November 2017

DECISION ANALYTICAL METHODS FOR ROBUST WATER INFRASTRUCTURE PLANNING UNDER DEEP UNCERTAINTY

Mehmet Umit Taner

DECISION ANALYTICAL METHODS FOR ROBUST WATER INFRASTRUCTURE PLANNING UNDER DEEP UNCERTAINTY

A Dissertation Presented

by

MEHMET ÜMIT TANER

Submitted to the Graduate School of the
University of Massachusetts Amherst in partial fulfillment
of the requirements for the degree of

DOCTOR OF PHILOSOPHY

September 2017

Department of Civil and Environmental Engineering
Environmental and Water Resources Engineering

DECISION ANALYTICAL METHODS FOR ROBUST WATER INFRASTRUCTURE PLANNING UNDER DEEP UNCERTAINTY

A Dissertation Presented

by

MEHMET ÜMIT TANER

Approved as to style and content by:

_____
Name, Chair

_____
Name, Member

_____
Name, Member

_____
Richard N. Palmer, Department Head
Civil and Environmental Engineering Department

DEDICATION

To my family for their unwavering support and encouragement over the years

ACKNOWLEDGEMENTS

Foremost, I wish to express sincere thanks to my advisor, Dr. Casey Brown for his support during my time at the University of Massachusetts Amherst. This work would never have been possible without his patient guidance. I would also like to thank Dr. Patrick Ray for his input and suggestions in my work over the past four years as well as his continuous encouragement and friendship. I would like to extend further gratitude to my committee members Dr. Senay Solak and Dr. Richard Palmer for their valuable feedback and comments.

I would like to thank the current and the previous members of the Hydrosystems Research Group for their friendship and collaboration. Special thanks are also due to Scott Steinscheineider, Ethan Yang, and Sungwook Wii, who generously provided technical help whenever I needed. Finally, I would like to thank my family, especially Alev and Fugen Pekun, and Sinasi Taner. Without their support and encouragement, this thesis could not have been completed. I would like to also thank Julieta Chaparro for her incredible support during this journey.

Individual studies in this dissertation work were funded through different projects. The first study on hydropower design in Malawi was funded through a subcontract from the Stockholm Environment Institute as part of the World Bank study "Enhancing the Climate Resilience of Africa's Infrastructure." The second study on water supply design in Kenya was funded by the World Bank as part of the project "Including Climate Uncertainty in Water Resources Planning and Project Design Decision Tree Initiative." The third study on water infrastructure planning in the Niger River Basin was funded by the World Bank as part of the project "Climate Risk Assessment for the Niger River Basin."

ABSTRACT

DECISION ANALYTICAL METHODS FOR ROBUST WATER INFRASTRUCTURE PLANNING UNDER DEEP UNCERTAINTY

SEPTEMBER 2017

MEHMET ÜMIT TANER, B.A., YILDIZ TECHNICAL UNIVERSITY

M.A., BOGAZICI UNIVERSITY

PH.D., UNIVERSITY OF MASSACHUSETTS AMHERST

DIRECTED BY: PROFESSOR CASEY BROWN

Deep uncertainties resulting from climate change, demographic pressures, and rapidly evolving socioeconomic conditions are challenging the way that water planners design and operate large-scale infrastructure systems. Conventionally, water infrastructures have been developed using stationary methods, assuming that the underlying uncertainties can be derived from historical data or experience. However, these methods are less useful under deeply uncertain climate and socioeconomic conditions, in which the future can be substantially different from the past and cannot be expressed by well-defined probability distributions. The recognition of deep uncertainties in long-term water resources planning has led to the development of "decision-analytical" frameworks that do not require predictions or prior probabilistic inference about the future. Instead, these approaches seek for alternatives that perform well across a broad range of conditions (robust) and can adapt to changing conditions (flexible). This dissertation aims to develop three new decision-analytical frameworks that build upon the previous work. The first study presents a generalized framework for water infrastructure design under climate change using regret-based robustness criterion and compares the findings to more conventional, predict-then-act based analyses of infrastructure design. The method is demonstrated for the design of a run-

of-the-river hydropower system in Malawi. The second study further develops the framework by considering multiple climatic, demographic, and socioeconomic uncertainties in the context of a water supply design project in the Coastal Kenya. This improved framework incorporates a Bayesian belief network to blend multiple sources of subjective information from model projections and expert opinions elicited from stakeholder workshops. The third framework develops a decision-analytical approach for flexible river basin planning under climate change and applies to the problem of long-term water supply and irrigation planning in the Niger River Basin. The framework makes use of a stochastic programming model to search for optimal planning pathways under a wide range of scenarios that represent both natural climate variability and climate changes. In this process, the framework explores uncertain beliefs associated with the probability weights assigned to each scenario and identifies "belief dominant" pathways that are insensitive to underlying probabilistic assumptions and are more promising based on climate projections.

TABLE OF CONTENTS

Page

LIST OF TABLES

LIST OF FIGURES

LIST OF ABBREVIATIONS

AOGCMs:	Atmosphere-ocean general circulation models
BNDS:	Bayesian networks decision scaling
BNs:	Bayesian networks
CMIP:	Coupled model inter-comparison project
DAPP:	Dynamic adaptive policy pathways
DS:	Decision scaling
EEV:	Expected value problem
ENSO:	El niño–southern oscillation
EV:	Expected value
GAMS:	General algebraic modeling system
GCMs:	General circulation models
IGT:	Info-gap theory
IPCC:	Intergovernmental Panel on Climate Change
ITCZ:	Inter-tropical convergence zone
KNN:	K-nearest neighbors
LCE:	Levelized cost of energy
LHS:	Latin hypercube sampling
NBA:	Niger Basin authority
NPTs:	Node probability tables
NRB:	Niger River Basin
NSE:	Nash-Sutcliffe efficiency
PCD:	Per capita demand for water
PDF:	Probability density function
PMF	Probability mass function
PRCC:	Partial rank correlation coefficient
PRIM:	Patient rule induction method
QBO:	Quasi-biennial oscillation
RCMs:	Regional climate models
RCPs:	Representative concentration pathways
RDM:	Robust decision making

RI:	Robustness index
RO:	Robust optimization
RP:	Recourse problem
SMIP:	Stochastic mixed-integer programming
SOW:	State of the world
SP:	Stochastic programming
SSTs:	Sea surface temperatures
SSY:	Specific sediment yield
VSS:	Value of stochastic solution
WARM:	Wavelet autoregressive model
WEAP:	Water Evaluation and Modeling System
WRMA	Kenya Water Resources Management Authority

CHAPTER 1

INTRODUCTION

Long-term decisions in water resources planning are one of the most compelling and wicked policy problems due to their broad and in many cases unforeseen implications for societies subject to many factors including climate variability, population growth, value tradeoffs, environmental regulations and technology (Rittel and Webber 1973; Priscoli 1998; Loucks et al. 2005). Water resources planning decisions, especially those related to infrastructure design and planning are irreversible and may produce unintended consequences, and in many cases, the long-term consequences of such decisions are highly uncertain if not entirely unknown.

Uncertainty from future climate change will add another layer of complexity to water resources planning, and will likely increase the magnitude and multiplicity of risks faced by water system planners (Fankhauser et al. 1999a; Arnell and Gosling 2013; Vorosmarty et al. 2014). The developing world will face a greater challenge under a changing climate regime due to their general geographical settings, their heavy dependence on climate sensitive socio-economic sectors as well as their overall lack of adaptive capacity (Mendelsohn and Williams 2006; Millner and Dietz 2011; Bhave et al. 2016). Given this greater and urgent need in water resources development, this dissertation focuses on the challenge how to better design and plan water infrastructure systems in the developing regions of the world. By taking an analytical and engineering-based perspective, the dissertation will focus on three different types of studies that are hydropower development in Malawi (Chapter 2), domestic water supply development in the Coastal Kenya (Chapter 3), and integrated planning of new water supply and irrigation infrastructures in the Niger River Basin (Chapter 4).

Development of an effective, long-term water strategy necessitates an adequate understanding of the level and the nature of the underlying uncertainties. The level of uncertainty ranges from statistical uncertainty, in which we can express uncertainty through known probability density functions to total ignorance that describes conditions where we do not even know that we do not know (Rotmans et al. 2003). Many types of problems compelling problems experienced today in water planning, including climate change are associated with deeply uncertain conditions, where it is not possible to define the underlying probability distributions of the future conditions and their consequences with precision (Lempert et al. 2004).

As water resources planners become more aware of a rapidly changing world and the limitations in conventional, stationarity-based planning to tackle the new challenges (Milly et al. 2008a), they become more interested in new, improved approaches for decision-making. Over the past few decades, the dominant paradigm been the so-called predict-then-act approaches that focus on climate model projections for predicting what may happen in the future. However, climate model projections are inherently uncertain due to unknowable, subjectively defined scenarios future greenhouse gas emissions (Stainforth et al. 2007b), inadequate sampling of initial conditions and natural variability. (Deser et al. 2012), and model inadequacies due to ill-defined earth-climate system processes (New and Hulme 2000).

Realizing the shortcomings of predict-then-act approaches, a number of decision-analytical approaches have emerged over recent years. These approaches shift the emphasis from climate science to local level decision-making (Brown et al., 2011; Walker et al. 2013; Wise et al. 2014; Herman et al. 2015), and aimed to seek decisions that are robust (insensitive to future conditions), resilient (able to recover quickly from failures), or flexible (able to

adapt to new circumstances). Most widely applied methods include (many-objective) robust decision making (RDM) (Lempert et al. 2006; Kasprzyk et al. 2013), info-gap theory (IGT) (Ben-Haim 2006), dynamic adaptive policy pathways (DAPP) (Haasnoot et al. 2013) and decision scaling (Brown et al. 2012). In comparison to the predict-then-act planning approaches, decision-analytical methods avoid making probabilistic assumptions about the future and rather aim to reduce the vulnerabilities in the system, by increasing the system's ability to perform adequately or acceptability under uncertainty, to adapt to changing conditions, or to recover quickly from undesired states or failures. Additional sources of information such as climate and demographic projections, paleodata or expert judgments can also be integrated to these analyses to provide insight on the likelihood of future changes to estimate risk (Brown et al. 2012).

The primary purpose of this dissertation is to improve the decision-analytical planning methods to water resources planning in a number of directions. The second chapter of this work addresses the challenge of how to identify robust, low-regret hydropower project designs under climate uncertainty. In this context, the work provides a comparison between the robust-based analysis and an implementation of more conventional, GCM-based predict-then-act approach regarding the representation of natural climate variability and the sampling of future climate changes, which are not explored so far. Also, the study also illustrates the use of three commonly used decision criteria for making decisions under uncertainty, namely i) planning for the most-likely outcome, ii) planning based on the expected outcome, and iii) planning for ensuring a low-regret across a wide range of conditions.

The third chapter of the dissertation expands on the second by considering multiple demographic and socioeconomic uncertainties in addition to climate change, and by

developing a new approach to improve the use of imprecise probabilistic information in robustness-based planning. Among the previous decision-analytical frameworks, there is no generalized method for blending in probabilistic information from diverse knowledge domains such as hydrology, water quality, and social sciences. This methodological gap is addressed by integrating decision scaling and Bayesian networks, a highly flexible probabilistic framework that can blend in multiple types and sources of information including stakeholder elicitations, expert judgments, and model projections. In this work, the Bayesian networks are used to propagate a posterior joint probability distribution of system vulnerabilities. This represents a novel application of Bayesian networks to the issue planning under deep uncertainty and environmental risk assessment. Also, the analysis also shows how the probabilistic inference obtained from Bayesian networks can be used further to identify ex-post scenarios regarding risk. This is done by coupling the results with a data-mining algorithm (Patient Rule Induction Method) to identify few, lower dimensional ex-post scenarios based on the identified range of risks. The proposed approach is demonstrated for a water supply project in the Coastal Kenya.

In the last chapter of this dissertation, decision-scaling concepts are further developed for multi-stage water infrastructure planning to assess the timing, sizing, and sequencing of multiple projects. The proposed framework uses a multistage stochastic programming model to search for optimal planning pathways under a range of stochastically generated transient climate scenarios. In doing this, a new sequential decision-making framework is developed that reduces the dependency on the assumptions made about the probability distribution of the scenarios. This is done by systematically varying the probabilities assigned to the scenarios, and resolving the stochastic optimization model under each case. This repeated optimization analysis results to a large set of optimal planning

pathways over a broad range of conditions. Finally, a post-optimization analysis is carried out to find one or few prosing development pathways to identify robust outcomes that are less sensitive to the underlying climate scenarios and probabilistic assumptions. GCM projections are also incorporated at this phase, to inform the decision-making process on the solution pathways that are associated with 'more likely' futures. The presented approach is illustrated for the planning of new dam and hydro-agricultural expansion projects in the Niger River Basin over a 45-year planning period from 2020 to 2065.

The primary contribution of this dissertation is to present new tools and methodologies for water resources decision-making under a deep uncertainty world, through means of exploring new, improved ways to use of imprecise probabilistic information in risk management, and by better assessment of the value of flexibility in large-scale infrastructure planning problems.

CHAPTER 2

ROBUSTNESS-BASED EVALUATION OF HYDROPOWER INFRASTRUCTURE DESIGN UNDER CLIMATE CHANGE

2.1. Abstract

The conventional tools of decision-making in water resources infrastructure planning have been developed for problems with well-characterized uncertainties and are ill-suited for problems involving climate nonstationarity. In the past 20 years, a predict-then-act-based approach to the incorporation of climate nonstationarity has been widely adopted in which the outputs of bias-corrected climate model projections are used to evaluate planning options. However, the ambiguous nature of results has often proved unsatisfying to decision makers. This paper presents the use of a bottom-up, decision scaling framework for the evaluation of water resources infrastructure design alternatives regarding their robustness to climate change and the expected value of performance. The analysis begins with an assessment of the vulnerability of the alternative designs under a wide domain of systematically-generated plausible future climates and utilizes downscaled climate projections *ex-post* to inform likelihoods within a risk-based evaluation. The outcomes under different project designs are compared by way of a set of decision criteria, including the performance under the most likely future, the expected value of performance across all evaluated futures and robustness. The method is demonstrated for the design of a hydropower system in sub-Saharan Africa and is compared to the results that would be found using a GCM-based, scenario-led analysis. The results indicate that recommendations from the decision scaling analysis can be substantially different from the scenario-led approach, alleviate common

shortcomings related to the use of climate projections in water resources planning, and produce recommendations that are more robust to future climate uncertainty.

2.2. Introduction

Investments in water infrastructure typically involve trade-offs between large capital costs and difficult-to-quantify delayed benefits ranked by current societal values, all subject to large uncertainties regarding future climatic, demographic, technological, and socioeconomic conditions (Fankhauser et al. 1999b; Pahl-Wostl 2007b; Jeuland 2010; Furlong et al. 2016). The design process for new water projects can be lengthy and highly complex, as such projects may often cause societal and environmental impacts, both positive and negative, that go well beyond the lifetime of the investment (Bednarek 2001; Hallegatte 2009; Hall et al. 2015). And though the complexities and uncertainties inherent in the design of new water infrastructure often warrant lengthy cautious discussion that delays investment, the world's poor living in conditions of high climate variability (e.g., in sub-Saharan Africa) suffer through the delays (Brown and Lall 2006; Hall and Murphy 2012; Strzepek et al. 2013; Groves et al. 2015). The primary purpose of this work is to improve the process of water infrastructure planning such that cost-effective, sustainable design alternatives can be more confidently identified and implemented considering climate variability and change.

The conventional modeling paradigms in water systems planning have assumed stationarity in long-term natural processes and estimated decision-relevant climate or hydrological statistics, for example, annual mean flow or 100-year flood from historical data (Hirsch 2011; Jeuland and Whittington 2014). This statistical information allowed planners to define generally few number of possible future states with known occurrence probabilities, and subsequently identify optimal or near-optimal project designs through

expected utility maximization (Maas et al. 1962; Loucks et al. 1981; Wurbs 1993; McInerney et al. 2012). However, recent evidence of climate change, including unprecedented changes in the precipitation patterns, and the frequency and intensity of storms, the timing and magnitude of surface runoffs has raised questions regarding whether water system planners shall continue to use stationarity-based methods, when making long-term, costly investment decisions (Milly et al. 2008b, 2015; IPCC 2013a; Arnell and Lloyd-Hughes 2014; Koutsoyiannis 2014). There is now a general agreement that climate-related uncertainties in water planning are deep due to unknowable trajectories of future greenhouse gas emissions (O'Neill et al. 2014), natural variability dominating at decision-relevant time scales (Deser et al. 2012; Enserink et al. 2013), and our understanding of the how the biophysical systems would respond to climate change, particularly at finer scales needed for decision-making (Hawkins and Sutton 2011; Forster et al. 2013; Hall 2014).

Over the past few decades, growing concerns on the use of conventional planning methods have resulted in interest in new, risk-based planning approaches for better consideration of climate uncertainty in decision-making (Lempert et al. 2004; Brekke et al. 2009; Hall and Borgomeo 2013; Kwakkel et al. 2016). As an initial response, many water system planners have focused on climate information from the coupled Atmosphere-Ocean General Circulation Models (AOGCMs, hereafter GCMs) to understand and assess the possible range of outcomes under climate change. This predict-then-act approach typically begins with selecting a subset of scenarios describing the state of future global development and demographic conditions, such as the Intergovernmental Panel on Climate Change (IPCC)'s "representative concentration pathways" (RCPs) (Moss et al. 2010). The selected set of scenarios is then evaluated through a subset of GCMs to assess the global climate response to greenhouse gas concentrations and then downscaled to a finer temporal and

spatial resolution needed by the decision-makers. The downscaled climate projections are then evaluated through linked simulation models, e.g., hydrology, water quality, and reservoir operations to assess the outcomes of climate change. As a result, the findings of the predict-then-act analyses rely heavily on the probability distribution of climate or hydrologic variables that are affected by the subjective assumptions and the source of information defining the scenarios and modeling procedures (Dessai and Sluijs 2007; Dessai and Hulme 2009).

Decision-centric frameworks attempt to address the shortcomings of predict-then-act approach by shifting the emphasis from climate science modeling to climate vulnerability at the local level (Walker et al. 2013; Singh et al. 2014; Wise et al. 2014; Herman et al. 2015). These approaches use exploratory modeling to examine a broad range of outcomes under future climate uncertainty, then identify decision alternatives or management actions to reduce vulnerability to climate change. Vulnerability reduction can be expressed in various ways, for example by increasing the system's ability to perform adequately or acceptability under uncertainty (robustness), to adapt to changing conditions (flexibility), or to recover quickly from undesired states or failures (resiliency). Decision-centric frameworks typically apply structured sensitivity analyses to identify critical outcomes across a broad range possible futures, and commonly aim to cover extreme or surprise futures often described as 'black swans' (Taleb 2007). The decision rules employed in decision-centric frameworks are typically non-probabilistic and show a departure from the conventional, expected utility based decision rules to accommodate for greater risk-aversion. For example, they rank choices based on the worst possible outcome, *maximin* (Wald 1950), a weighted score from the worst and best possible outcomes, *optimism-pessimism* (Hurwicz 1951), or based on acceptable performance on a specified performance benchmark, *satisficing* (Simon 1955). The

most prominent decision-centric frameworks are Robust Decision Making (Groves and Lempert 2007; Lempert and Collins 2007; Bryant and Lempert 2010), vulnerability-based or scenario-neutral planning (Prudhomme et al. 2010; Nazemi et al. 2013; Nazemi and Wheater 2014), Info-Gap Decision Theory (Ben-Haim 2006; Korteling et al. 2013), and decision scaling (Brown et al. 2011b; Whateley et al. 2014).

It is common in both decision-centric frameworks and predict-then-act analyses that the scenarios defining the domain of plausible future climates are derived from GCM-based climate change projections. However, this *ex ante* use of climate projections presents potentially biased inputs, which potentially bias the evaluation of design or planning alternatives. The use of an ensemble of projections reveals the performance of designs for the futures those models happen to produce, which is not an unbiased representation of possible climate change (Stainforth et al. 2007a; Weigel et al. 2010; Knutti et al. 2013), notwithstanding bias correction techniques, which map projections to historical conditions but do not address biases in projections of the future or sampling bias in the selection of GCMs used. The emission or concentration scenarios used in climate models incorporate numerous assumptions and subjective choices about how the future would unfold that cannot be verified. For example, all RCP scenarios from the IPCC's 5th Assessment Report assume a large reduction in the atmospheric aerosol emissions by the end of the 21st Century, which is argued to be too narrow (Stouffer et al. 2017). Also, many GCMs share basic structural assumptions, numerical schemes, and data sources, and consequently respond quite similarly to related models (Weigel et al. 2010; Knutti et al. 2013) leading to biases when viewed as independent realizations of possible future climate (Steinschneider et al. 2015a). They perform poorly in simulating interannual variability in precipitation (Brown and Wilby, 2012; Rocheta and Sugiyanto 2014), the frequency and intensity of extreme

events (Sillmann et al. 2013; Crétat et al. 2014), especially at fine scales relevant for the water system planners (Schiermeier 2007). The choice of downscaling method (Pielke 2012) and methodological challenges related to model calibration, e.g., model overfitting (Rougier and Goldstein 2014) introduces additional concerns in the use of GCM projections in decision-making. Consequently, careful consideration is warranted in the sampling of future climate conditions in scenarios used for infrastructure design, whether using a decision-analytical or climate-science based approach.

If GCM projections are not to be used as possible futures, how can this uncertain but potentially useful information be incorporated into climate risk analysis? An alternative is to use GCM projections *ex post*, i.e., after a broad range of future climate changes are explored for making posterior inference about the future. The *ex post* use of climate science information in water systems planning is presented by decision scaling (DS) applications (Moody and Brown 2013; Whateley et al. 2014; Steinschneider et al. 2015b; Culley et al. 2016). In DS, a *climate stress test* is first applied to reveal vulnerable outcomes across a broad range of climate uncertainties using climate/weather simulator and stochastic simulation analyses. The results of the stress test identify sensitivity to climate change, rather than sensitivity to the climate change projections and their associated and often untested biases that happen to be available from the current generation of GCM runs. Summary statistics from GCM projections, such as long-term trends in mean conditions are then considered to make a subjective judgment on whether identified problematic outcomes are likely to occur in the future. Finally, the system robustness is quantified by decision rules by considering both vulnerabilities as well as the probabilistic information derived from climate projections.

This manuscript demonstrates the first application of the DS framework to the design of water facilities, specifically related to hydroelectricity. In doing this, we present a

detailed comparison of the proposed framework to a conventional top-down analysis on two key aspects: the use of climate information in the decision analysis process and the choice of the decision rule for the preference ranking of the design alternatives respectively. For the former aspect, we compare and discuss using GCM projections at the initial phase of the process to describe the possible states of the world (which we refer to as the *ex ante* use) versus later in the process following the vulnerability analysis for making a probabilistic inference (which we refer to the *ex post* use). In the latter case, we compare infrastructure design preference under robustness criterion to more conventional criteria based on expected value of performance and performance under the expected future. Although numerous studies discuss the use of climate information from a methodological point of view (Dessai and Hulme 2004, 2007; Prudhomme et al. 2010), and the choice of decision rule in decision-making processes (Lempert and McKay 2011; Budescu et al. 2014; Giuliani and Castelletti 2016), we are not aware of any studies that evaluate both aspects together and demonstrate the practical implications quantitatively.

This manuscript is organized as follows: Section 2 introduces the adapted DS framework for water infrastructure design; Section 3 provides a comparative analysis of the proposed framework for a hydropower design case study in Lower Fufu River in Malawi; Section 4 provides a further discussion of the key findings, limitations, and conclusions.

2.3. Methods

The proposed framework consists of three main stages: [1] a stakeholder-led project screening of the essential processes and components of the analysis, [2] a climate stress test for exploring system performance under different design alternatives and plausible futures,

and finally [3] an *ex post* analysis for comparing and ranking the alternatives using alternative climate futures and innovative decision rules (Figure 2.1).

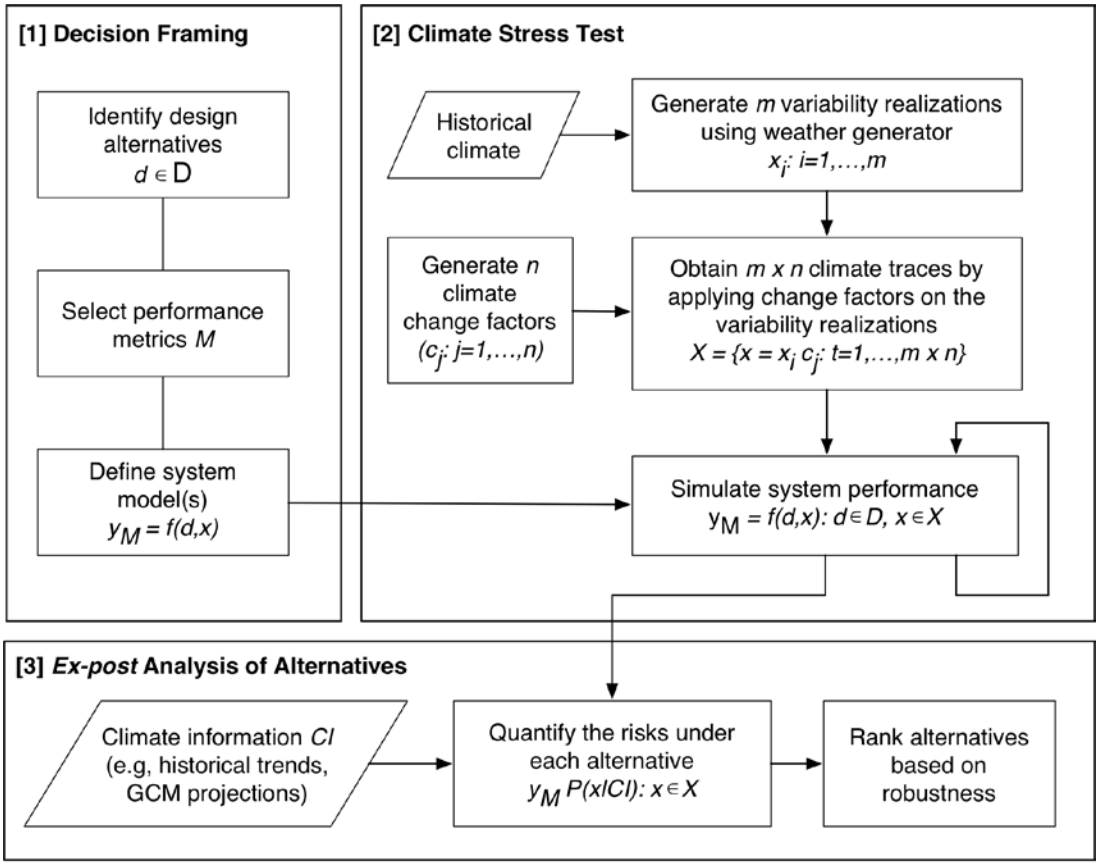

Figure 2.1 The proposed decision scaling framework for water infrastructure design under climate uncertainty. The rectangles and the parallelograms mark major model processes and information inputs respectively.

The first step of the process is the stakeholder-driven decision framing to describe the essential features of the analysis, including the design alternatives *d* to be evaluated through the process; the performance metrics *M* for expressing the performance of the alternatives, and the system model(s) $y_M = f(d, x)$ to relate design alternatives d to the consequences y_M contingent on the climate conditions *x*. Prior to the analysis, a set of discrete design alternatives can be specified jointly with the stakeholders, e.g., associated

local organizations, project partners, funding agencies. It is also possible to specify the options through a computational search based on Monte Carlo methods (Korteling et al. 2013) or evolutionary algorithms (Kasprzyk et al. 2013; Reed et al. 2013). The system models(s) are built based on the principal hydroclimatic, economic and operational processes, and the relevant temporal-spatial scales of the infrastructure design problem. As mentioned, although the framework presented here focuses on climate uncertainties, the same approach can be extended to include non-climatic factors, including uncertainties associated with price, population, or water demand change, although achieving unbiased sampling of those uncertainties has yet to be explored.

The second step is the climate stress test, a procedure to systematically explore how the infrastructure design may perform across a wide range of plausible future climate conditions, including changes in mean climate as well as climate variability. Typically, climate change studies use time-series of projections from GCMs to evaluate future performance. However, GCM projections do not systematically explore plausible climate changes, especially variability changes. They offer a glimpse based on what the projection happens to produce. The results indicate the performance relative to the projection that happens to be used. Finally, climate change projections are contingent on the emissions scenario used, downscaling and bias correction used, and a host of other subjective choices that obfuscate the final results of the analysis. In contrast, the climate stress test is specifically designed to systematically evaluate response to alternative climate futures that are represented unbiasedly and precisely. Climate stress test is implemented by first systematically sampling new realizations of the past climate using a stochastic weather generator (Steinschneider and Brown 2013). In this process, the weather generator is conditioned on the s historical climate statistics such as its mean and variance to produce an unbiased sample. The weather

generation process yields n realizations $x_i: i = 1 \ldots n$ each consisting of a set of time-series of climate variables at the desired temporal scale and spatial resolution. Long-term changes in the climate system, such as trends or shifts in mean temperature and/or precipitation conditions are represented through m delta factors $c_j: j = 1 \ldots m$. The variability realizations and the delta factors are then combined, resulting in a matrix of $n\ x\ m$ climate traces $X = \{x_t = x_i \cdot c_j : t = 1 \ldots, n\ x\ m\}$, where $(\cdot)$ is the operator used for modifying a given climate variable time-series. The system model $y_M = f(d, x)$ is then simulated for each climate trace $x \in X$ and design alternative $d \in D$ to evaluate the consequences under each case. The climate stress test thereby explores performance across systematically generated samples of climate variability and change, going beyond a conventional scenario-led analysis, in which the vulnerabilities are only estimated for the climate changes and variability that happen to be sampled by the available climate projections.

The final step is the *ex post* analysis of alternatives to identify one or few low-risk options for the project of interest. First, the risk associated with each option is quantified by weighting the set of consequences $\{y_M(d, x)\}$ based on available sources of climate information *CI*, such as including historical trends, paleoclimate data, GCM projections or expert views. The conditional probability weights assigned to future climate states $P(x|CI)$ $x \in X$ can be obtained from the most credible information or decision-relevant statistics extracted from the information source. For example, in recognition that the climate model projections are most credible at reproducing mean climate conditions (versus higher order moments, i.e., variability and extremes) at broader spatial scales (versus a single grid cell), only long term mean precipitation and temperature are used from the climate model outputs. Extracted climate information can be treated within a formal probabilistic framework to set

the conditional probability weights of the conditions evaluated in the stress test (Moody and Brown 2013). Finally, the quantified risks are summarized by a choice of robustness criteria, including stakeholder-defined robustness index (Whateley et al. 2014), satisficing metrics (Lempert and Collins 2007) or conditional-value-at-risk (Webby et al. 2007). The choice of decision criteria in robustness-based performance assessments allows creating a spectrum of attitudes reflecting the decision-maker's behavior, from full optimism, e.g., maximax, to extreme pessimism, e.g., minimax regret (Giuliani and Castelletti 2016).

2.4. Case study: hydropower plant design

The case study used to demonstrate the approach is the design and analysis of a hydropower facility currently in the planning phase. The results of the analysis are compared to the results of a scenario-led evaluation of the same project. The implications of the use of climate information and alternative decision criteria are discussed for both methods.

2.4.1. Project description

The planned investment in northern Malawi combines water resources from the North Rumphi and South Rukuru rivers for generating hydropower through a run-of-the-river plant (Figure 2.2). The required flow is diverted via two equally sized intake weirs and underground supply tunnels. The design problem consists of the choice of an economically viable hydropower facility size among the twelve prespecified design alternatives from 84 to 148 MW, which were defined by the project stakeholders before the analysis. The present value life cycle costs of these twelve options increase linearly from $223 to $342 million with increasing plant size. The design variable of the analysis is the combined maximum flow

allowed through the supply tunnels (design flow) that range from 29 to 51 m^3/s, depending on the selected hydropower plant size (Table 2.1).

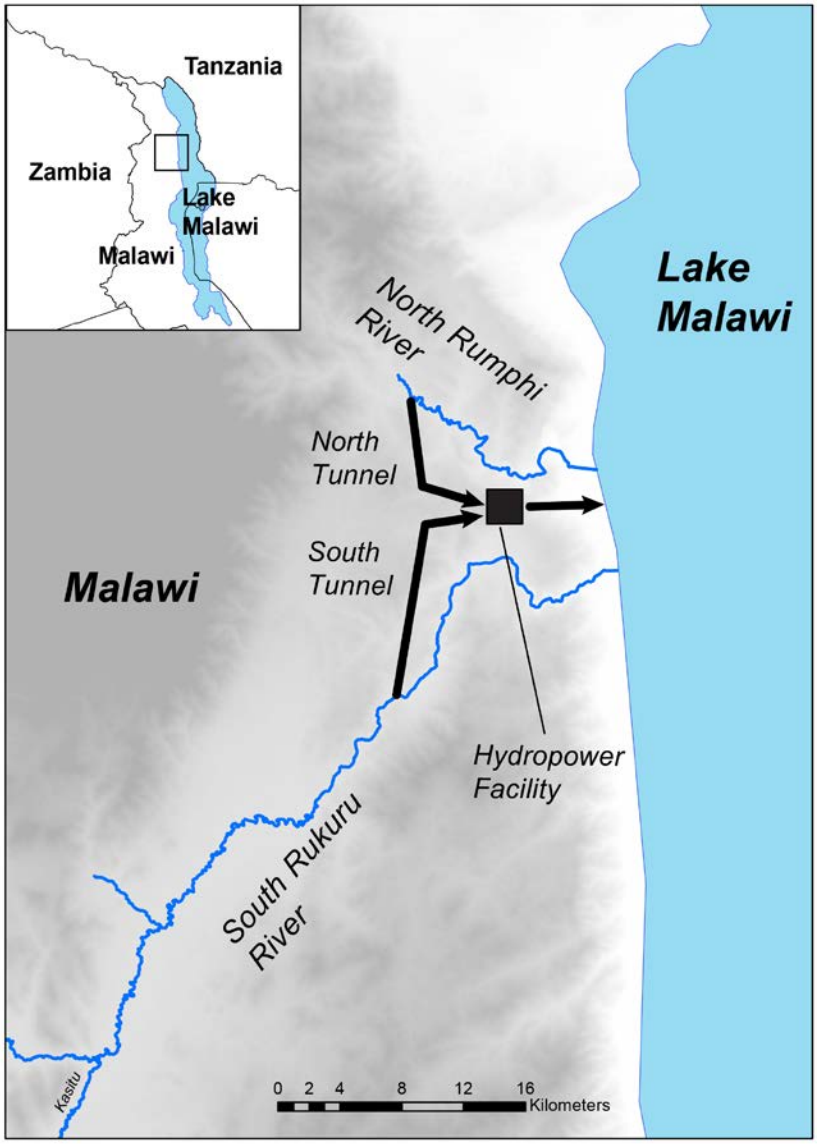

Figure 2.2 An illustration of the planned hydropower development project. The arrows indicate the direction of the diverted streamflow for hydropower generation.

Table 2.1 Design alternatives for the proposed hydropower facility. Design flow indicates the combined maximum flow allowed through the supply tunnels. The project cost shows the summation of the project capital costs and the estimated operations and maintenance costs over the project lifetime

Design capacity (MW)	Design flow (m^3/s)	Project cost (M USD)
84	29	223.0
90	31	231.0
96	33	238.8
102	35	246.4
107	37	253.9
113	39	261.2
119	41	268.4
125	43	275.4
131	45	282.3
137	47	289.1
142	49	295.8
148	51	302.4

The climate of northern Malawi is mild tropical with Austral rainy summers from December to April, and very dry winters from July to October. The primary driver for precipitation is the migration of the Inter-Tropical Convergence Zone (ITCZ) that separates the southeast trade winds and the north-east monsoon of the Indian Ocean (Jury and Mwafulirwa 2002). The historical climate conditions of the study region were evaluated for the period 1974-2008 using the combined reanalysis with observation data from the Terrestrial Hydrology Research Group at Princeton University (Sheffield et al. 2006). According to the available data, precipitation ranges from 700 to 1350 mm/yr, with a mean of 1001 mm/yr. The marked variability in the annual precipitation can be attributed to large-scale teleconnection effects, such as El Niño–Southern Oscillation (ENSO) and the stratospheric Quasi-Biennial Oscillation (QBO) (Nicholson 2000). Historical mean

temperature over the same period shows a linear increase of about 0.9 ˚C, with a mean of 20.6 ˚C.

2.4.2. Modeling of system performance

The hydropower generation from the run-of-the-river facility is simulated using an application of Water Evaluation and Modeling System (WEAP), a decision support tool for integrated water resources management. For this particular case study, the WEAP model was developed by Cervigni et al. (2015).The WEAP schematic of the study area includes two source nodes that simulate monthly surface flow from time-series of rainfall (mm) and temperature (°C); and two withdrawal nodes that divert simulated flow to the hydropower plant. Since the planned hydropower facility does not dam the river to create a reservoir, the hydropower output is approximated as a linear function of combined diverted flow (m^3/s) with a fixed hydraulic head of 336 m and a plant efficiency factor of 88 % based on the project feasibility study (Norconsult 1996).

The economic performance of the project is assessed by the Levelized Cost of Energy (LCE) based on the stakeholder preference. The LCE metric gives the price at which the electricity must be sold to break even financially over the lifetime of the project in $ per GWh:

$$LCE(d,x) = C(d) * \left(\sum_{t=1}^{T} P_t(d,x) * (1+r)^{-t} \right)^{-1}$$

Equation 2.1

where C is the present value cost of the project under design d ($), $\mathrm{P_t}\ (d,x)$ is simulated hydropower output in year t (GWh) under design d and climate condition x, *T* is the project

lifetime (35 years), and r is the economic discount rate (set to be 5%, based on stakeholder preference).

2.4.3. Assessing Design Alternatives under Climate Uncertainty

The twelve designs are subjected to a climate stress test to explore the performance of each under a large domain of future climate conditions. The input data for the climate stress test is obtained through the procedure described in Section 2, by first generating a set of new climate variability realizations, and then applying a set of change factors to the climate realizations to reflect gradual climate changes.

The new climate realizations are generated by a first-order wavelet autoregressive model (WARM) (Kwon et al. 2007; Steinschneider and Brown 2013). For this process, the historical precipitation record (from 1974 to 2008) for the two upstream catchments are area-averaged and aggregated to annual values. Next, ten annual, thirty-five-year precipitation realizations are sampled from the WARM, with approximate means and standard deviations of 1001 mm and 150 mm respectively, and with power spectrum similar to the observed record. The generated annual precipitation realizations are then disaggregated to multi-site monthly time-series using a K-Nearest Neighbors (KNN) resampling scheme (Lall and Sharma 1996). The outcome of the weather generation process is a relatively unbiased sample of the observed climate record with matching mean, standard deviation, and low-frequency variability. Next, delta factors are applied to the climate realizations to simulate long-term trends in the precipitation and temperature. For temperature, six additive factors applied from -1 to 4°C, with increments of 1°C. For precipitation, thirteen multiplicative factors are applied ranging from 0.4 to 1.6 with increments of 0.1. These climate change factors increase linearly by starting from zero-change at year one and ending at the specified

level (e.g., 3°C). The choice of delta factors is made to span a broad range of climate changes for the study area, exceeding the range of projected temperature increases (up to 2.5ºC) and precipitation changes (up to 30%) in 2060's relative to 20th Century means (Cervigni et al. 2015).

By applying all possible combinations of change factors over the ten realizations, a total of 780 climate traces is obtained. The climate stress test is then executed for each design alternative by simulating the WEAP model of the system under each climate trace to obtain monthly hydropower outputs. LCE metric is calculated for each simulation run (Equation 2.1), and then are transformed to regret to identify the design(s) that would give a relatively low level of regret over the range of climate conditions assessed:

$$regret_M(d,x) = |LCE(d^*,x) - LCE(d,x)|$$

Equation 2.2

where the regret $regret_M(d,x)$ is the absolute difference between the Levelized cost of design d in some future condition x, $LCE(d,x)$, and the levelized cost of the best-performing design, d^*, under the same future condition, $LCE(d^*,x)$. Note that the presented approach of comparing the design alternatives, i.e., by assessing the range of low regret outcomes in each option, does not make use of climate information. In order to aid the decision-making process, downscaled GCM projections are used to set the likelihood of future climate conditions (see the following section).

2.4.4. Robustness Analysis of the Alternatives

In the final phase, the twelve alternatives are evaluated regarding their ability to perform acceptably under the future climate conditions evaluated. This is done by calculating

the robustness of each alternative from the set of LCE regret values calculated through the climate stress test (Section 2.3.3). Climate science information is incorporated at this phase to assign relative weights to alternative futures.

The robustness of the options is expressed using a modified version of the Robustness Index *(RI)* (Whateley et al. 2014). The first step of RI calculation is parsing the stress test results into regions of acceptable and unacceptable outcomes concerning a pre-defined performance threshold I^T:

$$\Lambda(d,x) = \begin{Bmatrix} 1, & if\ regret_M\ (d,x)\ \leq I^T \\ 0, & if\ regret_M\ (d,x) > I^T \end{Bmatrix}$$

Equation 2.3

where, I^T is the performance threshold that is set to a LCE regret of 200 \$/GWh, and $\Lambda(d,x)$ is a binary variable that takes a value of one when the computed regret value is less than or equal to the threshold value and zero when the regret is higher than the threshold. The threshold value is set based on the stakeholder opinion among a range of alternatives. Next, a *RI* value is computed from the weighted sum of the binary variable $\Lambda(d,x)$ conditional on the climate information CI:

$$RI_{d^*} = \underset{d}{argmax}[\sum_{x} \Lambda(d,x)\ .P(x|CI)]$$

Equation 2.4

where, $P(x|CI)$ is the relative weight assigned to each climate state x conditional on the climate information. For this study, the climate information is obtained from the World Climate Research Programme Coupled Model Intercomparison Project Phase 5 (CMIP5) multi-model ensemble (Taylor et al. 2012). The ensemble has a total twenty GCM models

that consists of twenty model runs forced with the historical conditions (the atmospheric composition of the 20th century), and a total of fifty-four model runs forced with the IPCC's representative concentration pathways (RCPs) 4.5 and 8.5 respectively (IPCC, 2013). The GCM outputs from all model runs are statistically downscaled to a monthly temporal resolution and a 0.5º spatial resolution according to the Bias Correction Spatial Disaggregation (BCSD) method (Cervigni et al. 2015).

Using the CMIP5 ensemble, the relative weights assigned to the climate states are obtained in four steps. First, the vector of mean annual precipitation and temperature changes are calculated from all future climate projections. Second, the computed mean changes from twenty GCMs are then reduced to eight data points to account for the potential sampling biases due to the structural similarities in GCMs (Knutti et al. (2013). In doing this, we treated all model runs equally, and by simple averaging within each model group. Third, the computed eight data points are used to define a probability distribution function (PDF) for the domain of climate changes. In this work, we used a bivariate Cauchy distribution:

$$g(x,y) = \frac{1}{2\pi}\left[\gamma\left((x-x_0)^2 + (y-y_0)^2 + \gamma^2\right)^{-1.5}\right]$$

Equation 2.5

where, x_o and y_o are the location parameters that are set to the mean temperature and precipitation value of the eight data points; and γ is the scale parameter that is set to the covariance matrix obtained from the eight data points. The reason for using a heavy-tailed Cauchy distribution over a more common Gaussian (Whateley et al. 2014) is assign higher relative weights to extreme changes for greater risk-averseness. Finally, we the contingent normalized probability weights of the 78-plausible mean temperature and precipitation

changes are obtained (Equation 2.5). The RI calculation is repeated for each climate variability realization and then averaged over with an assumption that each variability realization is equally likely to occur.

In addition to the RI criterion, we also show design preference under two more commonly applied decision rules for comparison. The first additional criterion is the design choice based on the most likely (ML) future state:

$$ML_d = LCE(d,x): \max_X P(x|CI)$$

Equation 2.6

where, $\max_X P(x|CI)$ is the 'most likely' climate future conditional on the imperfect climate information; $LCE(d,x)$ is the LCE value under that most-likely climate state. The latter criterion of EV is the weighted sum of the computed LCE values contingent on relative probability weights obtained from the climate information CI:

$$EV_d = \sum_x LCE(d,x)\ P(x|CI)]$$

Equation 2.7

2.4.5. Design Evaluation Based on Scenario-led Analysis

The twelve design alternatives are also evaluated under the historical climate conditions, and by way of a conventional top-down, GCM-based analysis to demonstrate differences on the proposed framework. In this case, climate information is used *ex ante* to describe the domain of climate scenarios and the evaluation process is carried out based on the results obtained from those scenarios.

For the analysis under historical climate, the WEAP system model is simulated under a single forcing scenario representing the historical climate of the 1974-2008 period. For the

latter case of GCM-based analysis, the model is forced with all downscaled GCM outputs over the 2016-2050 period. In both cases, the simulated hydropower output and the present value costs are used to calculate the LCE (Equation 2.1). The results are then summarized using the same decision criteria of RI, ML, and EV respectively. For the RI and EV criteria, it is assumed that each GCM-based climate scenario is independent and equally likely to occur. For the ML criterion, the most likely climate scenario is determined based on the empirical density of the projected climate changes in the multi-model ensemble.

2.5. Results and Discussion

2.5.1. Design Preferences under Decision Scaling (DS) Application

The LCE values obtained from the stress test range from 18,400 to 32,800 $/GWh for the smallest design (29 m^3/s) and from 17,000 to 37,000 $/GWh for the largest design (51 m^3/s), respectively. We note that the order of magnitude of differences among the LCE values may be relatively small for real-world decisions; however, the results illustrate the application of the evaluation process despite the small magnitude of the economic values. The differences in results become more noticeable in regret terms, as the computed regret for the smallest and largest design sizes are up to 1,400 and 4,300 $/GWh, respectively.

Figure 2.3 shows the regret for each alternative under evaluated climate changes. The relatively sharp changes over the y-axis (precipitation change) indicate that the results are more sensitive to precipitation than to temperature. Among the twelve alternatives, the smallest (29 m^3/s) results in a regret of less than 200 $/GWh, and therefore performs acceptably when the mean annual precipitation is less than the historical mean. However, for the smallest option, the regret increases to 1500$/GWh under wetter futures. In contrast,

larger options, i.e., 45 m^3/s or greater, are vulnerable to drier futures, with a maximum regret of 2,000 $/GWh or greater. As no single option dominates, and the choice varies whether the future would be drier or wetter, climate likelihood information is useful at this stage for making a judgment on the relative risks presented.

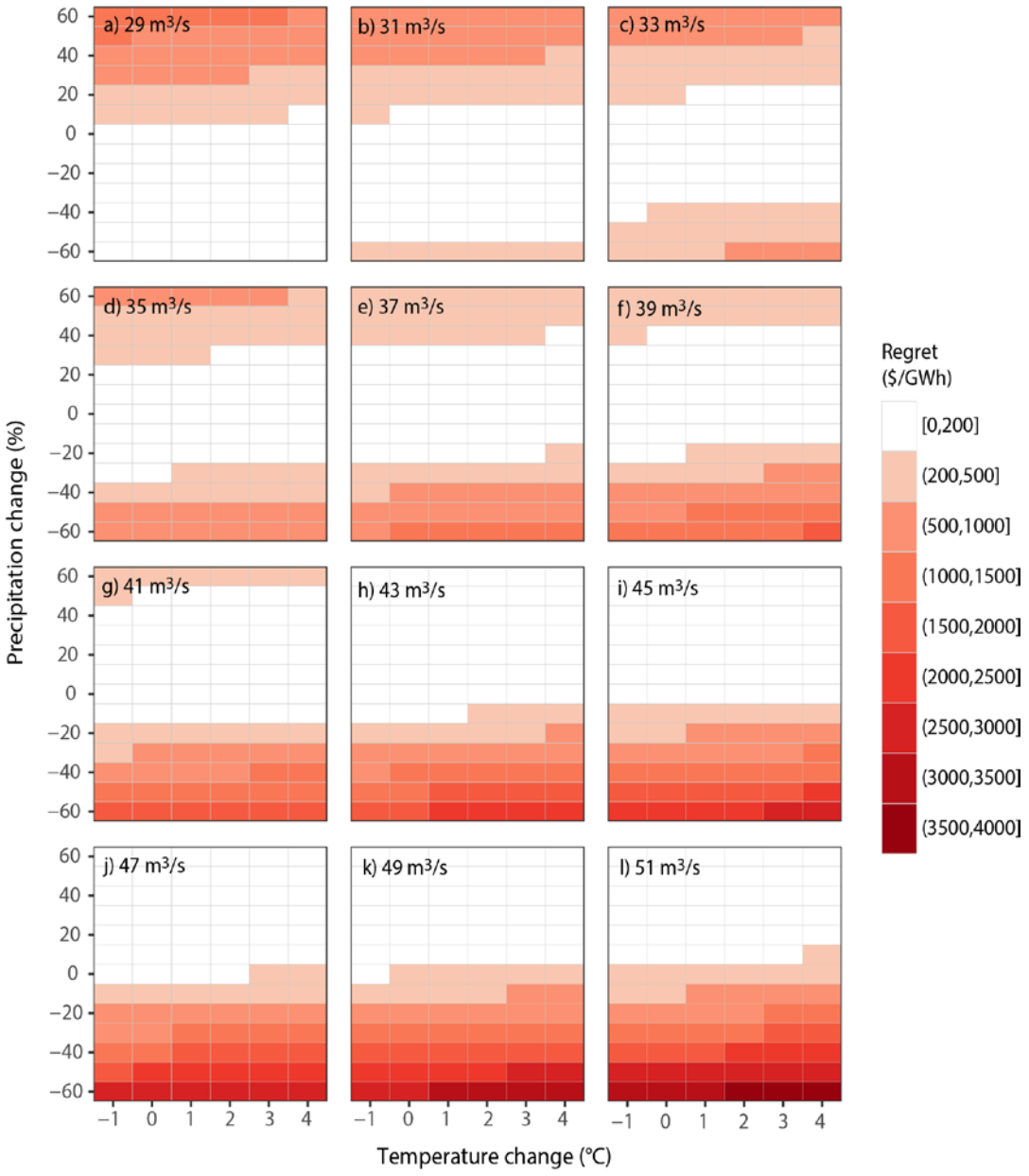

Figure 2.3 Computed LCE regret across the domain of climate changes in USD/GWh. Panels a through k show the results for the indicated design flow in m3/s. The cells shaded with white color mark the climate conditions that result in a low (acceptable) level of regret.

Figure 2.4 shows the scatter plot of annual mean climate changes from the CMIP5 ensemble of GCM output. The multi-model ensemble shows a large range of outcomes for both the direction and the magnitude of change in mean annual precipitation (-30% to +20%) and a relatively small range of outcomes in the magnitude of increases in mean annual temperature (1˚C to 2.2 ˚C) relative to the historical averages.

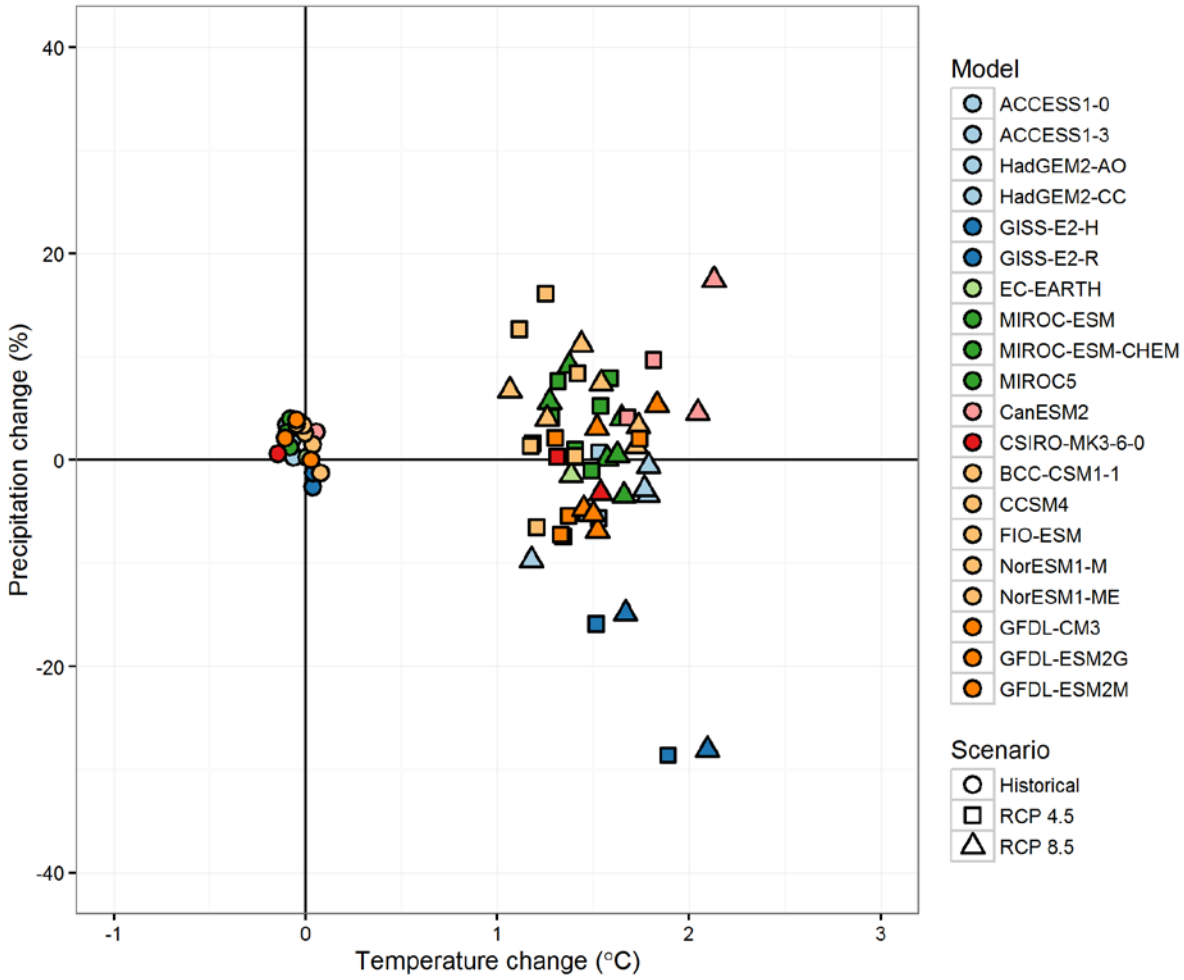

Figure 2.4 Projected mean changes in annual temperature (˚C) and precipitation (%) in the seventy-four GCM runs relative to the historical period 1974-2008. GCMs sharing similar model code are shown in the same color. Shapes represent a model response to different climate forcing scenarios. The intersection of the vertical and horizontal line marks the value of mean observed temperature (20.6 ˚C) and precipitation (1001 mm).

The results from the vulnerability analysis (Figure 2.3) and the climate information derived from the CMIP5 ensemble (Figure 2.4) can be combined to for the risk analysis of alternatives. Figure 2.5 depicts the climate conditions under which each design is the no-regret choice or the best performing alternative. In Figure 2.5, eight data points representing the mean climate changes from each GCM group (see Figure 2.4) are superimposed to provide a graphical indication of the GCM-based likelihood of evaluated climate changes. It is seen that most designs are optimal for a narrow band of plausible climate changes, while the smallest and largest design flows, 29 and 51 m^3/s respectively, outperform the others over a relatively larger domain of climate changes. However, these represent extreme climate changes that are less likely to occur according to the mean changes from the model groups. As Figure 2.5 shows, most model groups indicate little change in mean precipitation and a temperature increase between 1 and 2 ºC, although there is one warmer-and-wetter and one dryer.

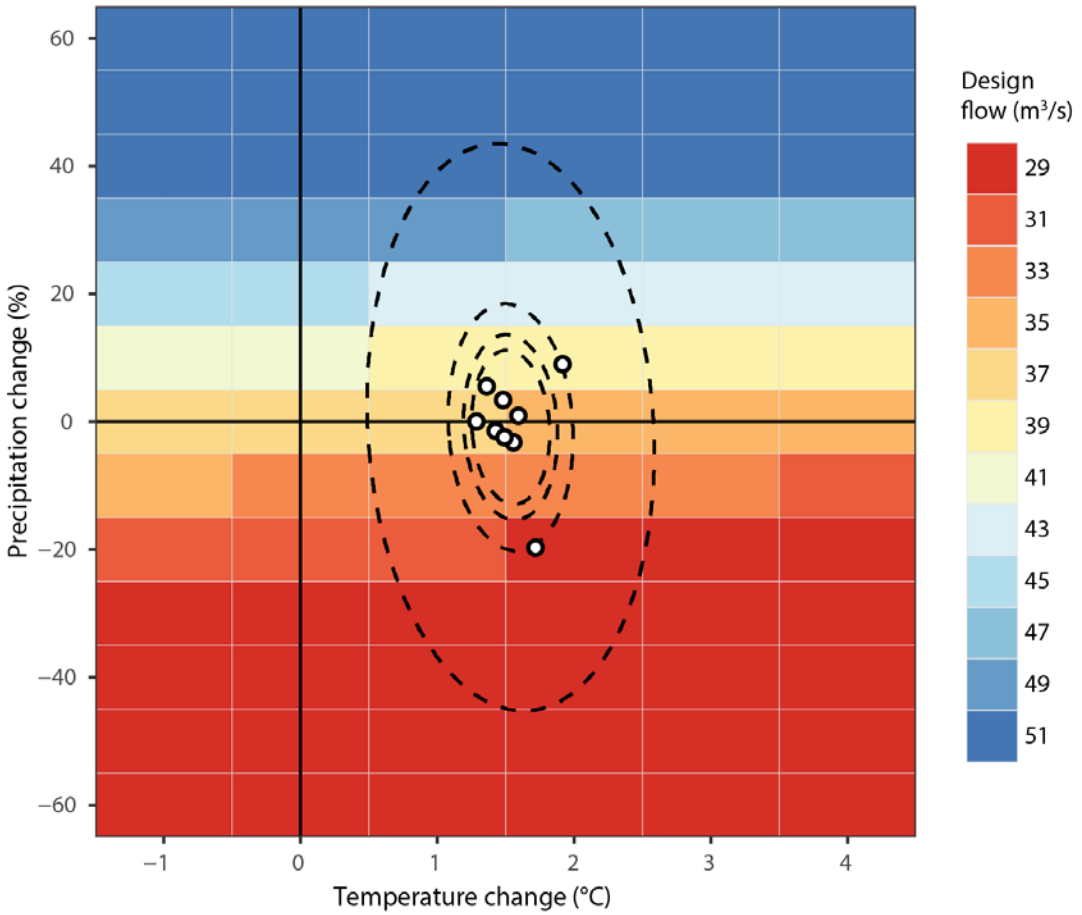

Figure 2.5 No-regret domains of the designs under the evaluated range of climate changes. Each color region marks a design's zero-regret performance domain regarding LCE. The intersection of the vertical and horizontal line marks historical mean temperature and precipitation (1974 – 2008 period). The circles mark projected means from 11 GCM groups in the CMIP5 ensemble for the period of 2016-2050. The contours indicate the levels ($1x10^{-3}$, $3x10^{-3}$, $5x10^{-3}$, $7x10^{-3}$ and $9x10^{-3}$ respectively) of the bivariate Cauchy distribution derived from the GCM data.

The computed decision criteria applied to the design question reveals a single best design of each evaluation criteria. For the ML criterion, the 35 m^3/s design gives the lowest LCE, with a value of 23,400 $/GWh under the most likely conditions of a mean temperature increase of 2 ºC and historical precipitation means (no-change). Figure 2.6 shows the results under the EV and RI criteria for each climate realization, as well as for the conditions averaged over their means. The EV criterion indicates design 35 m^3/s as the best choice. Note that the role of variability, however, as the design preferences vary from the 33 to 37

m^3/s based on the choice of climate realization (Figure 2.6-a). The RI criterion also indicates design 35 m^3/s as the best choice, with results ranging from 31 to 39 m^3/s over the ten individual variability realizations (Figure 2.6-b).

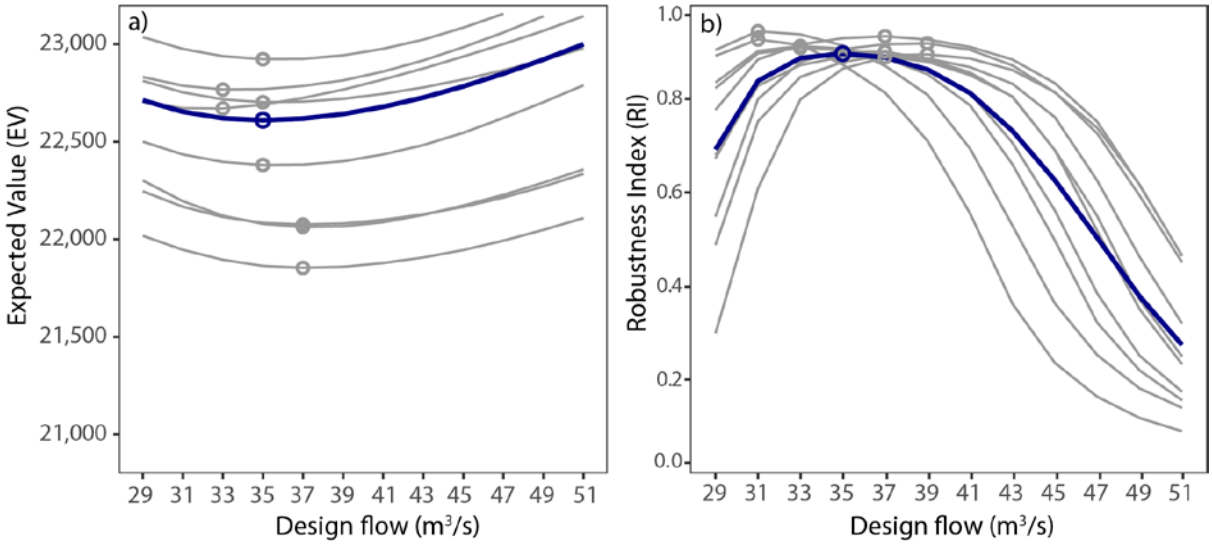

Figure 2.6 a) Variation in EV criterion, in US/GWh. b) Variation in RI criterion. The gray lines show the variation of results across the ten stochastic climate variability realizations. The blue lines show the mean results averaged over the individual variability realizations. The gray and blue circles mark the preferred design choices for each condition.

2.5.2. Comparison to results under scenario-led analysis

The simulated LCE values under the historical climate period (1974-2008) across the twelve alternatives show 39 m^3/s as the optimal design option. Under the scenario-led analysis, the LCE metric ranges from 19,300 to 31,500 \$/GWh for the smallest size (29 m^3/s), and from 18,400 to 35,400 \$/GWh for the largest size (51 m^3/s). The design preference is found to be highly dependent on the choice of criterion, as the choices were 39 m^3/s for the ML, 31 m^3/s for the EV, and 29 m^3/s for the RI respectively.

Table 2.2 summarizes the preferred choices under the past climate, and the scenario-led and decision-scaling analyses on the three decision criteria applied. Considering the RI

criterion, the best alternatives are identified as the 39 m^3/s for the historical climate, 29 m^3/s for the scenario-led analysis, and 35 m^3/s for the decision-scaling analysis respectively. To illustrate the differences between these three optimal choices, we focus on their relative performances under future climate. Figure 2.7 depicts the regret from the options of 29, 35, and 39 m^3/s versus the potential future mean streamflow based on 780 stochastic climate traces used in the stress test analysis. If the mean streamflow were to decline in the future, the historical choice performs very poorly, while the two alternatives that accommodate climate change perform better. Therefore, it remains helpful to bring in a representation of the information from both climate projections as well as the historical mean value to assess alternative designs. Shown as pdfs of climate change in parallel coordinates (lower panel), the 35 m^3/s (based on DS) and 39 m^3/s (based on historical conditions) perform better over the conditions indicated to be probable by the available climate evidence.

Table 2.2 The summary of findings from each decision criteria under the historical climate conditions, and based on the scenario-led and the decision scaling analyses. The values in bold show the final preference in each case.

Decision criteria	Historical climate	Scenario-led analysis	Decision scaling analysis
ML	39 m^3/s	37 m^3/s	35 m^3/s
EV	-	31 m^3/s	35 m^3/s
RI	-	29 m^3/s	35 m^3/s

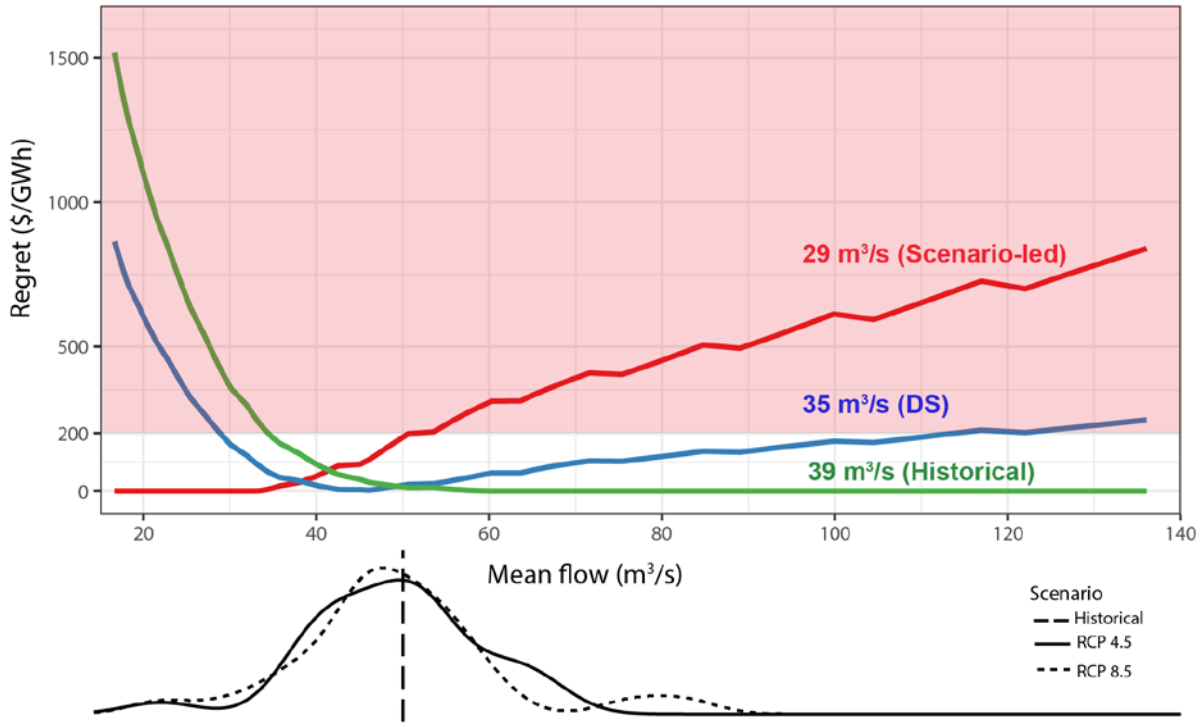

Figure 2.7 - LCE regret (in $/GWh) versus mean flow at the upstream the project site (m^3/s) for the best performing designs under the historical climate, and under future climate with the scenario-led and decision-scaling approaches. The region shaded in light red shows the unacceptable performance when regret is above 200 $/GWh. The lower panel shows the historical mean, and the density distribution of mean streamflow from the GCM runs with the RCP 4.5 and 8.5 forcings respectively.

2.5.3. Implications of *ex ante* and *ex post* uses of GCM projections on the design preference

The differences in the results of the two methods presented (Table 2.2) can be explained by the underlying methodological choices, and mainly by how climate uncertainty is sampled in each case. The DS approach provides a fuller and more systematic exploration of the climate change uncertainties through a stress test, in this case, with a full factorial design consisting of six additive factors of mean temperature increases up to 4°C and thirteen multiplicative factors of mean precipitation changes from -40% to 40%. In contrast, the scenario-led approach explores system sensitivity to the downscaled range of CMIP5 projections, consisting of twenty GCM models and two RCP scenarios. These GCM

projections represent a relatively narrow range of climate changes (e.g., for precipitation from about -30% to 20%) and a clustered sample set of mean climate changes based on the underlying assumptions such as the forcing scenarios used, the downscaling method or the structural similarities among the climate models. The clustering of model estimates in the given multi-model ensemble (e.g., the clustering of mean annual precipitation around the historical mean of 1000 mm/year in Figure 4) imposed an *ex ante* probability distribution over the evaluated range of uncertainties. The preference for relatively smaller project design capacities in the scenario-led analysis can be attributed to this implicit probability distribution, with a higher density on the lower range of potential precipitation changes.

Second, the DS and scenario-led analyses represent historical climate variability differently. In DS, historical climate variability is represented by ten stochastic realizations from a wavelet auto-regressive model. The statistical properties of these ten realizations match well with the historical record. For example, the differences in standard deviation are less than 3%, and the correlation between the power spectra of each realization and the historical data ranges from 0.5 to 0.7 (Figure 2.8). In contrast, the GCM time-series used in the scenario-led analysis are biased in the representation of historical climate variability. The downscaled GCM runs overestimate the historical standard deviation by 14%, on average, with particular runs deviating from the true standard deviation by -20% to +63%. The downscaled GCM runs perform particularly poorly with regard to precipitation persistence. Half of the models carry a negative correlation with the observed power spectrum (with values ranging from -0.6 to 0.7) (Figure 2.9).

In addition to the biases associated with the historical GCM runs, the sensitivity of results to climate variability could not be observed in the scenario-led approach, as no GCM model had more than a few realizations of the possible future climate under the given

concentration forcing assumption. Moreover, no data were available to indicate the degree to which the inherent climate noise influenced the downscaled GCM runs, or if the design preferences from the scenario-led analysis would change in a repeated analysis with different climate time series obtained from the same GCM projections and concentration scenarios. We are aware that the sampling of climate variability can be improved by making use of GCM data from large perturbed physics experiments such as the UKCIP scenarios (Murphy et al. 2007), but such were not available for this study.

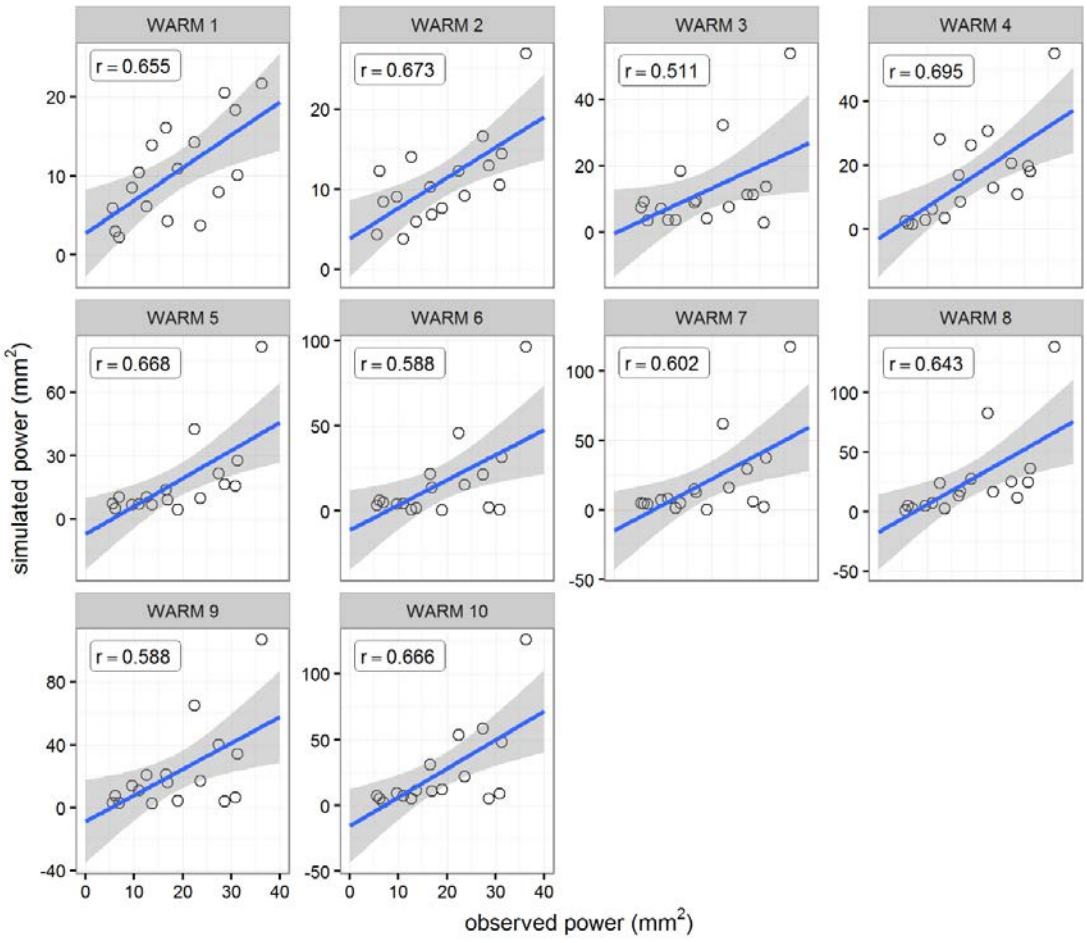

Figure 2.8 Power correlations between the observed precipitation (1974-2008) and the precipitation realizations generated by WARM. In each panel, the blue line shows the linear regression line and the gray ribbon represents the 95% confidence interval of the regression.

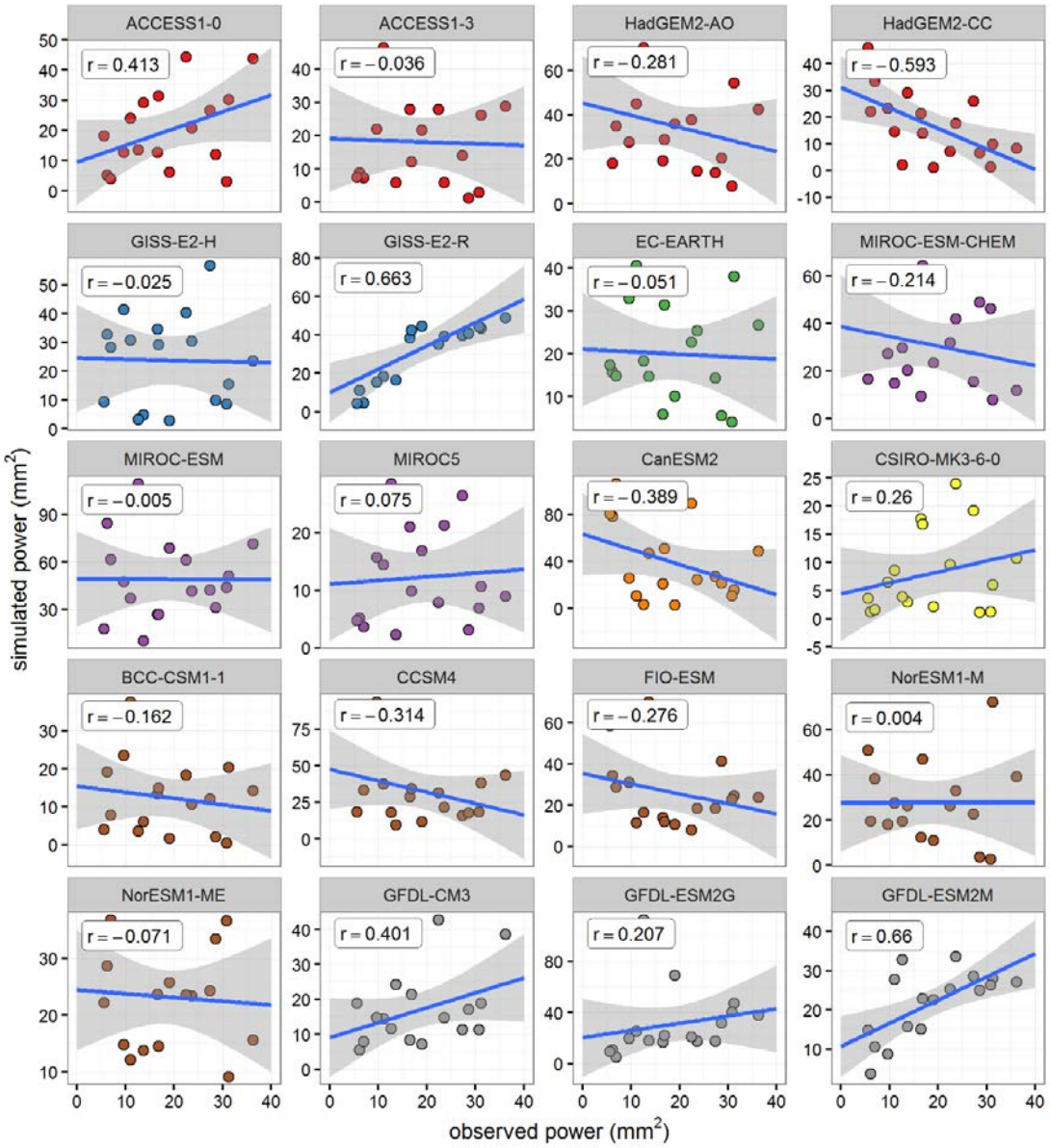

Figure 2.9 Power correlations between the observed annual precipitation of the 1974-2008 period (x-axis) and the historical GCM runs (y-axis). In each panel, the blue line shows the linear regression line, and the gray ribbon shows the 95% confidence interval of the regression line. Colors indicate GCM family scheme.

2.5.4. Implications of decision criteria on the design preference

Faced with a deeply uncertain climate, the water systems planning community has commonly agreed that long-term, costly investment decisions would do well to emphasize robustness, the ability of the system to perform satisfactorily across a broad range of futures.

This marks a departure from the conventional decision theory, by which analysts commonly prescribe uncertainties *ex ante*, commonly through a single, well-defined PDF, and then model the system using a "most likely" future, or run the model for a number of scenarios and make a recommendation to decision makers based on the single expected value of outcomes. The limitations of conventional criteria in contrast to robustness-based based approaches have been discussed in detail, particularly on results sensitivity to underlying probabilities (McInerney et al. 2012; Walker et al. 2013; Heal and Millner 2014) and underestimation of risks from low-probability-high-impact events (Weitzman 2009). However, the implications of their use in planning problems in comparison to robustness-based criterion have not been demonstrated. To address this point, we have shown a comparative analysis for a hydropower design problem.

The preferences under the decision criteria of RI, ML, and EV (Table 2.2) show high sensitivity to underlying experimental design, in this case, how the domain of future changes is defined and weighted. In the scenario-led case, the RI criterion results in the most 'conservative' choice of 29 m^3/s (i.e., the alternative with the lowest capital cost) to maintain a low regret regarding economic efficiency across all projected climate changes. However, under the decision-scaling analysis, both RI and the conventional criteria of ML and EV resulted in the same mid-sized design choice (35 m^3/s). This result is not necessarily generalizable, but is indicative in its demonstration for this case.

2.5.5. Limitations of the analysis presented

The case study explored the future vulnerabilities across a broad domain of climate states considering both natural variability and long-term climate change. We represented future climate changes through simple change factors applied to annual mean temperature

and precipitation. However, the changes in extremes (e.g., future monthly maximum precipitation) or in intra-annual variability (e.g., seasonality of precipitation) remains as an important concern in long-term planning (IPCC 2013b) and could also be explored. For this purpose, Steinschneider and Brown (2013) describe a quantile mapping method to alter frequency distributions of precipitation time-series (e.g., monsoon arrival time and duration) that could be integrated into the presented framework.

We represent climate information for the area of interest based on a set of fifty-four downscaled GCM projections. Although the multi-model GCM ensembles are standard inputs to many top-down climate risk assessment studies, it is possible to improve the sampling of uncertainty in model projections using more rigorous approaches. For example, Borgomeo et al. (2014) present a risk-based approach to water systems planning, where they define the probability distribution of future climate states using a large perturbed physics ensemble (PPE). In their work, Borgomeo et al. (2014) couple data from UKCP09 PPE with a transient stochastic weather generator for better sampling of natural climate variability and model parameterization. Various other decision-centric analyses show similar ways of using GCM projections using large model experiments and stochastic sampling or downscaling algorithms (Groves et al. 2008; Lopez et al. 2009; Bussi et al. 2016; Turner et al. 2016). However, these more rigorous frameworks still lack proper treatment of uncertainties due to model structures or underlying emission scenarios.

Another important point related to the use of climate information in decision-making is the approach to account for the sampling bias due to the similarities among the climate models. In this work, we address the bias due to model similarity using a single representative value (the mean) from each GCM family based on the model genealogy scheme given by Knutti et al. (2013). We are aware that this is a coarse approximation of the

probabilistic information that can be extracted from a multi-model climate projections ensemble. More sophisticated methods can be used to maintain model diversity without replication, for example through a performance-based weighting scheme (Haughton et al. 2015), k-means clustering (Cannon 2015), or by assessing the correlations in the error structure of the model projections (Bishop and Abramowitz 2013; Evans et al. 2013).

2.6. Conclusions

This paper has applied DS concepts to the design of the turbine capacity for a run of the river hydropower facility. Previous applications of DS have been *risk assessment* applications: assessments of the impact of possible climate changes on a water resources system. Here, the approach is used for *risk management*, to identify a specific design under climate change. Design outcomes were explored under multiple dimensions of climate uncertainty, on natural climate variability, long-term climate change, and climate projections. Design alternatives were compared and ranked by way of a formal decision analysis procedure, using optimality and robustness-based decision criteria. In this framework, subjective information regarding the future, such as climate projections, was applied *ex post* (following the process of stress test analysis) and indirectly (to set the conditional likelihoods of the stress test outcomes). The approach was compared to a conventional scenario-led framework through a hydropower project design study, and the decision outcomes under both frameworks were discussed.

The framework provides a systematic procedure to incorporate the effects of natural climate variability, through a stochastic weather generator conditioned on the historical climate record. In contrast, scenario-led analyses provide limited means to explore these kind of climate variability effects, for example through the use of perturbed physic ensembles

(Lopez et al. 2009; Fung et al. 2013), or by the use of stochastic downscaling methods (Groves et al. 2008; Fatichi et al. 2014). We note that the uncertainty effects of natural climate variability are likely to outweigh the uncertainty effects of global climate change in the next couple of decades (Deser et al. 2012; Ledbetter et al. 2012; Fatichi et al. 2014); hence need to properly be addressed in the frameworks of infrastructure planning and design.

Given the biases and structural problems in GCM projections, an important issue for the decision-makers is to what extent they should trust these model results, and how to use these (often conflicting) model outputs in their analysis frameworks. Through the *ex post* application of appropriate information from GCM projections (e.g., long-term changes in mean climate conditions), the analyst can *explicitly* set the statistical properties of the valuable information, for instance, the choice of probability distribution used to fit the climate statistics. In contrast, the *ex-ante* use of information in the scenario-led framework provides no flexibility, as the analysis is entirely dependent on the time-series data from the GCMs. An important implication of this *ex ante* use of GCM projections is the bias due to the empirical distribution of the parameters, e.g., the repeated sampling of certain projected conditions due to model similarities.

Under deep uncertainty regarding future climate conditions, irreversible and costly infrastructure planning decisions need to be made with risk-aversion. However, the level of acceptable risk, and the trade-offs between performance and robustness are highly subjective and dependent on the decision maker's (stakeholder's) perspective. Examples of the ramifications of such risk aversion perspectives (ML, EV, RI) have been quantitatively demonstrated here. The influence of the decision criterion applied was found to be higher under the scenario-led analysis in comparison to decision scaling.

2.7. Acknowledgments

This work is funded by a subcontract from the Stockholm Environment Institute (SEI) as part of the World Bank study "Enhancing the Climate Resilience of Africa's Infrastructure". The authors are grateful to David Groves and Zhimin Mao from RAND Institute and Brian Joyce from Stockholm Environment Institute (SEI) for generously sharing their climate data and WEAP model application for the case study, to Brent Boehlert from Industrial Economics for providing the downscaled climate model projections, and to Scott Steinscheineider for providing the model code for the stochastic weather generator used in the analysis. Please contact the corresponding author by e-mail to obtain the data used to produce the results of this paper.

CHAPTER 3

LINKING BELIEF INFORMATION TO ROBUSTNESS-BASED PLANNING: BAYESIAN NETWORKS DECISION SCALING (BNDS)

3.1. Abstract

The widespread recognition of a highly uncertain future due to the changes in climate, socioeconomic conditions, demographics and technology has resulted in an increased interest in risk-averse robustness-based frameworks for the long-term water planning. The common characteristic of these robustness-based frameworks is that they do not rely on a narrow range of impacts and vulnerabilities identified by model projections, but rather attempt to reduce vulnerabilities across a wide range of plausible future conditions. Decision scaling is an example of robustness-based frameworks that uses stochastic simulators to sample climate uncertainty by generating a wide range of futures with specified variability and mean statistics and then identifying and evaluating vulnerabilities with respect to stakeholder-defined performance thresholds. Climate projections are then used to in a quasi-Bayesian approach to identify the posterior likelihood of the vulnerabilities. This work presents an improved framework, in which a Bayesian network is used to explore multiple demographic and socioeconomic factors in addition to climate change uncertainties within the robustness-based framework. The proposed framework incorporates varied information types including expert judgments, demographic projections and subjective opinions elicited from stakeholder workshops to obtain a posterior joint probability distribution of system vulnerabilities. The Bayesian network framework provides the basis for representing the joint probabilistic behavior of uncertain factors, while the robustness framing is retained through the distinctive ex-post identification of vulnerability scenarios and application of

probabilities as sensitivity factors to aid decision making. The proposed framework, which we call as Bayesian Networks Decision Scaling (BNDS) is demonstrated for design of a new water supply system in the Coastal Province of Kenya.

3.2. Introduction

Long-term planning of water resources systems has become increasingly complex over recent years, facing compounding, deep uncertainties from climate variability and change, as well as from nonclimate factors including population growth, urbanization, living standards, and societal preferences (Hansman et al. 2006; Kwakkel and Walker 2010; Giordano 2012; Jeuland and Whittington 2014; Hall et al. 2015; Young and Hall 2015; Furlong et al. 2016). Realizing this complexity, a growing body of researchers have begun questioning whether the traditional techniques for the appraisal of water infrastructure projects, such as cost benefit analysis, cost efficiency analysis, multi-criteria assessment, are still adequate to meet the goals of the decision-makers (Fankhauser et al. 1999a; Lempert 2002; Ranger et al. 2013; Dittrich et al. 2016; Furlong et al. 2016). A fundamental input to these planning techniques is the prior assumptions on how the future may unfold over the course of the planning period, expressed as by way of probability distributions or a most-likely estimate of the future world (Hallegatte 2009; Jeuland and Whittington 2014; Hall et al. 2015; Maier et al. 2016). These assumptions about the future are then used within an expected utility framework to rank multiple planning options with respect to one or more objectives (Keeney et al. 1982; Dittrich et al. 2016; Furlong et al. 2016). Anthropogenic climate change complicates this process by altering many climate statistics, including rainfall patterns, frequency of storms, duration of heat waves and others (Strzepek et al. 2010; Shongwe et al. 2011; IPCC 2013a; Kunkel et al. 2013), and thereby reduces our ability to

identify one or few most-likely futures for decision analysis. This necessitates new, improved analytical approaches for planning under deep uncertainty, i.e., conditions where the possible range of future conditions or the prior probabilities of those conditions are highly subjective if not unknown (Lempert 2003; Walker et al. 2013).

A number of analytical frameworks have emerged over the past few decades to deal with deeply uncertain conditions, including (many-objective) robust decision making (RDM) (Lempert et al. 2006; Kasprzyk et al. 2013), info-gap theory (IGT) (Ben-Haim 2006), dynamic adaptive policy pathways (DAPP) (Haasnoot et al. 2013) and decision scaling (Brown et al. 2012). A distinguishing feature of these new frameworks is that they envision future through many possible states of the world (SOWs), without focusing on whether they are likely to occur (Maier et al. 2016). These frameworks then use simulation or optimization models to seek for planning alternatives that are robust, i.e. can function effectively over a wide range of possible SOWs (Herman et al. 2015). The way that robustness is operationalized changes from one framework to another, for example, in RDM and decision scaling, it is the ability to achieve low regret or satisfactory performance (Lempert and Collins 2007; Whateley et al. 2014); in IGT, it the distance from an expected future state before the system fails to perform adequately (Ben-Haim 2006); and in DAPP, it is a measure of flexibility to adapt to changing conditions over time (Haasnoot et al. 2013; Walker et al. 2013). However, independent of the framework being applied, a good representation of the uncertainty space through the SOWs is essential, to reveal the true range of vulnerabilities that may be faced in the future, including those associated with surprise conditions or so-called "Black Swans" (Taleb 2007).

An ongoing debate in the field of planning under deep uncertainty is how to make the best use of highly uncertain but potentially useful sources of information about the

future. Examples to these include downscaled Global Circulation Model (GCM) projections of future climate change, extrapolated trends from observed environmental conditions, expert elicitations or stakeholder opinions about future living standards and many others, which we will simply refer as "belief information" in this paper. There is now a large consensus on that belief information shall not be seen as "predictive scenario machines" to describe the plausible range of futures (Walker et al. 2013; Wise et al. 2014; Herman et al. 2015; Dittrich et al. 2016). Such use, often referred as "top-down" only spans a very narrow and potentially biased fraction of the true range of possible futures (Lempert 2003; Weaver et al. 2013), and results in a cascading pyramid of epistemic (knowledge-related) and/or stochastic uncertainties from one modeling step to another (Giorgi 2005; Wilby and Dessai 2010). An alternative to the top-down use of belief information is to employ them after the vulnerability analysis to assess the occurrence likelihood of future conditions. Decision scaling (Brown et al. 2012) demonstrates how climate information (e.g., GCM projections) can be used in this way. In brief, decision scaling uses stochastic weather generators to obtain a broad range of SOWs representing both natural climate variability and future climate change. Outcomes of those SOWs are then explored through simulation models in an attempt to reveal vulnerabilities or conditions that may lead to poor or unacceptable results. Climate information is incorporated after this phase, to assess whether those problematic climate conditions identified are likely to occur, and to rank the level of concern or priority for each vulnerability. This approach of linking climate information to robustness-based performance have been demonstrated over an increasing number of studies (Moody and Brown 2013; Turner et al. 2014; Steinschneider et al. 2015b). However, to date, incorporation of multiple beliefs, including climate and nonclimate information has

not been investigated. Our goal in this work is to develop a generalized probabilistic framework for improving the use of belief information in robustness-based planning.

Using multiple beliefs in the form of probabilistic information results in additional challenges over the baseline robustness-based planning framework. First, many types of social, economic, and environmental factors relevant for water planning decisions are not isolated, but rather conditionally dependent (Pahl-Wostl 2007a; Döll et al. 2014). Examples include climate or price elasticity of household water demand (Franczyk and Chang 2009; Schleich and Hillenbrand 2009), and effects of climate variability on regional economic development (Hurd et al. 2004; Brown et al. 2011a; Olmstead 2014), and climate change effects on land-use patterns (Syvitski 2003; Vörösmarty et al. 2003). To account for the co-dependencies, the beliefs about the probability distributions of those variables need to be expressed in conditional forms. However, this is difficult since the belief information about the variables are associated with different knowledge domains (such as hydrology, ecology, economics, public policy or others), and are available in many different forms (such as model-driven time-series data, point-estimate projections, qualitative survey results, or simply expert judgments). Thereby, establishing conditional probability distributions or blending those belief information to obtain a joint probability distribution of future conditions may be very difficult without a formal framework.

To address these points, we incorporate Bayesian network concepts to robustness-based planning. Bayesian networks (BNs), or Bayesian Belief Networks is a statistical modeling approach used for knowledge representation and reasoning across many fields from environmental science to medical research (Pearl 1988; Newton 2010; Aguilera et al. 2011). BNs provide a graphical network representation of a system of variables, in which the degree of belief on each variable is represented by conditional probability distributions. This

belief information is propagated based on the network structure for obtaining a posterior joint probability distribution of the system (Jensen and Nielsen 2007). From a water planning perspective, the use of BNs provides several well-established advantages. First, BNs are very flexible regarding data requirements and processing, allowing them to combine knowledge of different accuracies and sources in highly complex and multidisciplinary problems (Getoor et al. 2004). They can provide a transparent, participatory modeling interface, where information from multiple stakeholders or experts can be incorporated in the form of subjective beliefs or elicitations, and easily revised when needed (Kumar et al. 2008; Newton 2010; Kjaerulff and Anders 2013). They can handle situations where underlying data is missing or too sparse, through learning algorithms that iteratively provide maximum likelihood estimates of the parameters given the data and model structure (Uusitalo 2007). Finally, they can be easily incorporated to traditional decision analysis frameworks such as cost-benefit analysis (Lee et al. 2009; Åström et al. 2014), or used within dynamic contexts for making probabilistic inference over multiple time stages (Yet et al. 2016).

The use of BNs in water planning problems has a relatively long history and is still developing (Dawsey et al. 2006; Chan et al. 2010; Aguilera et al. 2011; Aller and Waller 2011). Kuikka and Varis (1997) shows one of the first applications of this kind by using expert knowledge to assess climate change effects on watershed level planning. Others used BNs for planning urban infrastructures (Noi and Nitivattananon 2015), irrigation systems (Batchelor and Cain 1999; Henriksen and Barlebo 2008), environmental flow allocations (Pollino et al. 2007; Stewart-Koster et al. 2010; Chan et al. 2012) or sea level rise adaptation (Catenacci et al. 2013) and flood risk reduction (Noi and Nitivattananon 2015). Some studies discuss the integration of BNs with other decision-analysis tools and modeling techniques in water planning or similar fields. Castelletti and Soncini-Sessa (2007) states that BNs can be

used to model an entire water resources system, or a specific component (e.g., hydrology, reservoir operations, water quality). They conclude that BNs can be particularly useful when there is no theory to support quantitative model formulations, in contrast to mechanistic models that quantify well-established theories about internal system processes. In this context, BNs have been integrated to rainfall-runoff (Dyer et al. 2014), groundwater (Martínez-Santos et al. 2010; Molina 2013), and water quality models (Mesbah et al. 2009). Aside from the coupling of BNs with mechanistic models, several studies show the use of BNs within decision support systems. Bertone et al. (2015) developed a risk assessment tool for managing the effects of extreme weather events, in which they use a BN to estimate the probability of meeting water quality targets, and a system dynamics model to assess the effectiveness of policy responses. Kocabas and (Dragicevic 2013) used a BN to obtain decision rules related to land-use management choices of individuals, which are then used in an agent-based modeling framework to simulate land-use dynamics. However, none of the past studies use BNs as part of a robust decision-making framework, in which, they are only used to provide probabilistic information about the future vulnerabilities.

Our framework, which we refer as "Bayesian Networks Decision Scaling" (BNDS) decouples the processes of vulnerability assessment from subjective inference. In our approach, we begin by generating a wide range of futures SOWs using efficient sampling techniques. Next, we reveal the vulnerability space over those SOWs to stakeholder-defined performance criteria through mechanistic system models. After this phase, we use a BN model for making probabilistic inference about the vulnerabilities identified through the use of multiple belief information. The outcome from the BN model is the posterior joint probability distribution function of future outcomes, which is then used for calculating and comparing the robustness of different planning alternatives. Uncertainty and disagreement

about future beliefs are addressed by the separation of vulnerability exploration, allowing the use of multiple and conflicting beliefs as a sensitivity factor. The remainder of this paper is structured accordingly. In Section 2, we provide a brief background on fundamental BN concepts. In Section 3, we describe the proposed framework in detail, with a focus on the linkages between vulnerability analysis and BN-based probabilistic inference. In Section 4, we illustrate the framework over a water supply design study in Mombasa, Kenya. Section 5 contains the results and the discussion of the case study application. Section 6 presents the conclusions.

3.3. Bayesian Networks

Stated simply, a BN is a multivariate statistical model that consists of a graphical network structure and a set of probability distributions corresponding to that structure (Figure 3.1). The graphical component of BNs, referred as a directed acyclic graph, is composed of nodes representing variables and arrows representing the direction of probabilistic relationships among those variables. The network structure is often defined based on the causal interpretation of the variables, although causality is not a strict requirement. BNs may consist of categorical (e.g., low, medium, high), Boolean (yes or no), discrete, continuous or mixed variables, with associated probability distributions simply referred as node probability tables (NPTs). A node is called as a child if it has an in-going arrow, and as a parent, if it has an outgoing arrow. The root nodes, which do not have any parents, are associated with marginal probability distributions that represent prior knowledge on those variables. All non-root nodes are associated with conditional probability distributions, specifying the probability of a variable taking a value given the values of its parent nodes.

A fundamental feature of BNs is the conditional independence or the absence of a connecting arrow between any two nodes. Conditional independence simplifies the modeling process by allowing NPTs to be generated "locally" that is by only considering the immediate parent nodes of the node being quantified (Kjaerulff and Anders 2013). Based on this property, the joint probability distribution of a BN with *n* discrete random variables $V = \{X_1, \ldots, X_N\}$, can be expressed using the chain rule as the product of local probability distributions:

$$P(V) = \prod_{i}^{n} P(x_i | \, pa(X_i))$$

Equation 3.1

where $pa(X_i)$ defines the parent nodes of X_i; and $P(x_i | \, pa(X_i)$ is the conditional probability of X_i given the values of its parent nodes. Once the network structure is generated, belief updating can be performed using Bayes rule (3.2), by obtaining the posterior probabilities of the nodes in the network when values of one or more nodes are observed and entered as evidence:

$$P(X|e) \; \propto P(e|X)P(X)$$

Equation 3.2

where, $P(X)$ is the prior knowledge about the variable X, $P(e|X)$ is the likelihood information on X given the evidence e, and $P(X|e)$ is the posterior probability distribution. In 3.2, e may represent hard evidence specifying a definite finding of the uncertain variable, or soft evidence specifying a new probability distribution of the random variable. In the case of hard evidence, belief updating may be implemented by instantiation of the variable X to

its finding x_i, so that $P(X = x_i) = 1$, whereas, in the latter case of soft evidence, the prior probability distribution of X can be directly replaced by the new soft evidence, $R(X)$. Belief updating with soft evidence is more relevant in the context of long-term water planning, as information about the future conditions never indicates a certainty, but rather (optimistically) a better belief about how the future conditions may unfold.

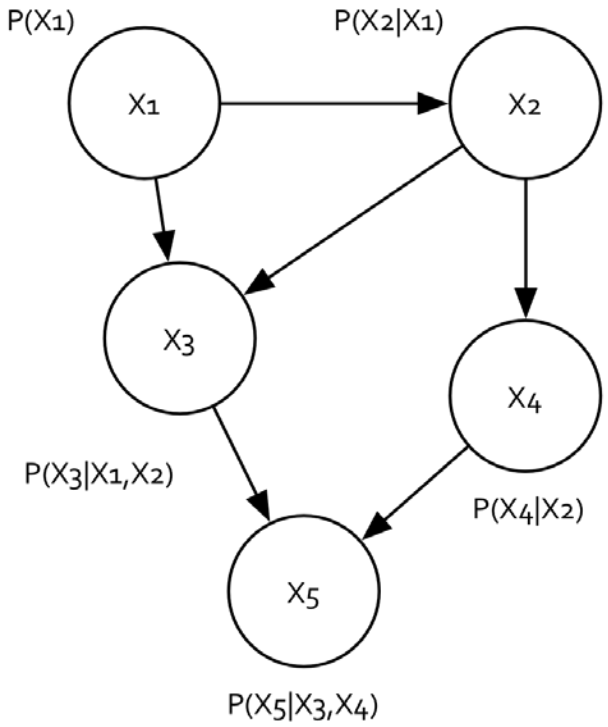

Figure 3.1 Conceptual representation of a Bayesian network with five nodes

3.4. Bayesian Networks Decision Scaling (BNDS)

The proposed framework consists of three phases: problem definition, vulnerability analysis, and bottom-up inference respectively (Figure 3.2). The process begins with a typical stakeholder-driven process to define the main planning problem, including the planning objectives and problem statement, decision alternatives, performance measures and criteria, and major uncertainties. Since this is the first step in most analytical planning frameworks,

readers can refer to other sources for details (Castelletti and Soncini-Sessa 2006; Black et al. 2014). The second phase of vulnerability analysis uses simulation-based mechanistic models to reveal the domain of conditions that result in poor or unacceptable performance under each decision alternative. In the third phase of bottom-up inference, a BN is used to evaluate the occurrence likelihoods of the vulnerabilities identified. Finally, the revealed vulnerabilities and their occurrence likelihoods are summarized for each decision alternative for a risk-based robustness analysis. On Figure 3.2, of particular note is the integration of the second and third phases through a BN model, defined over the same pre-generated set of SOWs. The components and steps in the second and third phases are discussed in more detail below, while an application of the entire framework is presented for the case study in Section 3.4.

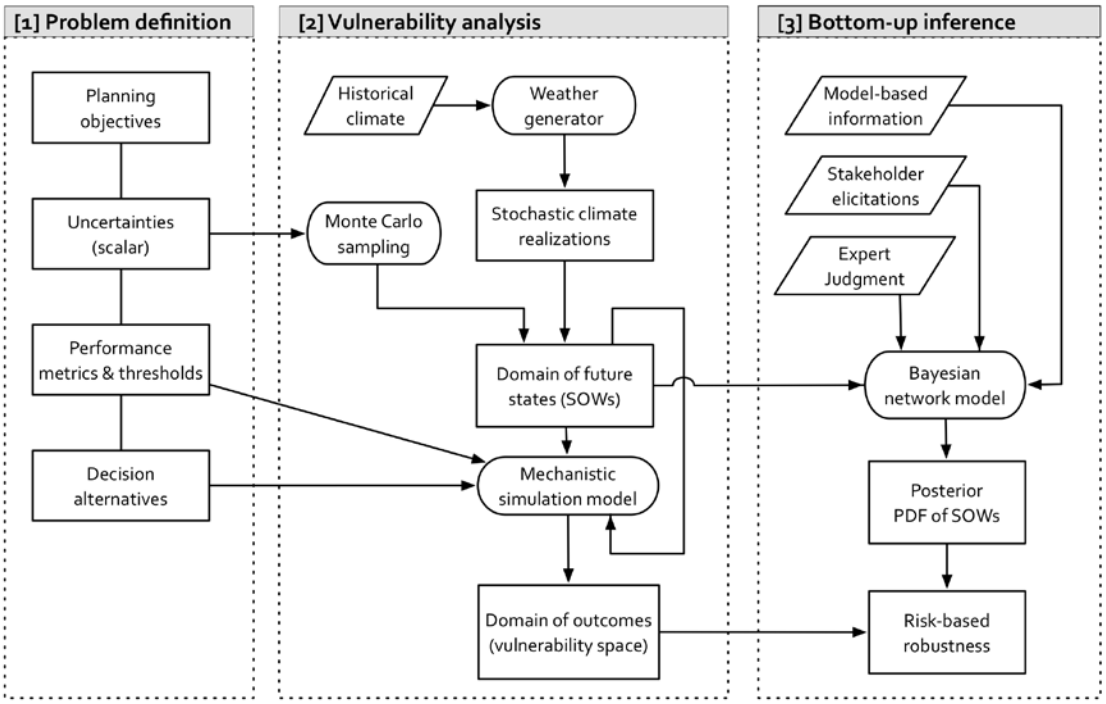

Figure 3.2 Conceptual flow chart of Bayesian Networks Decision Scaling (BNDS) representing the three main phases. On the flow chart, rectangles show main processes, squashed rectangles show various models, and parallelograms represent information inputs.

3.4.1. Vulnerability analysis

Vulnerability analysis begins with the process of generating a sufficiently large size of SOWs for providing a good coverage of conditions that may occur, given by the set $\Omega = \{\theta_1, \ldots, \theta_n\}$. In this process, a SOW is a particular realization of m factors $\{X_1,.., X_m\}$ that represent key uncertainties related to the planning problem. These factors can be determined through stakeholder workshops and may include first-order or higher-order statistics of climate variables such as mean, variance, skewness, etc., and natural climate variability, life span of the civil works, construction delays, operating and maintenance costs, the economic value of the services provided by the infrastructure or similar. The domain of SOWs is generated by stochastic sampling algorithms based on the nature of the uncertain factor - whether if it represents a scalar or a time-series data, such as historical climate variability (Figure 3.2). The samples of scalar variables are generated by Latin Hypercube Sampling (LHS), an efficient stratified Monte Carlo algorithm for higher dimensional data (McKay et al. 1979). Briefly, LHS is applied by first discretizing each factor into *n* equal intervals, and then randomly selecting an interval from each factor without replacement. Samples of historical variability are generated by a stochastic weather generator that generates new random climate sequences while preserving observed climate statistics such as mean, variance or low-frequency variability (Steinschneider and Brown 2013).

The outcomes under each planning alternative d_k and future state θ_i are then explored using mechanistic simulation models (such as hydrology, water system operations, ecosystem, etc.), resulting in output $\{y_{i,k}, \theta_i\}$ (Figure 3.2). Simulated performance can be then expressed regarding stakeholder-based vulnerabilities by transforming $y_{i,k}$ into a binary variable for distinguishing acceptable (satisfactory) and not acceptable (failing) performances (Whateley et al. 2014). This process, also called as a multidimensional stress test, aims to find

the factors that the system is most sensitive to and reveal the range of conditions associated with poor or failing performances. At this stage, note that no probabilistic inference is made on the vulnerabilities, i.e., whether those underlying conditions are likely or not likely to occur.

3.4.2. Bottom-up inference

The purpose of this phase is to place a posterior PDF over the vulnerability space to identify and prioritize underlying conditions that are more likely to occur than others. This posterior PDF, $P(Y)$ is obtained from a BN model describing the knowledge domain of planning problem (Figure 3.2). The BN model includes m random nodes representing all climate and non-climate variables used in the vulnerability analysis (X_1,.., X_m}. Also, each of these nodes is discretized into *n* intervals consistent with the LHS scheme (Section 3.1). This consistency allows BN model to propagate a posterior probability value for every SOW, i.e., $P(\theta_i) = P(X_{1,i},.., X_{m,i}), i = 1, \dots n$. Note that the relationship between a future state θ_i and its outcome contingent on a planning alternative d_k, $f(y_{i,k}, \theta_i)$ is obtained from the integrated mechanistic models, P($y_{i,k}$) = P(θ_i). Thereby, the joint probability distribution $P(Y)$ obtained from the BN can be directly linked to the vulnerability space.

One of the main challenges in BN development is populating the NPT of each variable. Possible sources of information to generate NPTs typically include empirical evidence or data, outputs of empirical or mechanistic models, expert knowledge or stakeholder consultations (Aller and Waller 2011). In the context of water planning, many examples are demonstrating how NPTs can be generated from observed data and expert knowledge (Batchelor and Cain 1999), from stakeholder workshops or one on one interviews (Borsuk et al. 2001; Richards et al. 2013). When multiple belief information about

a single variable exists, this information can be combined through linear information pools (O'Hagan et al. 2006). Learning algorithms can also be used to encode data or expertise into NPTs for problems with complex node-link networks such as NoisyOR (Fenton et al. 2006) or Expectation Maximization (Uusitalo 2007). For this work, we use a relatively simple, two-step approach for NPT generation. First, for each variable, we define a truncated Gaussian distribution, $P(X_i) \sim TNORM(\mu, \sigma^2, a, b)$, in which the parameters mean μ, standard deviation σ^2, and the lower/upper bounds a, b are obtained or extracted from belief information. This distribution is then used to obtain the normalized probability weights for each of the n discrete variable intervals. For the non-root nodes, we define selected parameters conditional on their parent node values, e.g., $P(X_j) \sim TNORM(\mu = f(pa(X_j), \sigma^2 = g(pa(X_j)), a, b)$.

Using BN, the bottom-up inference is made by propagating the joint probability weight of each future state $P(\theta_i), i = 1, \dots n$ by the chain rule (Equation 3.1). Note that the process described here does not sample future states or vulnerabilities, but only seeks how plausible those vulnerable conditions are. Thereby, it does not raise the risk of overlooking vulnerabilities that were believed, a priori, to be unlikely. The results from bottom-up inference only play a role in defining the risks, which is traditionally defined as the product of an outcome and its occurrence likelihood. This type of use of BNs is different than the common use of BNs, where BNs are used to describe the entire set of relationships in the system. One side benefit of our approach is that the BN model, in this case, does not require rigorous model validation since it does not attempt to replace results given by mechanistic models.

3.5. Application of the BNDS framework

3.5.1. Description of study

This work focuses on the engineering design of the Mwache Dam located in Mombasa located about 22 km away from Mombasa in the Coastal Province of Kenya (Figure 3.3). Upon completion, the Mwache Dam is expected to provide an additional supply of about 80 Mm^3 per year to the region, of which 80% will be used for augmenting Mombasa's domestic supply. The remaining supply will be used to support irrigated agriculture in Kwale County and maintaining ecosystem health downstream of the reservoir. Estimated water deficits in the greater Mombasa region correspond to as high as 60% of the total demand of 130 Mm^3 per year, which is expected to increase with socioeconomic growth (Tahal 2013). The Mwache River is the only stream feeding into the proposed dam, with a catchment area of about 2,250 square kilometers.

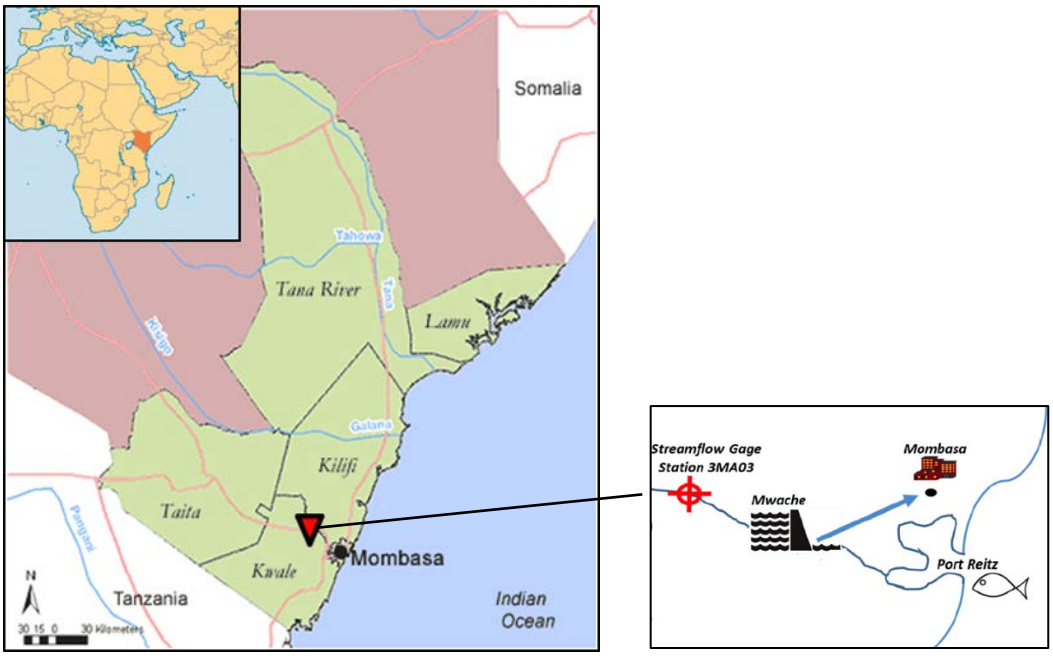

Figure 3.3 Coastal Kenya and the site of the proposed Mwache Dam

The analysis consists of assessing the robustness of four design capacity alternatives, with gross volumes of 80, 100, 120, and 140 Mm^3. Estimated present value costs of those alternatives are 75, 89, 100, and 109 M USD respectively (Groves et al., 2015). Before the analysis, a project inception workshop was performed in August 2015, to define the main features of the study, including the planning objectives, performance metrics, and key uncertainties are defined during the project inception workshop. The inception workshop brought together a diverse group of stakeholders from the Water Resources Management Authority, Coastal Water Services Board, Coastal County representatives, and local academic institutions. Based on this workshop, the target population for the reservoir is limited to Mombasa's Mvita, Kauni, and Changwamwe districts, with an estimated demand level of about 38 Mm^3 per year in 2015, which is expected to increase to 65-105 Mm^3 in the year 2035. Water infrastructure performance is expressed based on the metrics of volumetric reliability and NPV of the project. Volumetric reliability metric is defined as the volume of water supplied divided by the total target demand over the analysis period (Hashimoto et al. 1982). The latter metric of NPV is obtained from the sum of discounted benefits from the project minus the capital investments costs. For the evaluation, the project lifetime is assumed to be 50 years.

The key climate and nonclimate uncertainties for the project were determined during the project inception workshop. These include natural variability of the climate, gradual changes in mean annual temperature (°C) and precipitation (%) due to climate change, specific sediment yield* (m^3 per km^2 - year), annual water demand for municipal and

* Amount of sediment deposited in the reservoir normalized by the upstream area contributing sediment.

industrial use (Mm^3 per year), the price charged for municipal and industrial water use (USD per m^3), and the annual discount rate (%) respectively (Table 3.1).

Table 3.1 Key uncertainties of the robustness assessment of the Mwache Dam

Uncertain factor	Short name	Range
Natural climate variability	Nvar	New climate sequences conditioned on the observed meteorological data (1950-1999)
Change in long-term mean temperature	ΔTemp	No change to 5°C increase over the historical mean value (27 °C)
Change in long-term mean precipitation	ΔPrecip	50% decrease to 50% increase over the historical mean value (845 mm)
Annual demand for municipal and industrial use	Demand	60 to 100 Mm^3 per year
Specific sediment yield	SSY	150 to 600 m^3 per km^2- year
Price charged for municipal and industrial water use	Price	0.6 to 2.0 USD per m^3
Annual discount rate	DRate	2 to 10%

3.5.2. Data

Historical monthly climate data, including precipitation and maximum, minimum and mean temperatures were gathered from the Princeton University Terrestrial Hydrology Research Group's gridded meteorological data set from 1950 to 1999 (Sheffield et al. 2006). Based on this data, observed annual rainfall showed a marked variability between 1950 and 1999, ranging from 400 to 1600 mm, with a value of 845 mm on average. Rainfall patterns also show the effects of monsoon's, with 'long-rains' from March to May and 'short rains' from October to December that together correspond to about 70% of the annual rainfall. This variability in the observed rainfall can be attributed to the influence of the Inter-Tropical Convergence Zone (ITCZ) (Vetter et al. 2015).

Historical monthly stream flow data for the Mwache River was gathered from an existing monitoring study, which was available for near the proposed dam site and for a relatively short period of 1978-1990 (Tahal 2013). Observed streamflow during this period ranged from 5.4 to 18 Mm^3 per month with an average value of 10.4 Mm^3. Climate change projections over the region of the project site were obtained from the from the World Climate Research Programme Coupled Model Intercomparison Project Phase 5 (CMIP5) ensemble (Taylor et al. 2012). Land-cover information and associated specific sediment rates for the Mwache Dam's catchment was obtained from the Sediment management strategy study conducted by CES (2014). Volumetric water charges set by Kenya's Coastal Water Services Board are obtained from The Kenya Gazette (2012).

3.5.3. Vulnerability analysis of the proposed Mwache water supply

The analysis began with generating $n = 1{,}000$ SOWs spanning the range of uncertainty over the six key uncertainties (Table 3.1). The samples of natural climate variability were obtained from a stochastic weather generator of first order wavelet autoregressive model type (Steinschneider and Brown 2013). Using the weather generator, $n = 1{,}000$ 50-year monthly mean precipitation and monthly minimum, mean, and maximum temperature sequences are generated that match historical mean, variance, low-frequency precipitation variability of the observed historical period (1950-1999). Samples of the other factors besides natural variability was generated using LHS. To eliminate any potential correlations among the sampled factors, the sample matrix was reordered by the Huntington and Lyrintzist (1998) algorithm. Next, sampled natural variability realizations and mean climate changes were combined to obtain n transient climate trajectories. This is done by reflecting in each temperature change factor over the associated natural variability

sequence as an additive factor that starts from 0°C and linearly increases to the specified value (e.g., 3°C) at the end of the simulation period. Similarly, each precipitation change value was reflected in the associated natural sequence as a multiplicative factor that starts from 100% and linearly increases (or decreases) to the specified value in the final period. Overall, the process results in 1,000 unique SOWs describing a wide range of climate and socio-economic conditions.

Vulnerability analysis is then conducted by simulating water system operations under each SOW. Monthly streamflow response and reservoir operations for each design alternative were simulated through a coupled hydrology – water system operations model developed in R (See Appendix A). The outputs from the coupled simulation model were then summarized by the stakeholder-defined metrics of volumetric reliability and NPV respectively. Due to the relatively small magnitude of difference in results, calculated NPV values were transformed to regret. Regret is calculated as the difference in outcome between the best possible decision under a given state $NPV(d^*, \theta_i)$ and the decision that was made $NPV(d, \theta_i)$:

$$regret(d, \theta_i) = NPV(d^*, \theta_i) - NPV(d, \theta_i)$$

Equation 3.3

Next, most important factors to each metric are determined through a global sensitivity analysis. For this purpose, we used the Partial Rank Correlation Coefficient (PRCC), which quantifies the monotonic interactions between the model response and an input factor, after discounting the effects of all other input factors (Marino et al. 2008).

Finally, we transformed system performances into binary variables that express stakeholder-defined vulnerabilities. This is done by classifying the results either as acceptable

or unacceptable based on performance targets specified by the project stakeholders. For volumetric reliability, the acceptable level is greater than equal to 95% based on stakeholder preference. Therefore the system performance is accepted to be satisfactory over this threshold and insufficient or not acceptable below this threshold. Regarding NPV, an outcome is defined to be acceptable when the computed regret is less than or equal to 10 M USD, and not acceptable when greater.

3.5.4. Bottom-up inference through BN model

At this phase, we incorporate belief information about the future climate and nonclimate conditions to find the occurrence likelihoods of the vulnerabilities identified in Section 4.3. For this purpose, we developed a BN model and then used this model for propagating a posterior joint probability distribution.

The BN of the Mwache water supply planning problem consists of eight random nodes (Figure 3.4-b). The root nodes of the BN, which are natural climate variability (NVar), mean climate changes (MeanCC), target population level (Pop), economic development level (Dev), price charged for municipal water use (Price), and economic discount rate (DRate) are the main entry points for belief information. The BN includes two intermediate nodes of specific sediment yield (SSY) and per capita municipal water demand (PCD) that are represented by conditional probability distributions.

Within the BN (Figure 3.4), all random nodes except for population and economic development are discretized into n equal intervals in agreement with the LHS scheme applied in vulnerability analysis (Section 3.4.3). Population node is represented by three discrete levels, corresponding to values of 1.6 M (low), 2 M (medium), and 3 M (high), that span the range of population projections by Coastal Kenya's Water Resources Management

Authority in the year 2035 (CES 2014). The economic development node (Dev) also has three categorical levels (low, medium, and high) to indicate a qualitative belief on future socio-economic growth over the course of project lifetime.

The NPTs for the intermediate nodes (SSY and PCD) are defined through truncated Gaussian distributions, in which the parameters μ and σ^2 are expressed as functions of their parental combinations. The probability distribution of SSY is assumed to be conditional on future economic development through land-use practices based on previous studies conducted by CES (2014). Based on the historical studies carried out at catchment level, it is assumed that a higher economic development will result in more urbanization, which in turn will increase SSY at the upstream of the project site (see Appendix B). The conditional relationship $P(SSY|Dev)$ is given by:

$$TNORM(\mu,\ \sigma^2 = \mu/3, a =\ 200, b = 600)$$

Equation 3.4

where μ gets the values of 275, 325, and 35 m3 per km2 – year under low, medium, and high economic development respectively. In a similar way, the probability distribution of PCD is defined to be conditionally on three factors: economic development, the price charged for municipal water use, and mean annual temperature. For the Coastal Kenya region, it is assumed a higher per capita demand is more likely under higher economic development. Besides, increasing mean annual temperatures is assumed to increase per capita water demand, whereas increasing water pricing will decrease. The conditional distribution $P(PCD|Dev, \text{MeanCC}, Price)$ is given by:

$$TNORM(\mu = f(Dev, MeanCC, Price), \sigma^2 = \mu/4, a = 85, b = 150)$$

Equation 3.5

where, $f(Dev, \text{MeanCC}, Price)$ is a function that gives the mean of the distribution.

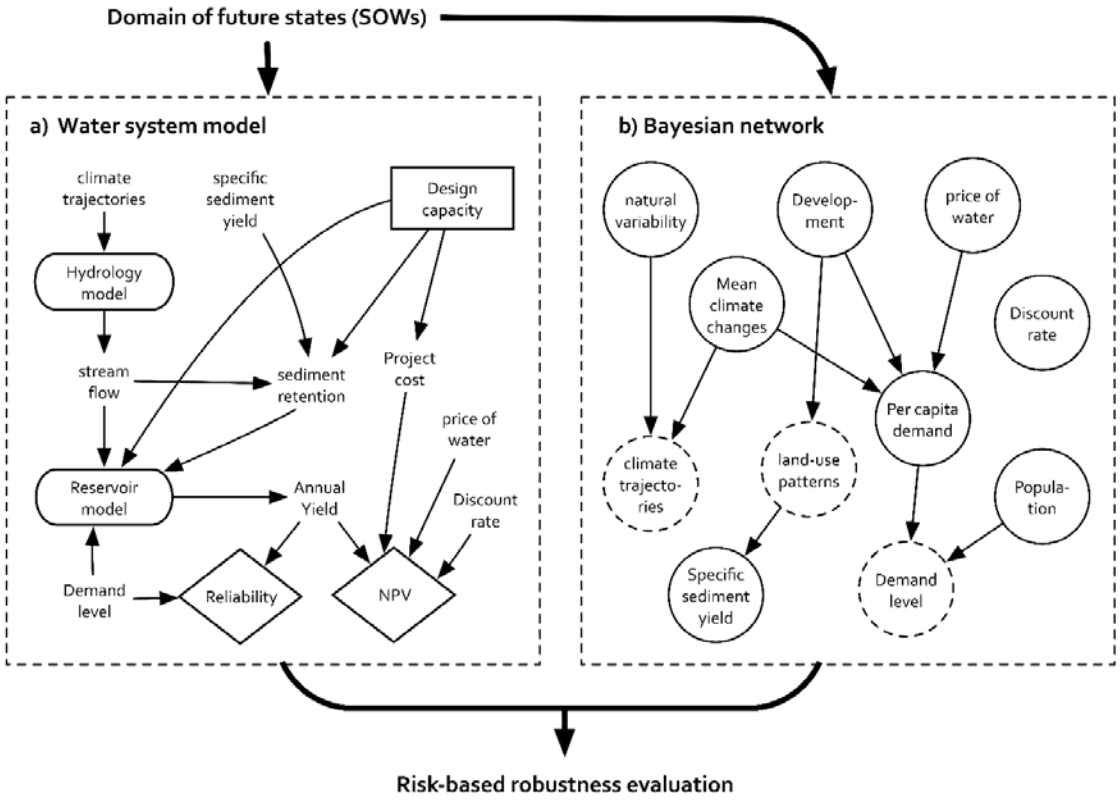

Figure 3.4 Illustration of the models used in the robustness analysis of the Mwache system: a) water resources simulation models used for vulnerability assessment; b) Bayesian network used for probabilistic inference. On Figure a (on the left), rectangles, rounded rectangles, and diamonds represent decision variables, mechanistic modeling processes and output performance (utility) respectively. On Figure b (on the right), solid circles represent chance nodes with probability distribution tables. Dashed circles represent deterministic nodes

Using the BN model, the bottom-up inference is conducted by updating the prior probabilities of the root nodes with belief information, and then calculating the joint probability distribution of the network over n = 1000 SOWs. For the natural climate variability node, a uniform discrete probability distribution is used since each climate variability realization is a new random sequence of the historical data.

The probability distribution of mean climate changes is set based on climate statistics from downscaled multi-model GCM projections. For this process, we used the data from the CMIP5 multi-model ensemble from a total of 65 model runs and calculated mean climate changes between the future period of 2020-2070 and the historical period of 1950-200. Computed mean changes were then fitted to a bivariate normal distribution:

$$P(MeanCC) \sim f(\Delta Temp, \Delta Precip) = \frac{1}{(2\pi)^{k/2}|\Sigma|^{1/2}} exp[-\frac{1}{2}(X-\mu)^T \Sigma^{-1}(X-\mu)]$$

Equation 3.6

where, μ is the means, and Σ is the covariance matrix of the mean annual temperature (°C) and precipitation changes (%) respectively (Figure 3.5). The belief information on economic development, population, discount rate, and price were set based on stakeholder opinion and best expert judgment. For development (Figure 3.5-b),t and population (Figure 3.5-c) the highest probability weights were given to medium levels, whereas for discount rate (Figure 3.5-d) and price of water (Figure 3.5-e), most likely values are set to be as 2% and 1.3 m^3 per USD respectively.

Using the BN, the posterior joint probability weight of each SOW is calculated from the chain rule and then normalized so that their sum equals to 1. This process is repeated for each engineering-design alternative to obtaining the probability mass function of the vulnerabilities under each case.

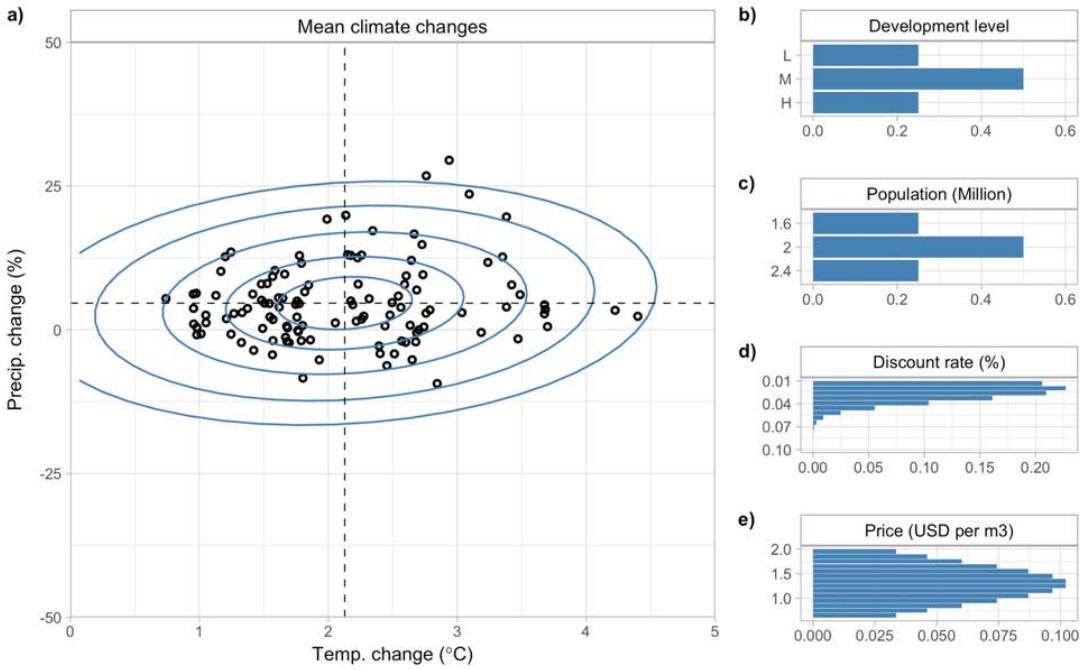

Figure 3.5 Prior probability distributions used for representing belief information in the BN model: a) mean climate changes, b) development, c) population, d) Discount rate, e) Price. On Figure a, the contour lines show levels of equal probability weights obtained by fitting CMIP5 data-points (shown by black dots) to a multivariate Gaussian distribution. The intersection of the dashed lines shows the mean value of the distribution.

3.5.5. Risk-based evaluation of the design alternatives

Finally, the posterior probability weights obtained from the BN model is used for a risk-based preference ranking of the alternatives. This is done by first weighing the binary performances with its associated probability weight, and then summing the outcomes to find the overall robustness score. The resulting robustness score has a scale from 0 to 1, in which 1 represents the ideal case with no failure risk, whereas a score of 0 maximum risk.

3.6. Results and Discussion

3.6.1. Performance sensitivity to uncertain factors

Figure 3.6 shows the relative importance of the uncertain factors based on the computed Partial Rank Correlation Coefficient (PRCC) values. Both reliability (Figure 3.6 -a) and NPV (Figure 3.6-b) are sensitive to only a fraction of the input factors. For reliability, the most important factors are precipitation change (> |0.85|) and demand level (> |0.6|), and to a lesser extent sediment flux rate (> |0.10|). In the case of NPV (Figure 3.6 -b), price and discount rate (both >| 0.95|) appears as the most important factors followed by precipitation (> |0.25|). The variation in the sensitivity analysis results on design capacity is negligible; all designs exhibit the sensitivity to the same factors and in the same fraction. The only exception for this is the sensitivity of reliability concerning demand level, for which estimated PRCC values ranged from 0.6 to 0.76, with greater sensitivity under smaller design capacities, i.e., 80 or 100 Mm^3 (Figure 3.6-a).

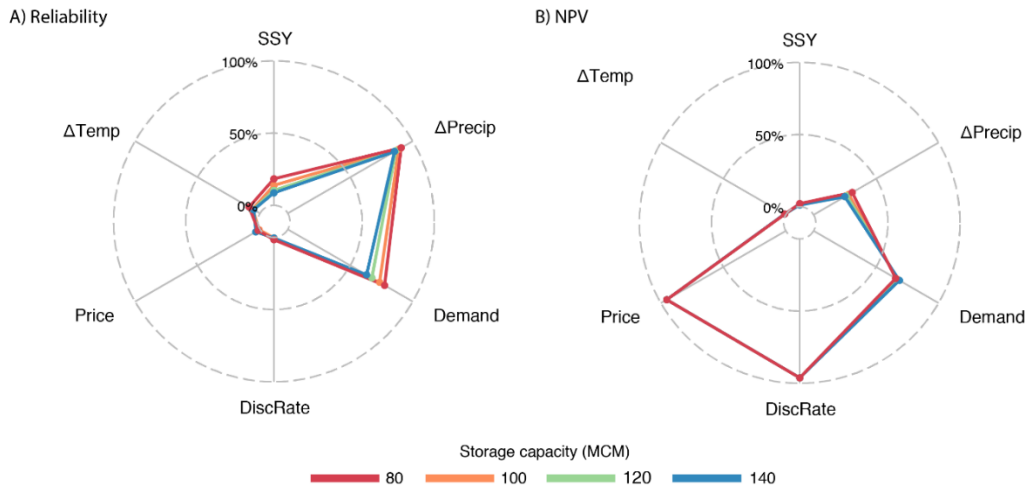

Figure 3.6 Global sensitivity analyses for the metrics of a) Reliability (%), b) Net Present Value (NPV) (%) respectively. Results indicate absolute values of the computed Partial Rank Correlation Coefficients (PRCC).

3.6.2. Preference with respect to vulnerabilities

The next step is to use multivariate visual analytics to explore the causes of vulnerable conditions. Common data patterns in the multivariate input data were revealed using Sankey (alluvial) diagrams. This was done by dividing the uncertainty range of each variable into few meaningful categories, and then binning the results from n = 1,000 data points accordingly. The binned results were then visualized through a set of alluvia, in which the thickness indicates the number of data points in each alluvium. Figure 3.7 shows the Sankey diagram depicts the relationship between reliability and the input variables of annual mean precipitation change, annual demand, and specific sediment yield for the selected design capacities of 80 Mm^3 (a) and 140 Mm^3 (b) respectively.

For the design alternative of 80 Mm^3 (Figure 3.7-a), it is seen that about 48% of all runs resulted in a reliability value of less than 95%, in which most of these runs are associated with low precipitation conditions (35%). Also, two major alluvium containing almost half of all failure runs (17%) are related to low precipitation (50 to 90%) and high demand level (80 to 100 Mm^3 /year) (Figure 3.7-a).

For the design capacity of 140 Mm^3 (Figure 3.7-b), unacceptable reliability outcomes represent 31% of all cases, of which 28% is associated with lower than normal future precipitation. Figure 3.7-b showed that a vast fraction of the failures is associated with lower than normal precipitation conditions (25%) and to a lesser extent with high demand conditions (21%) (Figure 3.7-b).

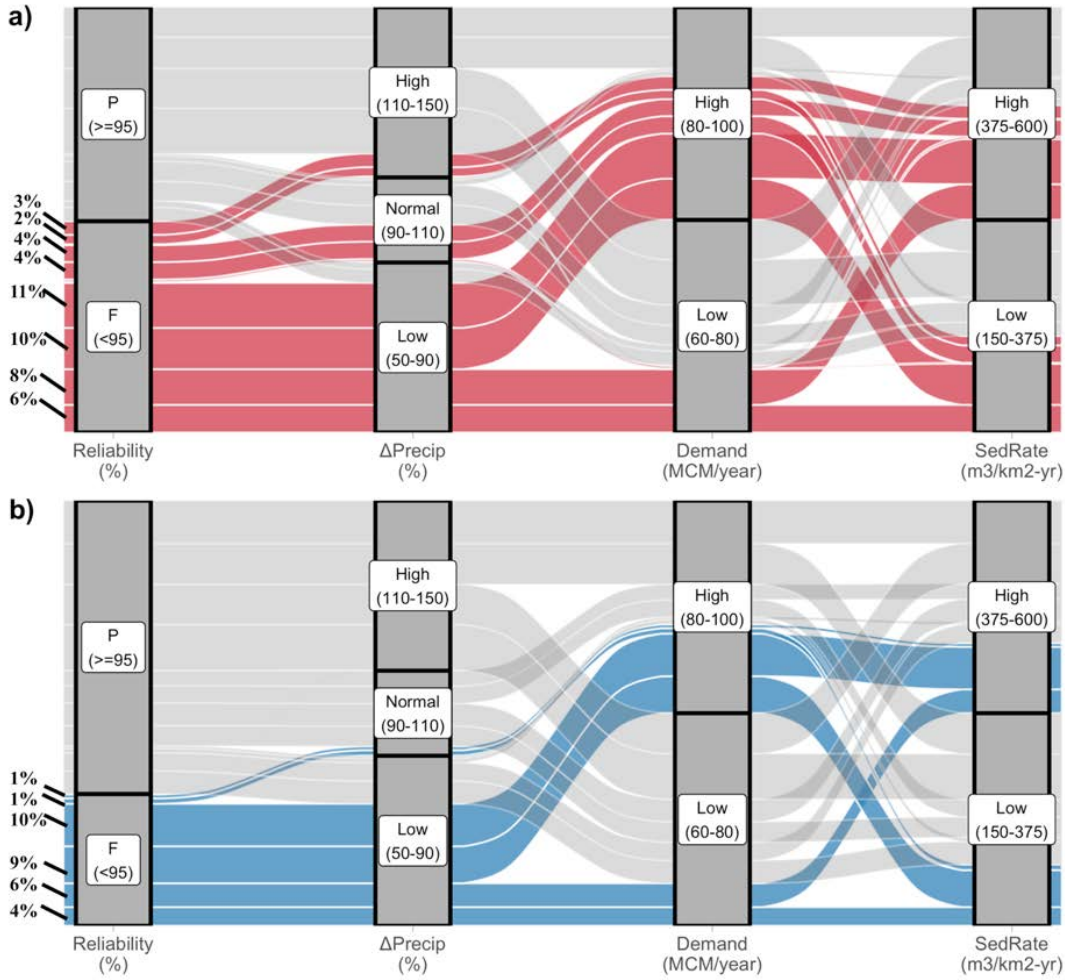

Figure 3.7 Sankey diagrams depicting vulnerabilities concerning the reliability metric for the design capacities of (a) 80 Mm^3, and b) 140 Mm^3 respectively. The results are shown by alluvia spanning across all the axes and indicated bins. Alluvia in red and blue represent outcomes that fail to meet the desired reliability threshold (95%). Alluvia thickness increase with the number of observations in each category. Values indicated on the left of the plots depicts the fraction of failing data points in each alluvium over all data points.

Figure 3.8 depicts vulnerability trade-offs concerning the reliability and NPV-regret metrics. On Figure 3.8, it is seen that the smaller alternatives (80 and 100 Mm^3) result in no or low NPV-regret over a large fraction of futures, meanwhile exhibiting relatively very high regret values (>100 M.USD) over a small number of futures. For the larger design sizes of 120 and 140 Mm^3, the NPV-regret values are more clustered within the 5-25 M.USD range. The relationship between reliability and design capacity size is more monotonic, as larger

alternatives always outperform the smaller (Figure 3.8). Figure 3.8-b summarizes the vulnerability of the design options with respect to the critical performance thresholds set for each metric. The summary figure shows that the preference ranking is from the smallest to largest (80 Mm^3 to 140 Mm^3) with respect to NPV-regret, whereas largest to smallest for reliability.

Note that the results considered in this section assess vulnerability over a wide range of SOWs generated through stochastic sampling, including conditions that are extremely less likely to happen. Thereby the occurrence likelihoods of the impacts need to be also considered to explore the plausible risks which will be discussed in the following section.

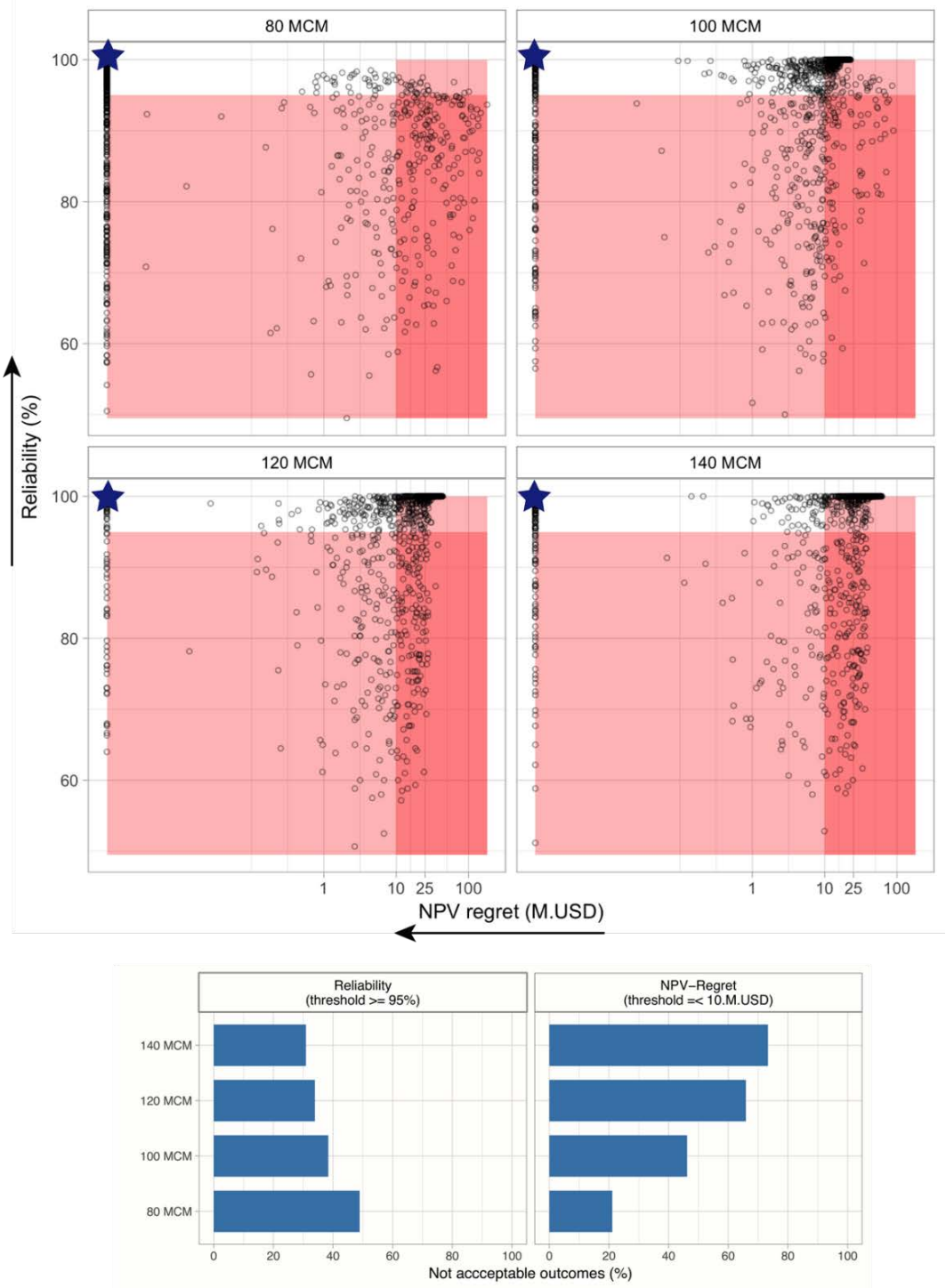

Figure 3.8 Vulnerability analysis of design alternatives: a) Individual results under each design alternative with respect to NPV-regret (x-axes) and reliability (y-axes), b) Summary statistics indicating the percentage of not acceptable outcomes under each metric. On Figure a, arrows indicate the direction of preference for each metric. The star symbol indicates the ideal solution. The shaded regions represent not acceptable conditions (e.g., when performance criteria are not met).

3.6.3. Design preferences with respect to risks

The results in this section consider future risks of alternative by weighting the identified range of vulnerabilities with the associated joint occurrence likelihoods obtained from the BN model. Figure 9 shows a variation of Sankey diagrams (Figure 7), in which time the thickness of each alluvium is scaled based on the underlying cumulative density of the data points. When occurrence likelihoods are considered, the relative importance of unacceptable futures is slightly less for the design size of 80 Mm^3 (Figure 9-a), and substantially less for 140 Mm^3 (Figure 9 -b). Note that in Figure 9, the low precipitation bin (50-90%) that is associated with most the failure outcomes has a very small value of marginal probability, reflecting the effects of GCM-driven belief information about the future climate.

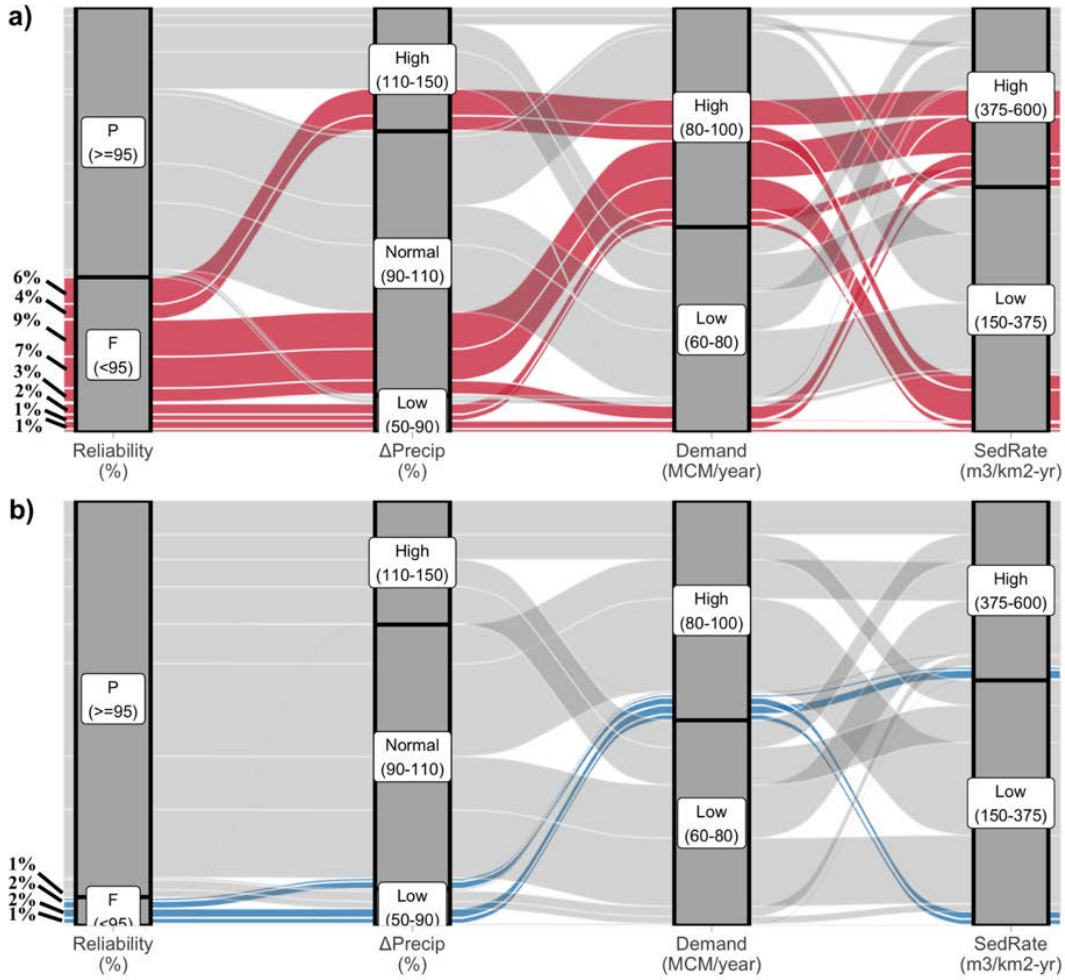

Figure 3.9 Sankey diagrams depicting the weighted vulnerabilities with respect to the reliability metric for the design capacities of (a) 80 Mm^3, and b) 140 Mm^3 respectively. The results are shown by alluvia spanning across all the axes and indicated bins. Alluvia in red and blue colors represent outcomes that fail to meet the desired reliability threshold (95%). Alluvia thickness increase with the cumulative likelihood of the data points. Values indicated on the left of the plots depicts the cumulative probability of each alluvium.

Finally, Figure 3.10 depicts the robustness trade-offs among the four engineering design alternatives under two distinct probabilistic assumptions: a) under uniform weighting, i.e., without the BN-based posterior distribution assigned to SOWs reflecting available information and b) weighting based on the posterior joint likelihoods obtained from the BN model. This represents a comparison of alternative beliefs about future conditions, one noninformative and one using available information and expert opinion. Under both

weighting schemes, robustness with respect to reliability increases with increasing storage capacity, with the most robust option being 140 Mm^3 with a robustness values 0.7 under uniform weighting (Figure 3.10-left panel), and 0.92 under posterior weighting (Figure 3.10-right panel). In contrast, smaller design alternatives are preferable with respect to the robustness of NPV-regret, with the smallest design size (80 Mm^3) giving an RS value of 0.8 under uniform weighting (Figure 3.10-left panel), and 0.55 (Figure 3.10-right panel) respectively. This implies that the weighting scheme did not affect the preference ranking, however, changed the scaling. Under uniform weighting, NPV-regret range substantially wider (0.2 – 0.8), compared to the robustness values under posterior weighting (0.4 to 0.6).

Overall, as two decision-criteria points the two extreme design choices (i.e., 140 Mm^3 with respect to reliability, and 80 Mm^3 with respect to NPV-regret), the final judgment can be made based on the trade-offs curves on Figure 3.10, depending on the relative importance of each criterion. However, based on Figure 3.10, one can argue the larger design alternatives (120 or 140 Mm^3) are more favorable under the posterior scheme due to the "flatness" of the trade-off curve. That is, with only a marginal loss in economic robustness (about 0.1 units), reliability robustness can be increased up to 0.3 units.

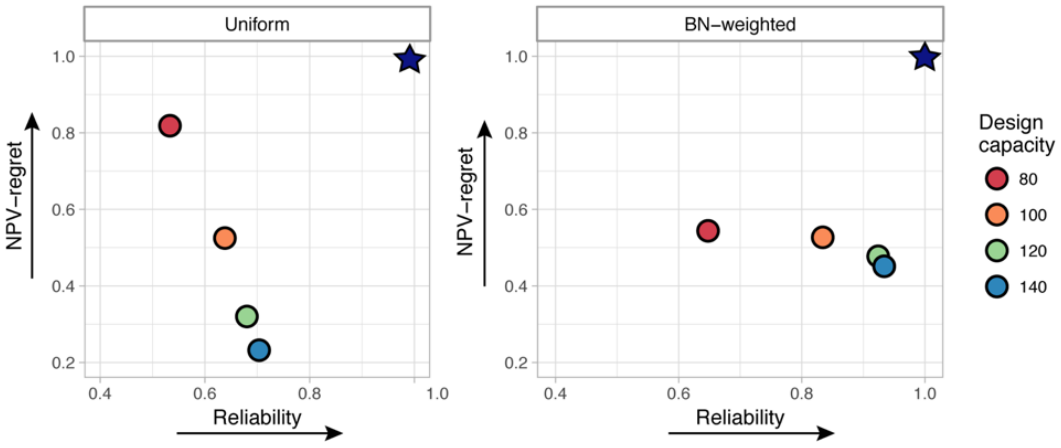

Figure 3.10 Robustness of the design alternatives under uniform likelihood (left), and under posterior probabilities calculated from the BN-model model (right)

3.6.4. Design preferences under climate uncertainty

To evaluate the robustness of the alternatives further, an additional analysis was conducted by only taking into account climate uncertainties, i.e., natural climate variability and mean annual temperature and precipitation changes. To do this, all non-climate factors were set to their most likely estimates, in which the price is 1.3 USD per m^3, annual demand level is 80 Mm^3, and the discount rate is 2%, and specific sediment yield is 325 m^3 per km^2 - year respectively. For the climate variables, the same $n = 1000$ samples were preserved. The robustness of the alternatives were then calculated under the uniform and BN-weighted case, using the same performance metrics and the same method described in Section 4.

Figure 3.11 showed the trade-offs under the case of uniform probabilities (a) and BN-weighted case (b) when only climate uncertainties were taken into account. The results indicate that the smallest design alternative is no longer the most robust choice with respect to NPV-regret metric in comparison to the case under full uncertainty analysis (Figure 10). Another finding is that the weighting scheme applied to the results does not affect the preference ranking, as 100 and 120 Mm^3 design capacities appear to be the most robust choices with respect to the NPV-regret and reliability metrics respectively (Figure 11). However, it is seen that robustness with respect to reliability is higher in the BN-weighted case (about from 0.70 to 0.95) in comparison to uniform weighting (0.55 to 0.70), which is similar to the findings on Figure 3.10.

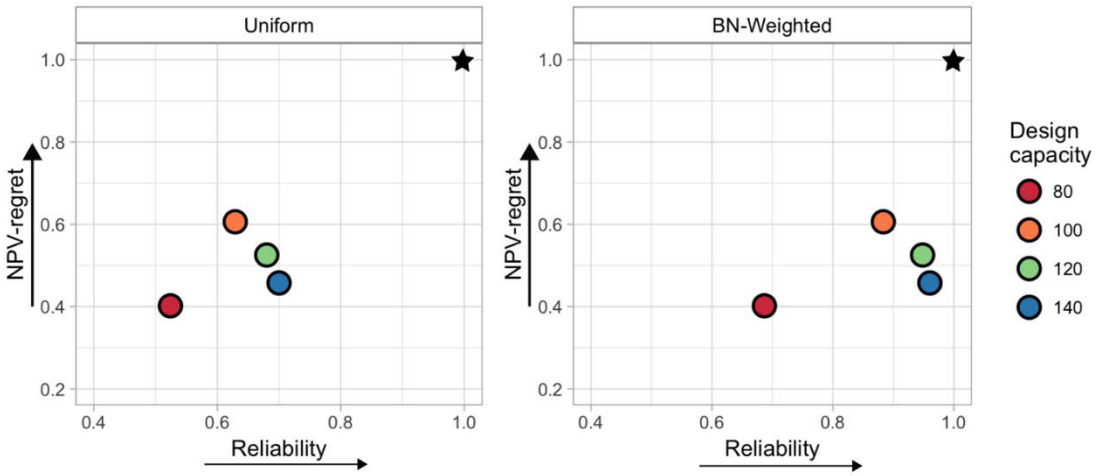

Figure 3.11 Robustness of the design alternatives under uniform likelihood (left), and under posterior probabilities calculated from the BN-model model (right) when only climate uncertainties are considered.

3.6.5. Identifying ex-post scenarios through data-mining

This section demonstrates the use of the Patient Rule Induction Method (PRIM), a data-mining algorithm as a complementary scenario analysis tool to the BNDS framework described earlier. Stated simply, PRIM seeks for data clusters within the uncertainty space that result in undesirable values (failures) for the response variable (Friedman and Fisher 1999). These data clusters, which are typically characterized by only a small number of uncertain factors, are used define "policy-relevant" scenarios to communicate vulnerabilities to decision makers (Groves and Lempert 2007; Bryant and Lempert 2010). The clusters identified by the PRIM are generally described by three major features: i) coverage, the percentage of failure cases contained within scenario, ii) density, the proportion of cases within the scenarios that result in a failure; and iii) interpretability, indicating how easily decision-makers can understand the information from the scenario (Bryant and Lempert 2010). Currently, PRIM is a commonly used scenario discovery tool in RDM, along with other rule induction methods such as Classification and Regression Trees (Hamarat et al. 2013).

In this work, we use a modified version of the PRIM algorithm to make use of the probabilistic information provided by the Bayesian networks, and more precisely to seek for "high risk" regions, rather than the conventional case of "high failure" regions. The motivation for this approach is that most decisions-makers dealing with long-term problems are interested in thinking regarding risks (the product of vulnerability and its occurrence likelihood), rather than only regarding vulnerabilities. Since the BN approach introduced earlier in this chapter intends to propagate a joint PDF of the vulnerabilities, a risk-based *ex-post* scenario analysis can be easily integrated into the framework. Below we give a brief description of the PRIM, along with the proposed modification.

3.6.5.1 PRIM method

This section provides a brief overview of the PRIM methodology from a vulnerability analysis perspective, and more in-depth discussion can be found in other sources (Lempert et al. 2008; Bryant and Lempert 2010; Polonik and Wang 2010). Suppose that we have a simulation model $y = f(x)$ that defines an outcome variable Y over an m-dimensional input variables space $x_j,\ j = 1, \ldots, m$, where each variable is defined within the specified lower and upper bounds $lb_j \leq x_j \leq ub_j$. Also suppose that Y is a binary variable and gets a value of 0 when the outcome is satisfactory or acceptable and 1 when it is not acceptable, with respect to a performance criteria Y^T:

$$y = \begin{Bmatrix} 0,\ y = f(x) > Y^T \\ 1,\ y = f(x) \leq Y^T \end{Bmatrix}$$

Equation 3.7

Our goal is to search for one or few lower dimensional boxes B within the uncertainty space that provide a good of explanation of the vulnerabilities $x|f(x) \leq Y^T$, with a high a relatively high mean $(\bar{y})$:

$$\bar{y} = \frac{\sum_{x_i \in B} y_i | f(x) \leq Y^T}{\sum_{x_i \in B} 1}$$

Equation 3.8

For this purpose, we can define a candidate box B_i over by the intersection of input variable values:

$$B_i = \bigcap_{k \in L} lb_k \leq x_k < ub_k$$

Equation 3.9

where L represents a subset of input variables that define the dimensions of B_i. The search process is implemented in two iterative steps, a top-down refinement (peeling) and bottom-up recursion (pasting) respectively. The top-down refinement or peeling begins with the box B that covers the entire uncertainty space. At each step, a small sub-box b^* is removed from the current box, in a way to obtain the highest mean within the remaining box $\mathrm{B} - \mathrm{b}^*$. The peeling process is controlled by the α (patience) and β_0 (support) parameters respectively. The former defines how much data will be peeled off at each step, with smaller values demanding greater computational time or "patience". The support parameter β defines the minimum number of cases to be included within the box, so that the peeling process stops when this value is reached. The bottom-up recursion (pasting) is to ensure that peeling process results in the best possible scenario. Since the peeling procedure

is applied without the knowledge of later peels, a readjustment on the final box may be necessary to find the best solution. At the stage of pasting, the size of the final box recursively until no further improvement is possible. Once the first box is chosen with the sequential process of peeling and pasting, the process can be iterated for finding other boxes or scenarios that explain vulnerable outcomes as desired. This is done by removing all the data points inside the first box (or prior boxes), and restarting the sequential process of peeling and pasting.

Three basic diagnostic features can be applied to PRIM-defined scenarios for further decision-relevant information. These features are coverage, density, and interpretability respectively. Coverage (also known as precision or positive predictive value) measures how completely the scenarios defined by box captures vulnerabilities. With binary output, coverage is simply the ratio of the total number of vulnerable cases in the Box to the total number of vulnerabilities:

$$Coverage = \frac{\sum_{x_i \in B} y_i \mid f(x) \leq Y^T}{\sum_{x_i \in \Omega} y_i \mid f(x) \leq Y^T}$$

Equation 3.10

Density measures the purity of the scenarios as is also called "precision" or "positive predictive value". With binary output, density is the fraction of cases within the box that are vulnerable relative to the total number of cases within the box, which is represented by (3.8).

The final feature, interpretability measures the ease of understanding and interpreting the results from a prim-generated box from a decision-making perspective. Interpretability is commonly expressed by the number of scenarios or boxes generated, and the maximum number of restricted dimensions by any box. Lempert et al. (2008) suggest that a scenario set

shall include about three or four boxes, each having no more than two or three restricted dimensions.

3.6.5.2 Modified PRIM method

For the purpose of identifying risk-based *ex-post* scenarios, we made several changes to the original PRIM algorithm shown previously. We start by assuming that the joint probability density function (PDF) of possible outcomes $\rho(x)$ is estimated through experts or by other modeling approaches such as Bayesian Networks. The original objective of the PRIM implicitly assumes that each outcome is equally likely (3.8). In the new formulation, this equation is modified as:

$$\bar{y} = \sum_{x_i \in B} \frac{\rho(x_i)\,\{y_i | f(x) \leq Y^T\}}{\sum_{x_i \in B} \rho(x_i)}$$

Equation 3.11

In Equation 3.11, incorporation of the $\rho(x)$ ensures that the search algorithm seeks for high density regions by placing a greater weight on cases that are more plausible than others. The stopping criteria (β), which originally sets the minimum number of cases to be included in any given box is also modified to represent the minimum cumulative probability of the cases.

To take into account of the non-uniform occurrence likelihood of the outcomes, the diagnostic features of coverage (Equation 3.10) and density (Equation 3.8) are redefined as weighted coverage and weighted density. In this new case, weighted coverage represents the cumulative occurrence probability of the vulnerable cases in the box to the total occurrence probability of vulnerabilities:

$$Weighted\ coverage = \frac{\sum_{x_i \in B} \rho(x_i)\{y_i \mid f(x) \leq Y^T\}}{\sum_{x_i \in \Omega} \rho(x_i)\{y_i \mid f(x) \leq Y^T\}}$$

Equation 3.12

Weighted density, on the other hand, is equal to the ratio of the total occurrence probability of vulnerable cases within the box to the total occurrence probability of all cases within the box as represented in Equation 3.12.

3.6.5.3 Illustration of the PRIM results over the case study

Figure 3.12 shows two clusters of scenarios identified from the case study analysis presented. The figure shows failure outcomes regarding reliability, where a computed reliability value of less than 95% is accepted as a failure (not acceptable) outcome. For simplicity, both scenarios indicate the same variables of precipitation change (%) and annual demand level (Mm^3 /year). The first scenario, which indicates a high vulnerability region is given by the precipitation changes from - 48% to -23% and the demand level from 78 to 100 Mm^3 /year. Scenario 1 covers about 66% of the identified risks and has a weighted density of 19%. The second scenario, on the other hand, seeks high-risk regions and defined by the precipitation changes from - 23% to 5% and the demand level from 85 to 100 Mm^3 /year. The scenario 2 on the other hand has a weighted coverage of 70%, and a weighted density of 87%. Overall, it is seen that the Scenarios 1 and 2 (Table 3.2) provide complementary information and their relevance depends on how much confidence is given placed on the probabilistic information. If one has high confidence on the joint PDF, scenario 2 becomes highly relevant as it captures a large fraction of the risks within the entire uncertainty space (%70) (Figure 3.12).

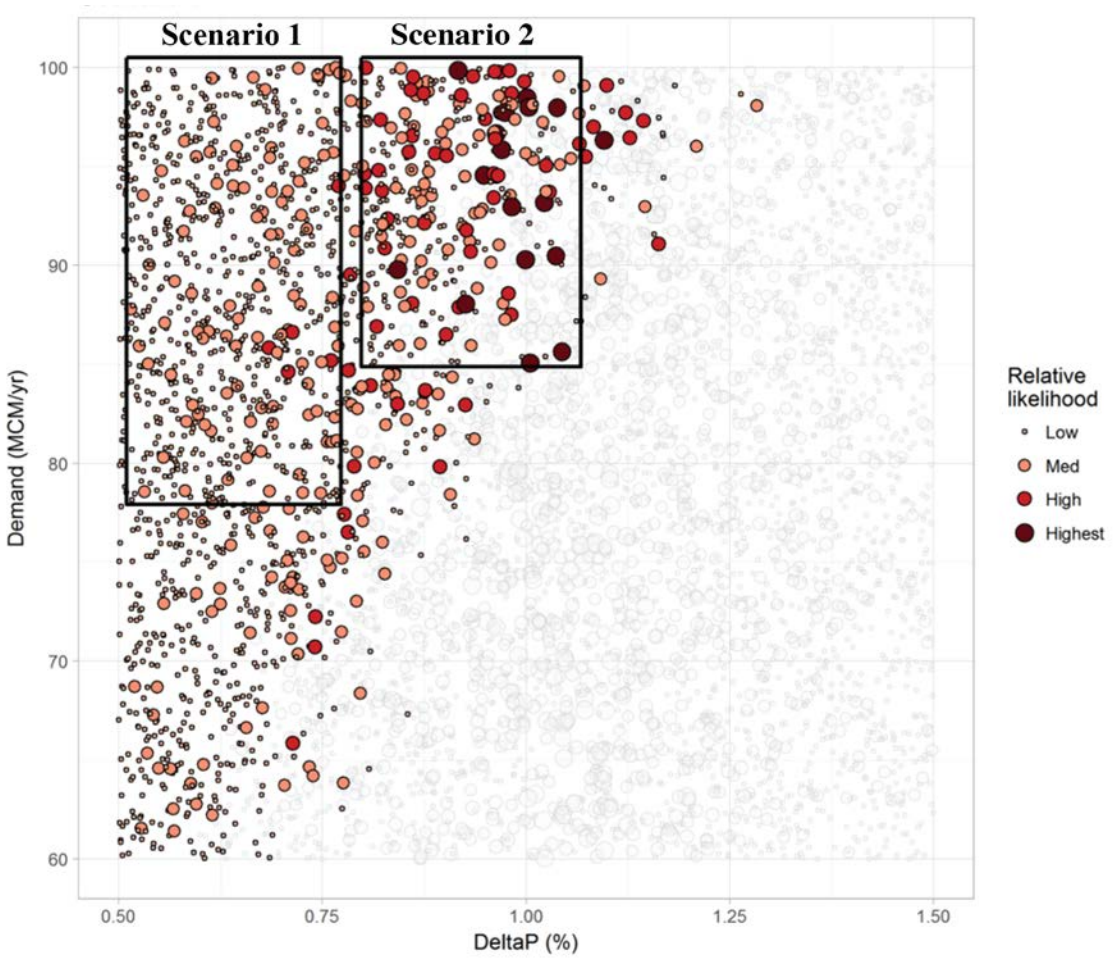

Figure 3.12 Scenarios identified through the conventional and modified PRIM methods. The data points indicated by the red color mark vulnerable scenarios (with a reliability value of less 95%). The size and the color of the data points represent the occurrence likelihood of each data-point, which are estimated from the Bayesian network model.

Table 3.2 Features of the scenarios obtained by conventional and modified PRIM

Scenario 1 - indicates high vulnerability	
Dimensions: Precip: 52% - 77% Demand: 78-100 Mm^3	Features: Weighted coverage: 66 % Weighted density: 19 %
Scenario 2 – indicates high risk	
Dimensions: Precip: 77% - 105% Demand: 85-100 Mm^3	Features: Coverage: 70 % Density: 87 %

3.7. Conclusions

This paper demonstrates an improved decision-analytical framework for making informed decisions in water systems planning under long-term climate and demographic uncertainty by explicitly considering subjective information or beliefs about the future states of the world. The framework integrates a bottom-up, robustness-based risk assessment approach called decision scaling with Bayesian network modeling, a popular tool for visualizing and propagating probabilistic information in complex systems. The coupled framework allows an explicit representation of conditional dependencies among various types of uncertainties and provides an estimation of the joint probability distribution of problematic conditions that were identified through an exhaustive vulnerability analysis. The framework follows the principles of bottom-up risk assessment by initially focusing on the exploration of stakeholder-defined system vulnerabilities. Probabilistic inference through subjective information or beliefs about the future world - in the form of model projections and forecasts, stakeholder opinions or historical data – only at the final stage of the analysis to assign likelihood weights to identified problematic conditions. Scenarios are then defined to provide the greatest coverage regarding plausible risks in the system.

The framework enhances the existing robustness-based decision-making approach in water systems planning in several different directions. First, the probabilistic network approach used allows stakeholder beliefs and local information to be quantified and incorporated into the risk assessment process and strengthens the "bottom-up" nature of the analysis. Stakeholder participation is not only limited to the first phase of project characterization, e.g., the definition of performance thresholds, but also at the final phase of risk analysis and scenario definition. Second, the framework allows blending of multiple sources of information in a transparent, coherent probabilistic framework that can be easily

communicated to the stakeholders and public. The framework allows analysis to evaluate the robustness of the alternatives by considering occurrence probability of the alternative futures in an "explicit" way. The presented framework can also be coupled with data-mining algorithms to define risk-based scenarios, such as Patient Rule Induction Method (PRIM) as shown in the case study.

3.8. Acknowledgements

This project was funded under World Bank Contract 717 4462: Including Climate Uncertainty in Water Resources Planning and Project Design Decision Tree Initiative. The authors are grateful to David Groves and Zhimin Mao from RAND Institute and Brian Joyce from Stockholm Environment Institute (SEI) for generously sharing their data and model application for the case study, to Brent Boehlert from Industrial Economics for providing the downscaled climate model data, and to Scott Steinscheineider for providing the code for the stochastic weather generator used in the analysis. The authors are also thankful for the local experts and stakeholders of the project from various institutions, including Kwale and Mombasa County governments, Water Resources Management Authority (WRMA) of Coastal Kenya, Coastal Water Services Board and the Mombasa Water and Sewerage Company.

CHAPTER 4

WATER INFRASTRUCTURE PLANNING BY MULTI-STAGE STOCHASTIC OPTIMIZATION WITH IMPRECISE PROBABILITIES

4.1. Abstract

Hydro-climatic nonstationarity due to climate change poses formidable challenges for making water infrastructure planning decisions in river basin systems. While decisions that are flexible or adaptive hold intuitive appeal, identifying sequences of well-performing decisions or planning trajectories requires rigorous quantitative analysis that addresses uncertainties directly while making the best use of scientific information on the expected evolution of future climate. Multi-stage optimization offers a potentially effective and efficient technique for dealing with this challenge; however, the necessity of assigning probabilities to future climate scenarios is an obstacle to implementation, given that methods to reliably assign probabilities to future climate states are nonexistent. In this work, we present a sequential decision-making framework that reduces the dependency on probabilistic assumptions, and rather evaluates probabilistic information after multi-stage optimization to aid selection amongst competing for alternatives. The framework represents natural climate variability and gradual changes in long-term climate through a scenario tree. A multi-stage optimization model is then solved repeatedly, by systematically varying scenario tree probabilities to capture a broad range of uncertainties. The iterative process yields a vector of planning trajectories that are optimal under associated scenario representation and probabilistic assumptions. In the final phase, the vector of optimal pathways is evaluated to identify the solutions that are least sensitive to the scenario probabilities and are more promising based on climate model projections. The proposed

framework is illustrated for the planning of new dam and hydro-agricultural expansion projects in the Niger River Basin in West Africa over a 45-year planning period from 2020 to 2065.

4.2. Introduction

Planners of large-scale, integrated water infrastructure systems deal with the problem of specifying the locations, design parameters, and scheduling (sequencing) of many types of facilities, for example, reservoirs, irrigation systems, pumping stations, hydropower turbines or treatment plants that will be in use over timescales up to fifty years or even longer (Loucks et al. 2005; Matrosov et al. 2013; Beh et al. 2014, 2015a; Jeuland and Whittington 2014). Planning over such long-time horizons poses a formidable challenge due to a myriad of uncertainties surrounding the decision-making process including future hydroclimatic conditions, population growth, changing socioeconomic standards or political interests (Molle et al. 2010; Haasnoot et al. 2013; Yang et al. 2016). Traditionally, decision-makers tackle with this problem by identifying a single, static 'optimal' plan considering historical or narrowly defined conditions through formal optimization methods, for example, linear programming (Lund and Israel 1995; Randall et al. 1997) or dynamic programming (Butcher et al. 1969; Becker and Yeh 1974; Braga et al. 1985). However, such a static optimal plan is likely to yield a poor or failing performance under conditions other than that is deemed 'most-likely (Ben-Haim 2006; Haasnoot et al. 2013; Maier et al. 2016). The risks from choosing a static optimal plan are even larger under deeply uncertain conditions, such as those associated with climate change, where planners have no credible, commonly agreed information about the probability distribution of the outcomes (Lempert 2003; Lempert and Collins 2007).

To better cope with a deeply uncertain future, it is suggested that the planners shall seek for robustness, the ability to perform well or satisfactorily over a broad range of plausible futures (Dessai and Hulme 2007; Lempert and Groves 2010; Walker et al. 2013; Herman et al. 2015). Most analytical approaches that seek for robust plans, for example, Robust Decision Making (Lempert 2003), decision scaling (Brown et al. 2011b), and Info-Gap theory (Ben-Haim 2006) focus on anticipatory adaptation, i.e., the actions that take place before the uncertainties over a predefined planning horizon are realized. However, in the actual practice, decision-makers are more interested in identifying flexible plans that can dynamically adapt to new conditions as the future unfolds (Haasnoot et al. 2012). This flexibility also referred as "dynamic robustness" allow adaptation to be anticipatory, concurrently (simultaneously with the observed changes) and in a reactive way (after observing the effects of change) (Walker et al. 2013). From a slightly different perspective, one can also classify flexible decisions into "here-and-now" actions that need to be implemented immediately to respond to current needs and challenges and those that are not urgent, and "prepare-and-monitor" actions that can be postponed until a certain predefined performance threshold (e.g., low reliability) or critical tipping point (e.g., sea level rise) is exceeded or triggered (Haasnoot et al. 2013; Barnett et al. 2014; Kirshen et al. 2014).

A number of planning frameworks focus on dynamically robust decisions under climate change, including Real Options Analysis (ROA) (Dixit and Pindyck 1994) and Dynamic Adaptation Policy Pathways (DAPP) (Haasnoot et al. 2013). ROA, originating from financial analysis, emphasizes the value of flexibility by considering the options of delaying, abandoning, expanding or switching decisions in response to unfolding uncertainties over multiple time stages (Neufville 2003). Such diverse sets of options allow decision makers to respond in a way to limit the downside of making a wrong decision and

capture the upside of new information and opportunities (Buurman and Babovic 2016). Gersonius et al. (2013) assessed real options for selection and timing of modifications in urban drainage infrastructure for enhancing resilience to climate change. More recently, Woodward et al. (2014) developed an optimization-based real options framework to assess flood risk management strategies for the Thames estuary, in London. A second way to conceptualize adaptation over time is through "critical tipping points" in which the system is no longer adequate, and modification is necessary (Haasnoot et al. 2011). DAPP combines the tipping points approach with the metaphors of route maps to evaluate the timing of scenario-dependent adaptation actions through a set of signposts specifying key information that should be tracked to determine if the critical tipping points are violated. The outcomes of DAPP are typically visualized regarding pathways or route maps over multiple stages to show a scenario-based representation no-regret actions, lock-ins, and the timing of actions (Haasnoot et al. 2012). Haasnoot et al. (2013) illustrated the DAPP framework for managing flood risks and freshwater supply planning in the Rhine Delta.

Developing dynamically robust infrastructure plans under climate change based on ROA, DAPP or any other method face at least two major analytical challenges: i) quantifying and representing the plausible range of climate uncertainties over time-scales relevant for the decision-making, and ii) developing an analytical procedure to evaluate a large array of adaptation options over the represented range of uncertainty (i.e., deciding when, where, and how to implement actions). The first challenge can be addressed by conceptualizing the future through multiple scenarios of transient, internally consistent storyline of future events (Schwartz 1996; Mahmoud et al. 2009; Maier et al. 2016). Within the body of climate change adaptation literature, long-term scenarios are commonly derived from the outputs of Global Circulation Models (GCM). This involves choosing a set of Global Circulation Model

(GCM) projections for the period of interest, and in some cases applying downscaling and bias-correction to those projections to obtain scenarios of regional or local climate changes. For example, Vicuna et al. (2010) developed a dynamic programming model for the adaptive management of water resources in California, where they represented climate uncertainty through eleven GCM runs under the two greenhouse gas emission scenarios from the IPCC's "Fourth Assessment Report" (the higher A2 and lower B1). Ray et al. (2012) developed a multi-stage water resources decision model for Amman, Jordan through a scenario-tree that depicts the gradual evolution of climate change at the years 2035, 2065, and 2085 based on eleven GCMs and three emission scenarios (B1, A1B, and A2). More recently, Haguma et al. (2014) developed a dynamic programming model similar to the work presented by Vicuna et al. (2010), considering thirteen GCMs and A1B, A2, and B1 emission scenarios. The problem with developing climate scenarios based on GCM projections is that they provide an incomplete and potentially biased sample of climate uncertainties due to inherent uncertainties related to climate forcings (Stainforth et al. 2005), model initial conditions (Deser et al. 2012), or the structural and computational limitations of climate models (New and Hulme 2000; Knutti 2008). As a result, the use of GCM-based climate scenarios in actual decision-making processes is limited (Brown and Wilby 2012; Dittrich et al. 2016). Alternatively, climate scenarios can be developed directly based on the vulnerability analyses of the system of interest (Brown and Wilby 2012). This approach makes use of weather generators and Monte Carlo sampling techniques for a fuller and more systematic sampling of future climate uncertainties, especially those associated with vulnerable or undesirable outcomes without being restricted by the assumptions of GCM projections (Steinschneider and Brown 2013). Examples of the use of "vulnerability-based" climate scenarios have become common in robustness-based water resources planning (Prudhomme

et al. 2010; Moody and Brown 2012; Singh et al. 2014; Whateley et al. 2014). However, their use in dynamic adaptation planning problems are very limited, majorly restricted to the application of simple sensitivity factors to the historical climate or streamflow records (Jeuland and Whittington 2014).

The second challenge arising from the need to assess multiple adaptation options over space and time analytically can be addressed through Monte Carlo analyses (Jeuland and Whittington 2014) or more efficiently by methods of 'optimization under uncertainty' (Sahinidis 2004). Multi-stage stochastic Programming with recourse (SP) is frequently used to assess the 'real options' in water resources planning, including flood risk management (Woodward et al. 2014), drought mitigation (Cai et al. 2015) or capacity expansion (Kang and Lansey 2014; Creaco et al. 2015). Stated simply, SP divides the planning horizon into multiple decision stages and then searches for a time-based solution by explicitly considering multiple future trajectories represented in the form of a scenario tree. The scenario tree structure reflects the evolution of random variables, e.g., mean temperature and precipitation changes in each stage through a set of joint probability mass functions (PMFs) (Birge and Francois 2011). An SP model can be also formulated as a robust optimization model (RO) by incorporating additional risk terms to model formulation, for example by minimizing expected cost and the cost variation over scenarios simultaneously (Markowitz 1952), or by considering variability in the objective and constraints (David et al. 1997; Mulvey et al. 2008; Ray et al. 2014).

When applying SP to planning under climate change, the requirement to assign *ex ante* probabilities to the scenarios at different decision-stages pose an important challenge. As noted earlier, determining the occurrence likelihoods of possible climate futures is not possible under a deeply uncertain climate due to a number of reducible and irreducible

uncertainties and thus results in a methodological problem. Past studies circumvent this issue by applying Laplace Principle of Insufficient Reason and treating all climate scenarios as equally plausible (Ray et al. 2012; Gersonius et al. 2013; Cai et al. 2015). The problem with assigning a single uniform probability distribution is that the solutions obtained from such analyses would be contingent upon the underlying probabilistic assumptions applied, and therefore do not inform the decision-makers about imprecise nature of probabilities (e.g., if the results would vary substantially under different prior assumptions). Recently, Kwakkel et al. (2015) present a multi-objective evolutionary optimization model to support the development of dynamic adaptation plans through DAPP that does not require prior probability assignment. In their work, they first develop a set of independent scenarios and then seek for a solution that simultaneously minimizes the median outcome across all scenarios as well as the dispersion around the median outcome. However, this type of a formulation requires all scenarios to be treated as independent, rather than a set of gradually evolving plausible futures from a common time origin. As a result, the outcomes do not provide a rich, detailed representation of decisions pathways representing nonanticipativity, but only a solution that heavily relies on the scenario with the median outcome.

In this work, we present a novel analytical framework to support multi-stage adaptation planning by combining the certain key principles of vulnerability-based climate risk assessment with SP. Our approach provides several key improvements over existing multi-stage adaptation planning frameworks regarding sampling climate uncertainties and identifying most promising decision pathways. First, we present an innovative scenario-tree generation procedure to systematically sample natural climate variability and gradual climate changes without depending on the highly uncertain outputs of GCM projections. Second, rather than making a prior preference on the likelihood of scenarios, we reapply stochastic

optimization considering a wide range of systematically generated probability distributions. From this repeated analysis, we produce an extensive inventory of decision pathways contingent upon the underlying assumptions. Finally, we post-process the resulting inventory of optimal portfolios in an attempt to identify dominating solutions that are frequently found in the database of scenarios. In this step, we also make use of GCM projects to extract additional information for the final preference ranking of the planning portfolios. This way, we only use GCM information at the final phase of the study, to weight the domain results. We demonstrate the method for the case of long-term water infrastructure planning in the Niger River Basin over a 45-year planning period.

Rest of this paper is organized as follows. The following section gives a brief overview of the bottom-up adaptation planning framework and introduces its steps. Section 4 presents the Niger River Basin application. It begins with a summary of main hydro-climatic and socioeconomic features in the context of long-term adaptation planning and then describes the specific modeling processes and the assumptions in each one. Section 5 reports the case study results. In section 6, we discuss the findings in a broader context and present the conclusions.

4.3. Proposed framework for adaptation planning under climate change

The purpose of this study is to develop a vulnerability-based, tractable framework for assessing multi-stage water infrastructure planning decisions. From this point and onward, these sequential planning decisions will be referred simply as "development pathways."

The proposed framework (Figure 1) consists of four major steps: [1] development of the modeling framework, [2] definition of the scenario space, [3] generation of planning

pathways, and finally, [4] identification of belief dominant pathways. Below, we provide a brief overview of each step shown in Figure 1, while reserving the detailed description of each step to the case study application (Section 5).

4.3.1. Step 1: Develop the modeling framework

The first step begins with a screening and model development process to describe the major features of the analysis including economic, social, and environmental objectives and constraints, the planning horizon and decision stages, and adaptation decisions to be evaluated, ideally through a stakeholder-driven process. The specified objectives are merged into a single one, in most cases expressed in monetary terms such as minimizing the economic cost of the water supply system (Becker and Yeh 1974; Chung et al. 2009) or maximizing net economic benefits of water operations and allocations for different uses (Draper et al. 2003). Alternatively, a 'multi-objective' model formulation can be used to explore possible non-dominated solutions or so-called 'Pareto frontiers' concerning the different objectives (see Beh et al. 2014, 2015b).

Next, the planning horizon of the water resources planning problem is subdivided into T subsequent periods. Long-term changes in the climate conditions is assumed to occur gradually, beginning from the time of origin and branching out further at each period. The gradual evolution of uncertainty over *T* subsequent periods can be represented through a set of scenarios $s \in S$ in the form of a scenario tree (see Step 2). A multi-stage SP model is then defined to explore sequential infrastructure decisions over this scenario space. The basic notation of a SP is introduced below with a more detailed description on Appendix C. The deterministic equivalent of the scenario-based SP model is defined as:

$$min\, E[F(x_1, {x_2}^s, \dots, {x_T}^s, \omega)]$$

$$s.t.\ \ g_l(x_1, x_2{}^s, \ldots, x_T{}^s, \omega) \leq 0 \qquad l \in L,\ \ s \in S,\ \ t \in T$$

Equation 4.1

where $\omega = \{\omega_1, \ldots, \omega_T\}$ is a stochastic process considered over T decision stages; x_1 is the decisions-made at the initial point in time, $x_2{}^s$ through $x_T{}^s$ are scenario-dependent decisions made at stages 2 to T; $\mathrm{g}_l(.)$ is the l^{th} constraint of the problem defined over the set $l \in L$. A unique feature of the SP model (4.1) is the nonanticipativity of the recourse decisions, which result from the fact that the decisions made at any point in time only depend on the past observations of the stochastic process (Birge and Francois 2011).

4.3.2. Step 2: Define the scenario space

The second step of the framework is the generation of the scenario space to represent the uncertainty in future climate conditions. The approach proposed here differs from the existing methods that use GCM projections to develop climate change scenario trees (Ray et al. 2012; Cai et al. 2015). Instead, it combines a relatively small set of carefully selected natural climate realizations with climate change factors defined over each decision period $t = 1 \ldots T$ to provide a rich representation of the possible ways that the climate system may unfold over course of the planning horizon.

In step [2.1], a large set of natural variability realizations are generated from a stochastic weather generator with statistical properties, e.g., mean, variance, and spatial-temporal correlations similar to the historical record. Repeated sampling of internal climate variability is critical to explore vulnerability to certain conditions, for example, particular sequences of wet or dry conditions. Also, natural variability will continue to be the primary source of uncertainty in water resources systems, at least for the over the next couple of

decades (Barsugli et al. 2012; Deser et al. 2012). However, using a large number of climate realizations is computationally expensive when exploring the effects of both natural variability and climate change, and a preprocessing might be necessary to reduce the size of sample size (Whateley et al. 2016). In step [2.2], a screening-level optimization model is used to select k realizations that represent the initial set of realizations.

The final step of the scenario generation process is to incorporate uncertainties from long-term climate changes. In step [2.3], a climate change scenario tree is constructed that yields a total of S scenarios providing a joint representation of gradual precipitation and temperature changes over T stages. This is done by specifying a range of change factors in a sequentially from stage 1 to stage T, in a way that covers a broad range of changes that go beyond the level of changes projected by climate models. The climate change scenario tree is then combined with k climate variability realizations obtained in step [2.2], resulting an ensemble of $S\ x\ k$ transient climate scenarios.

4.3.3. Step 3: Obtain an inventory of belief dominated pathways

The purpose of the third step is to get a large inventory of development trajectories under uncertainty. Due to the need to evaluate decisions across a multi-dimensional uncertainty space, i.e., from climate change, natural variability, and imprecise probabilistic assumptions, this step is the most computationally expensive part of the analysis.

In step [3.1], i bivariate PMFs are generated to set the probability weights of mean temperature and precipitation changes evaluated in the stochastic program. The purpose is to explicitly take into account the imprecise, and highly uncertain nature of probabilistic assumptions about the likelihood of future climate conditions and explore the effects of different beliefs about the future without being limited to climate science information. These

would include extremely wet to extremely dry and warm futures as well as more moderate and plausible climate changes. In step [3.2], the multi-stage stochastic optimization is repeated solved over each combination of i (PMFs) and k climate realizations to generate a large inventory of optimal development pathways.

4.3.4. Step 4: Obtain an inventory of flexible plans

The fourth step is a post-optimization analysis of the results to find one or few prosing development pathways that are most frequently found in the repeated optimization process in step [3]. The purpose of this post-optimization analysis is to identify robust outcomes that are insensitive (or less sensitive) to underlying climate scenarios and probabilistic assumptions. Note that here, we use "robustness" to refer to an optimal solution's appearance frequency within the inventory of solutions (in this case, over the combinations of i probabilistic beliefs and k natural variability realizations). This is slightly different than the formal meaning of "robust optimization", which offers a variety of models and algorithms to avoid worst-case outcomes or large risk from uncertain model parameters (David et al. 1997; Mulvey et al. 2008).

In the final step of the analysis, additional sources of information about future climate change such as climate model projections, paleodata or expert judgments can also be incorporated to rank and evaluate the results obtained under a broad range of 'beliefs.' For example, if an analyst would assign a higher subjective weight to solutions obtained from more plausible beliefs according to the results of climate models. Previous decision scaling studies present such *ex post* uses of climate information to assign weights to stochastically sampled climate scenario domains (Brown et al. 2012; Moody and Brown 2012; Whateley et al. 2014) but not to beliefs that are expressed by probability distributions.

Overall, the proposed framework inherits a number of useful concepts from two previously developed frameworks, namely DAPP (Haasnoot et al. 2013) and decision scaling (Brown 2011). We apply the visual analytics described as route or subway maps in DAPP to conceptualize river basin development pathways as dynamic plans that can adapt to new conditions or learn from previous experiences. Second, we employ a number of procedures that are commonly referred as vulnerability-based for distinguishing from more information-oriented predict-then-act analyses. First, the scenario generation technique in this work (step [2]) does not use climate projections but rather directly samples climate variability and mean climate changes. Second, the repeated optimization analysis (step [3]) aims to circumvent the necessity of assigning *ex-ante* probability weights to the scenarios before optimization. By varying the probability weights in a systematic way, we deemphasize on the role of scenario probabilities. This repeated optimization process over the probability space (step [3.1]) is compared to a "climate stress test" described in decision scaling (Brown et al. 2012). In decision scaling, the climate stress test explores system performance across a wide range of climate scenarios. In this work, we explore the probability domain associated with the scenarios rather than varying scenarios.

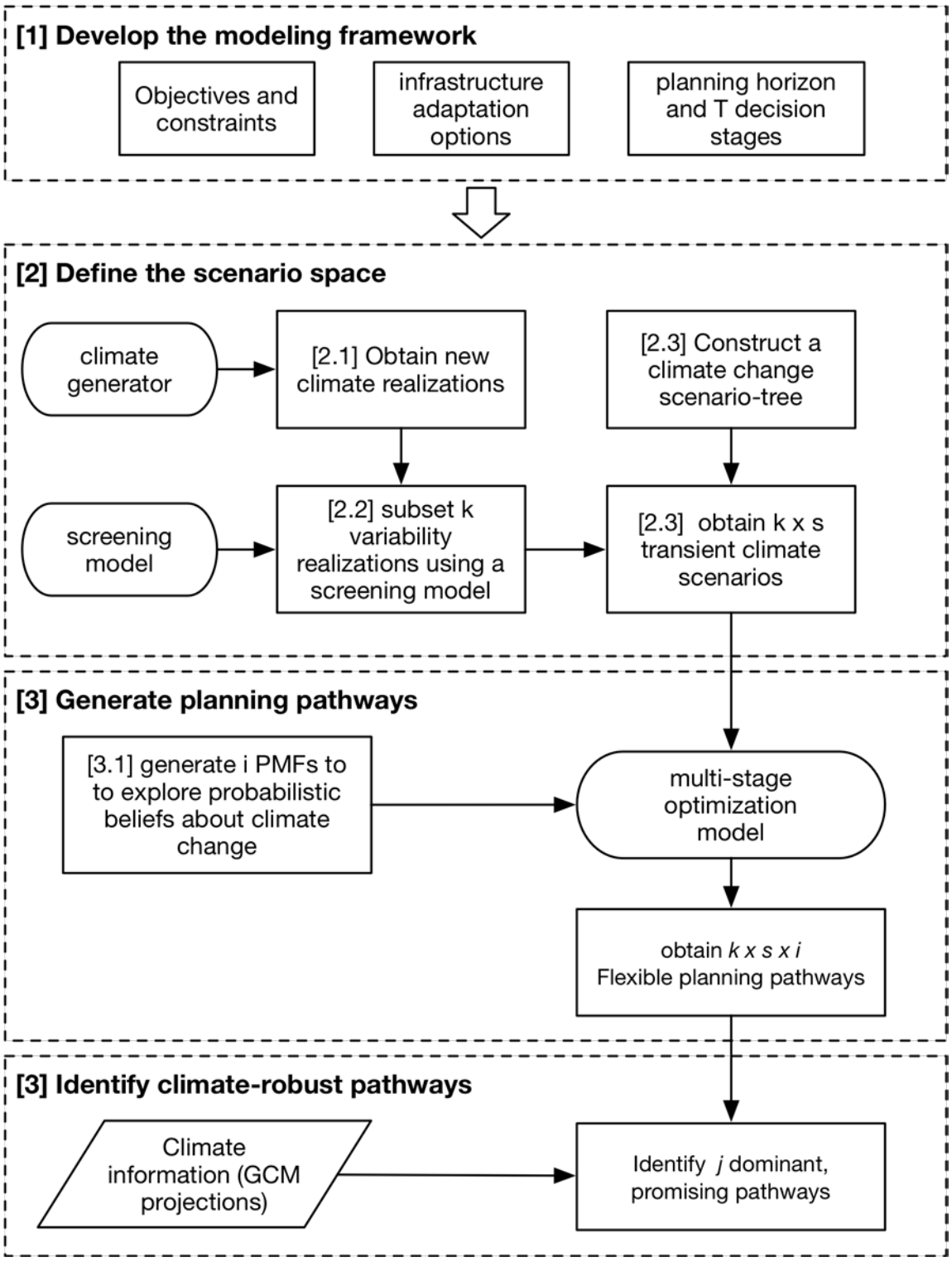

Figure 4.1 The proposed framework for multi-stage water infrastructure planning under climate change

4.4. Case study: Multi-stage infrastructure planning in the Niger River Basin

4.4.1. Background

The Niger River is the third longest river in Africa after the Nile and Congo, with a length of 4,200 km (Figure 4.2). It rises in the mountains of Guinea and Sierra Leone before flowing northeast towards the network of wetlands known as Inland Delta in Mali, then flows to the southeast and merges with the Benue River, and finally discharges to the Atlantic Ocean in Nigeria. The Niger River Basin (NRB) covers an area of about 2.27 km^2 which is shared among Benin, Burkina Faso, Cameroon, Chad, Côte d'Ivoire, Guinea, Mali, Niger, and Nigeria, which are also members of the Niger Basin Authority (NBA).

The NRB faces a number of complex socioeconomic and environmental issues including extreme poverty, vulnerability to droughts, and high child mortality due to water-borne diseases, which can be attributed to the poor state of built water and sanitation infrastructure (Ogilvie et al. 2010; Namara et al. 2011). As opposed to the state of the current conditions, there is a great opportunity for water resources development, with estimated irrigation and hydropower potentials of nearly 2.5 million hectares and 6,000-gigawatt hours respectively (Andersen et al. 2005; Lienou 2013). In 2002, the NBA declared a 20-year Sustainable Development Action (SDAP) worth 8 billion US dollars that includes the rehabilitation of existing water supply and hydropower sites, the construction of four new dams - Fomi, Diaraguale, Taoussa, Kandadji (Figure 4.2), expansion of the existing irrigated agriculture schemes across the eleven irrigation development zones of the NRB (Figure 4.3). Also new infrastructure investments, the plan includes a number of policy measures to support fisheries, livestock farming, and ecotourism, and to protect vulnerable

ecosystems including the Inland Delta in Mali, which is one the largest wetlands in Africa (NBA 2008).

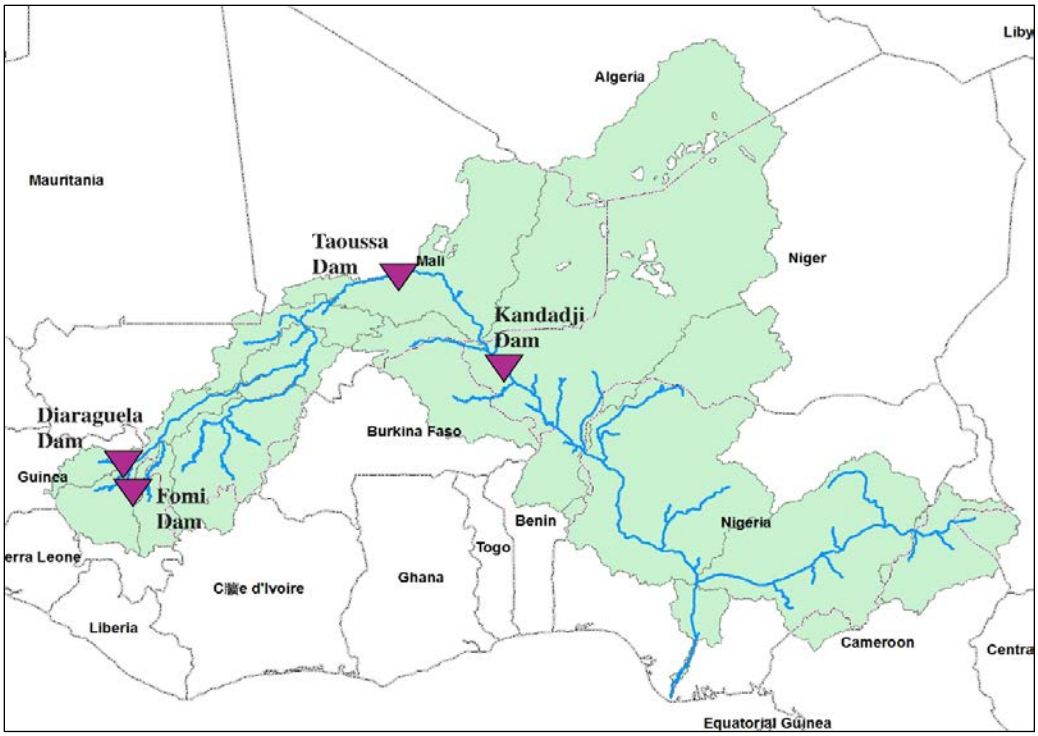

Figure 4.2 The geography of the Niger River Basin, along with the four new dam projects (Fomi, Diaraguala, Taussa, and Kandadji).

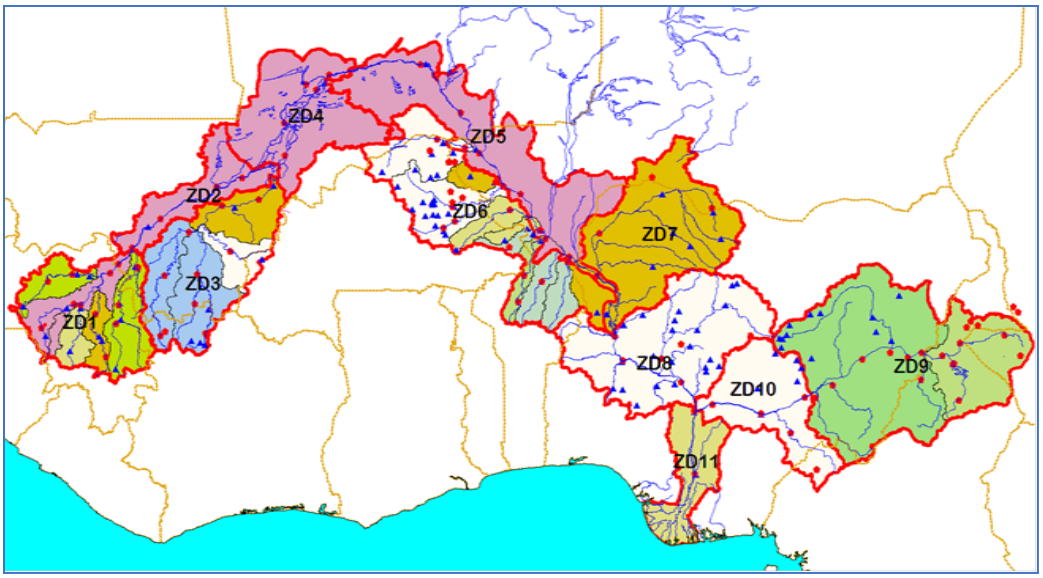

Figure 4.3 The geographic location of the eleven irrigation development zones in the Niger River Basin.

4.4.2. Historical climate variability and climate change

The climate regime in the NRB shows a high spatial and temporal variability due to the geographical setting. The primary force driving the regional climate system is the convergence of trade winds in the north and south of the equator, known as the Inter-Tropical Convergence Zone (ITCZ) (Sultan and Janicot 2003; Sultan et al. 2003; Nicholson 2009). The seasonal movement of the ITCZ tends to follow the sun's annual migration, advancing into the northern hemisphere in boreal summer and retreating into the southern hemisphere in austral summer (Wilby 2008). In relation to the ITCZ, the basin has a rainy summer season from May to October, and a dry winter from November to April, except for Nigeria, which receives rainfall over four seasons (Andersen et al. 2005). Average climate conditions across the basin vary substantially based on the latitude and season. For example, annual average rainfall is only 300 millimeters in the arid regions of the Sahel zone and is more than 2,000 millimeters in the tropical areas of Guinea (Grijsen et al. 2013).

Annual rainfall over the West Africa shows high year-to-year variability, which has been studied extensively (Le Barbe et al. 2002; Davidson et al. 2003; Brooks 2004; Giannini et al. 2008; Conway et al. 2009; Janicot et al. 2011; Tarhule et al. 2012). Over the past century, basin-wide mean annual precipitation was recorded to be above the long-term means from 1915 through the late 1930s, and from 1950s through the end of the 1960s, after which it was persistently below the long-term mean (Figure 4.4). The La Grande Se´cheresse, the great drought in the early 1980's, was an unprecedented catastrophe for the region that resulted in devastating famines (Zwarts et al. 2005; Sissoko et al. 2011). Beginning with the 1990's, annual rainfall has recovered and approached the century-long mean (L'Hote et al. 2003; Ozer et al. 2003; Held et al. 2005). Near mean conditions in terms annual rainfall continued past 1990's, with a relatively dry period for the years 2000 to 2003,

and an extremely high rainfall in 2010, and abnormally dry conditions in 2011 (Lebel and Ali 2009; Fontaine et al. 2011). This substantial interannual variability observed over the recent years is noted to be highest in the past forty years (Nicholson 2013). The complex dynamics of climate variability in West Africa is still a subject of ongoing research that is attributed to changing human activity and land-use conditions (Charney 1975) as well as anomalies in the sea surface temperature (SST) patterns in the Atlantic, Pacific, and Indian Oceans associated with El Niño–Southern Oscillation (Held et al. 2005; Biasutti and Giannini 2006; Janicot et al. 2011).

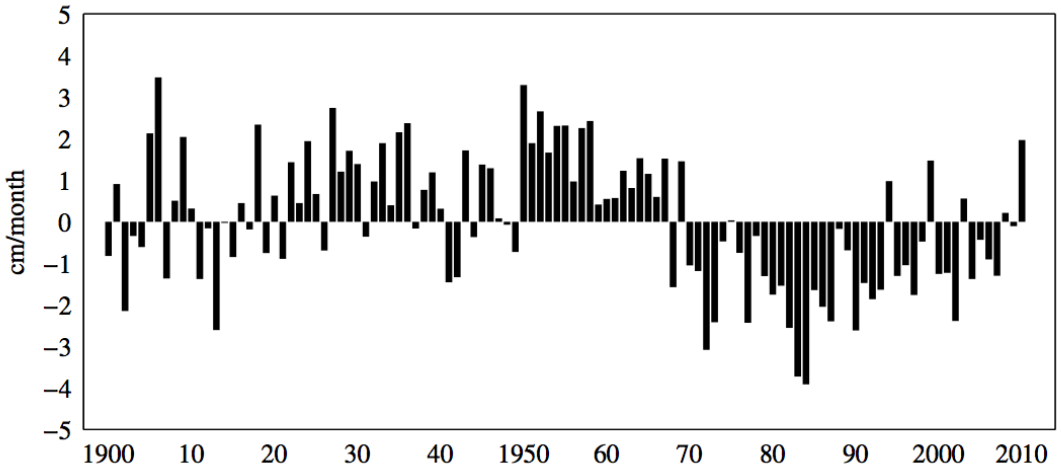

Figure 4.4 Rainfall anomalies in the Niger River Basin (Source: NOAA NCDC Global Historical Climatology Network Data)

Anthropogenic climate change may exacerbate the natural variability in West African climate (Wilby 2008; Roudier et al. 2014), resulting in new vulnerabilities, for example, from the acceleration of desertification (Oyebande and Odunuga 2010) and reductions in crop yields (Sissoko et al. 2011). However, there are large disagreements among the climate model projections regarding the direction and magnitude of potential climate change over the 21st Century. Figure 4.5 shows the range of projected changes in the mid-2060's and the

historical conditions (1950-2000 period) from the IPCC's latest Fifth Assessment Report. The underlying data on Figure 4.5 represents a large ensemble of climate model runs (110 in total) obtained from 23 GCMs, each forced by four Representative Concentration Pathways (RCP) scenarios (RCPs 2.6, 4.5, 6.0, and 8.5 respectively). Projected increases in the annual temperature range from about 1 to 5ºC concerning the historical period of 1950-2000 (Figure 4.5). However, there is no clear trend in the direction of precipitation change, as model projections range from a 10% decrease in a 25% increase for the same period (Figure 4.5).

The regional effects of climate change over West Africa are investigated in more detail through a number of studies using Regional Climate Models (RCMs) (Patricola and Cook 2010; Mariotti et al. 2011; Laprise et al. 2013; Dosio and Panitz 2016; Obada et al. 2017). Paeth et al. (2011) suggest a general drying trend over most of the West Africa in the first half of the 21st Century based on the results from multiple RCMs. Similarly, Sylla et al. (2016) evaluated the results from the CMIP5, CORDEX, and HIRES multi-model ensembles and concluded a shift toward more semi-arid and arid conditions. A majority of the past studies underline the sensitivity of the results to numerous assumptions made, for example, selection of GCMs or an application of a particular downscaling approach. Fontaine et al. (2011) note that the discrepancies in the projected precipitations among the GCMs can be partially attributed to their ability to simulate convective rainfall. Dosio and Panitz (2016) found that the use of RCMs can alter the sign of rainfall change of the driving GCM in West Africa, particularly regarding mean precipitation changes and extreme-events.

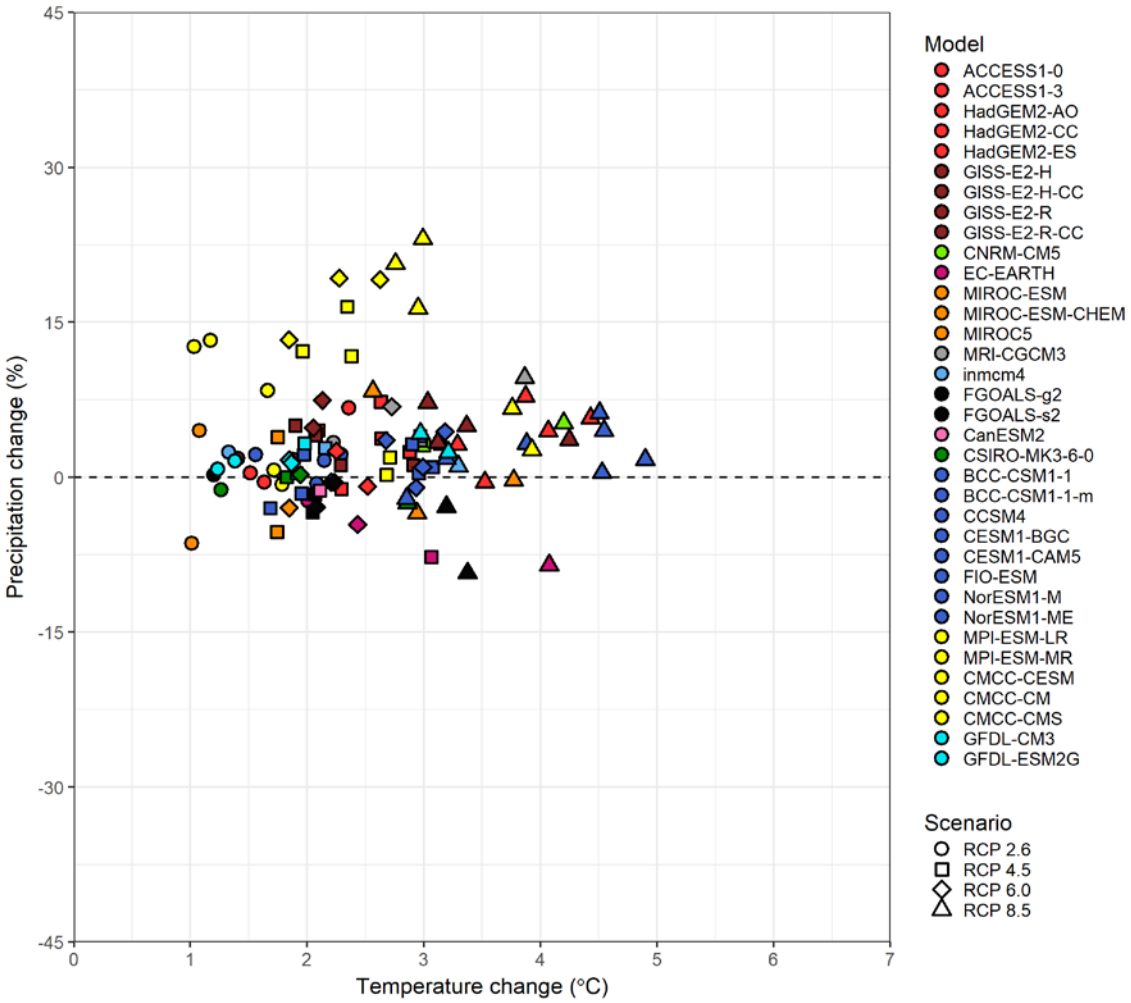

Figure 4.5 Mean climate changes from the IPCC's CMIP5 ensemble for the Niger River Basin for RCPs 2.6, 4.5, 6.0 and 8.5 respectively. The data shows the changes in the 2050-2080 future period relative to the historical period of 1950 - 2000. The models that share similar code are shown with the same color.

Overall, the scale of observed climate variability over the past century (Figure 4.4), and unclear, conflicting signals on the direction and magnitude of future climate change from the most recent GCM projections (Figure 4.5) mark a deeply uncertain future for West Africa. The presence of deep uncertainties necessitates a vulnerability-based planning approach by taking into account multiple, diverse range of plausible climate futures that goes beyond historical variability and projected a range of changes.

4.4.3. Data sources

This work makes use of a variety of hydroclimate and socioeconomic data sources from several previous studies. Data related to the physical basin and the water resources system, including the catchment locations, evaporative losses, the agricultural, industrial and municipal demand sites, the existing and planned reservoirs, the hydropower generation turbines and the minimum flow targets are obtained from the MIKEBASIN model of the Niger Basin (BRLi and DHI 2007a) and the WEAP of the Niger Basin (Schlef 2014). Data used for the calibration of seasonal water balance in the Inland Delta in Mali, including monthly inflows, evaporative losses, and inundated areas and water volume are obtained from the Niger RIBASIM model (Passchier et al. 2005) and the work of Zwarts et al. (2005). Data related to the use and allocation of water resources throughout the basin, and data used for estimating economic benefits and costs for agriculture, hydropower production, fisheries, and infrastructure and the capital cost estimates of infrastructure investments are obtained from BRLi and DHI (2007b). Historical climate data, including precipitation, maximum, minimum, and mean temperatures were gathered from the Princeton University Terrestrial Hydrology Group's gridded meteorological data set (Sheffield et al. 2006). Historical streamflow data across the NRB was gathered from Hydrological Cycle Observation System for West and Central Africa (AOCHYCOS 2015).

4.4.4. Application of the framework to the Niger River Basin

4.4.4.1 Development of the modeling framework

Application of the framework to the Niger River Basin begins with developing a large-scale river basin optimization model. The purpose of the model is to evaluate the sizing, timing, and sequencing of large-scale water infrastructure projects identified in the

Sustainable Development Action Plan (see section 4.2.1). These include construction of the Fomi, Diaraguala, Taussa, and Kandadji dams along the Niger River and its tributaries and the expansions in the irrigated agriculture infrastructure across the eleven agricultural development zones of the Niger Basin. The analysis covers a 45-year period, corresponding to the period from 2020 to 2065. The new infrastructure decisions are re-evaluated periodically, at years 2020, 2035, and 2050 respectively, whereas seasonal decisions related to reservoir releases and allocation of water are implemented every season (Figure 4.6). The problem is formulated as a stochastic mixed-integer programming (SMIP) model and implemented using the General Algebraic Modeling System (GAMS) (Brooke et al. 1988).

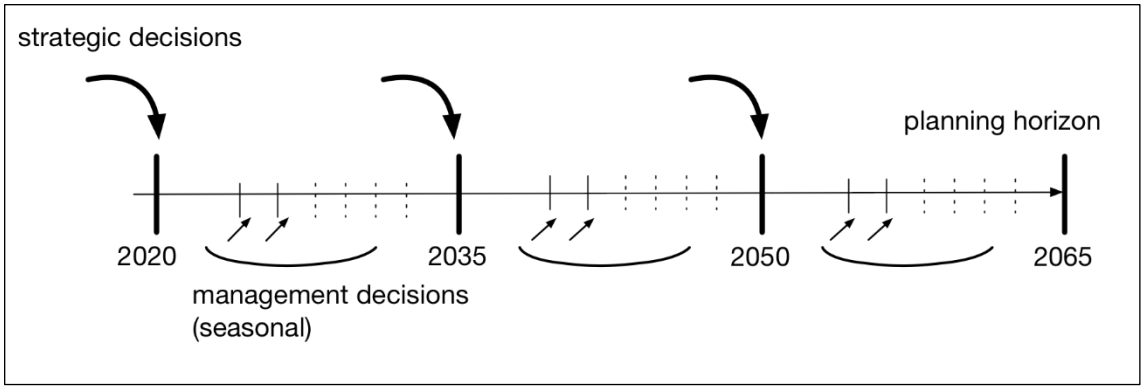

Figure 4.6 A conceptual representation of the sequential planning problem involving three decision stages (years 2020, 2035, and 250), and three subsequent observation periods.

The optimization model consists a set of mathematical equations to calculate: i) conservation of mass balance along the Niger River and its tributaries, as well as for the existing and new reservoirs, ii) investment decisions on the new water supply and irrigated agriculture infrastructures, iii) allocation of water resources to the domestic, irrigation, hydropower, fisheries and environmental sustainability sectors, and iv) net economic benefits from water use and allocation over the planning period. The model runs at a seasonal time step with a wet season from May to September and a dry season November to April.

Operational decisions related to the resources system including releases from the reservoirs, hydropower production, and crop production is simulated on a seasonal basis. Long-term climate uncertainty associated with natural variability and mean climate changes are represented by a multi-layered scenario tree (see Section 4.2).

The schematic of the NRB system is represented by a node-link network consisting of 155 nodes n representing various types of entities. These entities are subdivided into forty-nine hydrological catchments nodes ns, twelve natural or artificial lakes nodes r , eleven irrigation diversion nodes ni, and nineteen domestic diversion ns, and thirty minimum environmental flow nodes $neco$ (Figure 4.7).

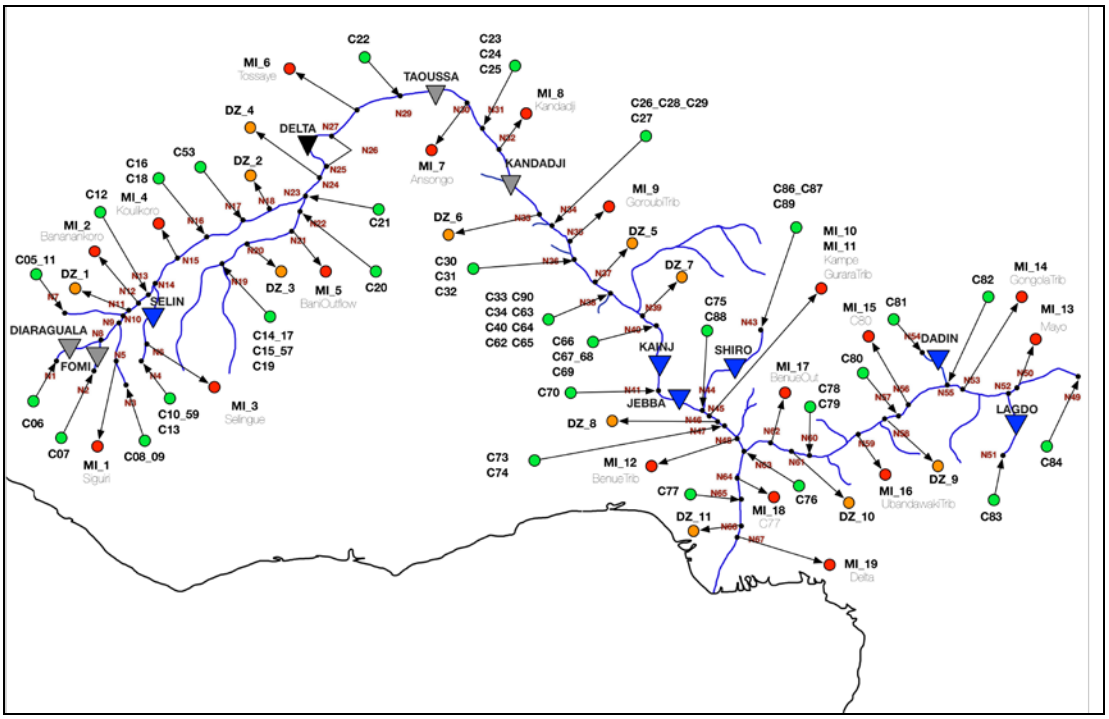

Figure 4.7 The schematic of the NRB water resources system. The green, red, and orange indicate the hydrological catchment (*ns*), domestic withdrawals (*nd*), and the irrigation nodes (*ni*) respectively. The triangles in blue, gray, and black colors represent the existing and planned reservoirs and the natural lakes (wetlands) respectively.

The seasonal time-series of basin runoff at 49 catchments are calculated using a series of simple, lumped parameter hydrology models (Thomas 1981). The runoff provided by the catchment nodes are then routed through the river basin network and allocated among various uses including municipal and industrial, irrigation, hydropower, fisheries and environmental sustainability.

The objective function Z of the model is to maximize the expected net present value (NPV) of the water resources system under climate uncertainty:

$$max\, Z = \sum_{v} p_v \left(- \sum_{nr} CK_{nr}^{v} - \sum_{ni} CIRR_{ni}^{v} - \sum_{neco} \sum_{y} \sum_{m} PECO_{y,m,neco}^{v} + \sum_{ni} \sum_{y} BIRR_{y,ni}^{v} + \sum_{nr} \sum_{y} \sum_{m} BHP_{y,m,nr}^{d} + \sum_{nr} \sum_{y} \sum_{m} BFSH_{y,m,nr}^{d} \right)$$

Equation 4.2

where v is the vertex index used in the scenario-tree representation of the problem, p_v is the probability weight associated with vertex v; y and m are time indices representing the year and the month; CK and $CIRR$ are the present value costs of new dams and hydro-agricultural infrastructure; $BIRR$, BHP and $BFSH$ are discounted economic benefits from irrigated agriculture, hydropower generation, and commercial fisheries respectively; and $PECO$ is the penalty term for not being able to maintain environmental flow targets. The optimization model also includes a series of constraints that defines the conservation of mass along the river, and the bounds for the municipal and industrial and agricultural water use, hydropower production as well as a series of nonanticipativity constraints to describe the scenario-tree structure.

A detailed description of the model formulations is given in Appendix C, and here we provide a brief description of each term included in the objective function (Equation 4.2). The cost of new dams CK is defined for three capacity alternatives, i.e., small, medium, and large sizes (Table 4.1). The cost of new hydro-agricultural infrastructure $CIRR$ is calculated based on new perimeter extension and new perimeter creation in each agricultural zone, which are constrained by given the predefined physical limits. Irrigation benefits $BIRR$ is obtained based on crop selection and calculated crop yields under the given land constraints. Hydropower generation benefits BHP is approximated from a series of linear regression equations that defines seasonal hydropower production based on releases through the turbines and lake levels. Finally, environmental flow penalties $CIRR$ are calculated by penalizing the negative deviations from the seasonal minimum flow targets at the predefined minimum flow check-points.

Table 4.1 Capacity alternatives for the Fomi, Diaraguala, Taussa, and Kandadji Dams (in Mm3). The associated present value capital costs are given in the parentheses.

Dam project	Size: small	Size: medium	Size: large
Fomi	5560 ($530 M)	6160 ($570 M)	6760 ($610 M)
Diaraguala	2400 ($250 M)	2700 ($280 M)	3000 ($310 M)
Taussa	2800 ($680 M)	3100 ($710 M)	3400 ($740 M)
Kandadji	1400 ($740 M)	1600 ($780 M)	1800 ($820 M)

Table 4.2 The upper constraints for development across the eleven irrigation zones

Irrig. zone	Current Irrigable Perimeter (Mm^2)	Max. Perimeter Expansion (Mm^2)	Max. New Perimeter 2020 (Mm^2)	Max. New Perimeter 2035 (Mm^2)	Max. New Perimeter 2050 (Mm^2)
DZ 1	147	71	283	707.5	707.5
DZ 2	1162	2280	253	633.5	633.5
DZ 3	44	236	944	2360.5	2360.5
DZ 4	208	35	139	346.5	346.5
DZ 5	541	334	1334	3335.5	3335.5
DZ 6	35	18	71	178.5	178.5
DZ 7	462	304	1217	3042	3042
DZ 8	214	323	2905	7262.5	7262.5
DZ 9	129	360	1442	3605	3605
DZ 10	50	156	1403	3508	3508
DZ 11	56	74	670	1674	1674
TOTAL	3047	4191	10661	26653	26653

4.4.4.2 Defining the scenario space

4.4.4.2.1. Generating climate variability realizations

The scenario generation process begins with sampling one hundred new stochastic realizations of the historical climate conditions (1955-2000 period) that consist of basin-wide, monthly time series of climate variables. The new climate realizations are obtained from a weather generator that couples a wavelet autoregressive model with a K-nearest-neighbors algorithm (Steinschneider and Brown 2013). The weather generator produces monthly time-series of total precipitation (mm) and minimum and maximum temperature (ºC) for the 49 sub-catchments within the river basin, while preserving: i) the spatial and temporal correlations among multiple sites and multiple climate variables, and ii) selected statistical properties of the historical, area-averaged annual precipitation, which are a mean of about 910 mm, a standard deviation of about 95 mm, and a low-frequency variability of

about 20-years. The climate traces produced by the weather generator show a good match to the historical data, with a periodicity of about 20 years (Figure 4.8-a), an annual mean of about 908 mm (Figure 4.8-b), and a standard deviation of about 90 mm (Figure 4.8-c).

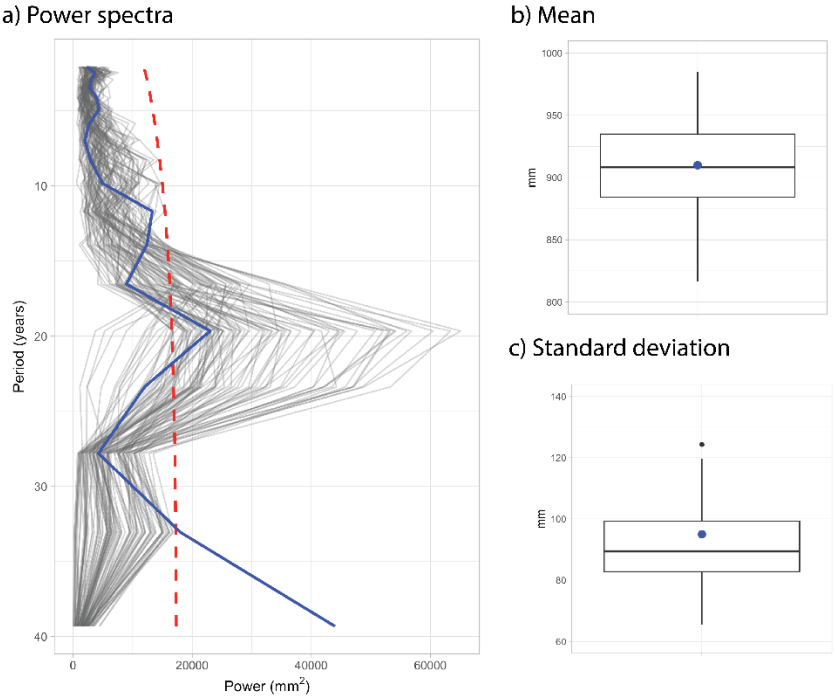

Figure 4.8 Comparison of annual precipitation realizations obtained from the weather generator and the historical data (1955-2000): a) Power spectra of annual precipitation realizations b) Boxplot of mean annual precipitation realizations, c) Boxplot of the standard deviation of annual precipitation realizations. In Figure a, the red line marks the confidence level at 0.90. In all figures, the blue color marks the indicated statistics of historical climate.

4.4.4.2.2. Identifying a small subset of representative climate realizations

The second step in the scenario development process is to identify a small subset of "representative" historical climate realizations within the initial set of hundred. The SMIP formulation used in this study is computationally demanding, and it is necessary to identify a small set of realizations that can represent the performance variation within the initial set.

This is done through a simplified optimization model and finding the maximum NPV achievable under each climate realization. The simplified optimization model evaluates

optimal decisions under perfect information, i.e., under known climate conditions over the course of the forty-five year planning period. The vector of NPV values computed from the hundred climate realizations ranges from about $95 B to $118 B, indicating that the system performance is sensitive to natural variability, even in the absence of climate change. Based on the outcomes, five representative climate traces are selected that correspond to the 5th, 25th, 50th, 75th, and 95th percentiles of the initial NPV distribution from the hundred historical realizations.

4.4.4.2.3. Constructing the climate change scenario tree

The third step is the development of a scenario tree to represent the gradual changes in mean temperature and precipitation over four stages (at years 2020, 2035, 2050, and 2065 respectively) and three consecutive intervals (at periods 2020-2035, 2035-2050, and 2050-2065 respectively). The climate change scenario tree is constructed in three sub steps:

1. *Develop a scenario tree of gradual temperature changes:* Gradual changes in mean temperature is represented by a binomial scenario tree (Figure 4.9-a). At every stage, temperature change scenarios transition either into a lower level DT_{low} or into an upper level DT_{up}, with associated transitioning probabilities of p(DT_{low}) and $p(DT_{up})$ respectively. The sequential branching process over three stages results in a total of eight scenarios spanning a range of final increases from 1 to 7ºC.

2. *Develop a scenario tree of gradual precipitation changes:* Gradual changes in mean precipitation is implemented by a trinomial tree (Figure 4.5). At every state scenarios branch into one of three options described by the lower DP_{low}, mid DP_{mid}, and upper DP_{up} levels with the probabilities of $p(DP_{low})$, $p(DP_{mid})$, and $p\left(DP_{up}\right)$ respectively. The trinomial scenario tree consists of a total of twenty-seven scenarios, spanning a range of relative changes from -45% to +45%.

3. Construct a joint scenario tree of precipitation and temperature changes: In the final step, the temperature and precipitation scenario trees (Figure 4.9 and Figure 4.10) are combined into a joint scenario tree of climate changes. This is done by enumerating all possible bivariate combinations at each stage. For example, scenarios at the first stage branch out into six possible paths described by each unique combination of possible temperature changes (0.5 and 1.5 ºC) and precipitation changes (-15%, 0%, and 15%). Each of those six scenarios further branches out into six pathways at the second stage and resulting in a total of $3^6 = 216$ climate change scenarios in the final stage (Table 4.3). Assuming that the precipitation and temperature variables are independent, the joint transition probabilities $p(DT_i, DP_j)$ can be expressed as:

$$p(DT_i, DP_j) = \frac{p(DT_i)\,.\,p(DT_j)}{\sum_i \sum_j p(DT_i)\,p(DT_j)}$$

Equation 4.3

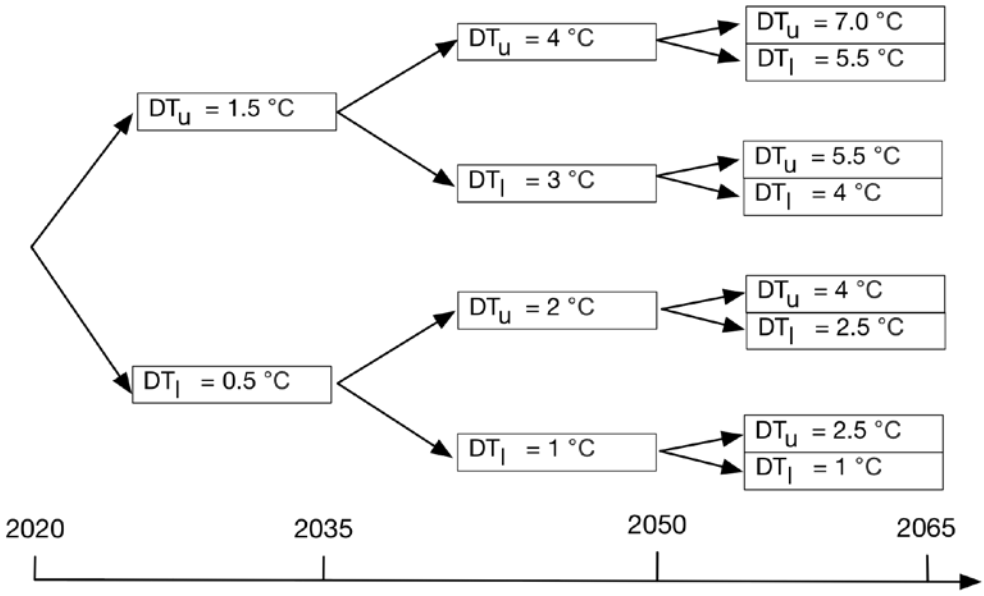

Figure 4.9 The binomial scenario tree representing future temperature changes. Each path shows the evolution of one possible scenario over the subsequent periods of 2020-2035, 2035-2049, and 2050-2065 respectively. Indices DT_l and DT_u represent scenario transitionings into lower and upper levels at each stage.

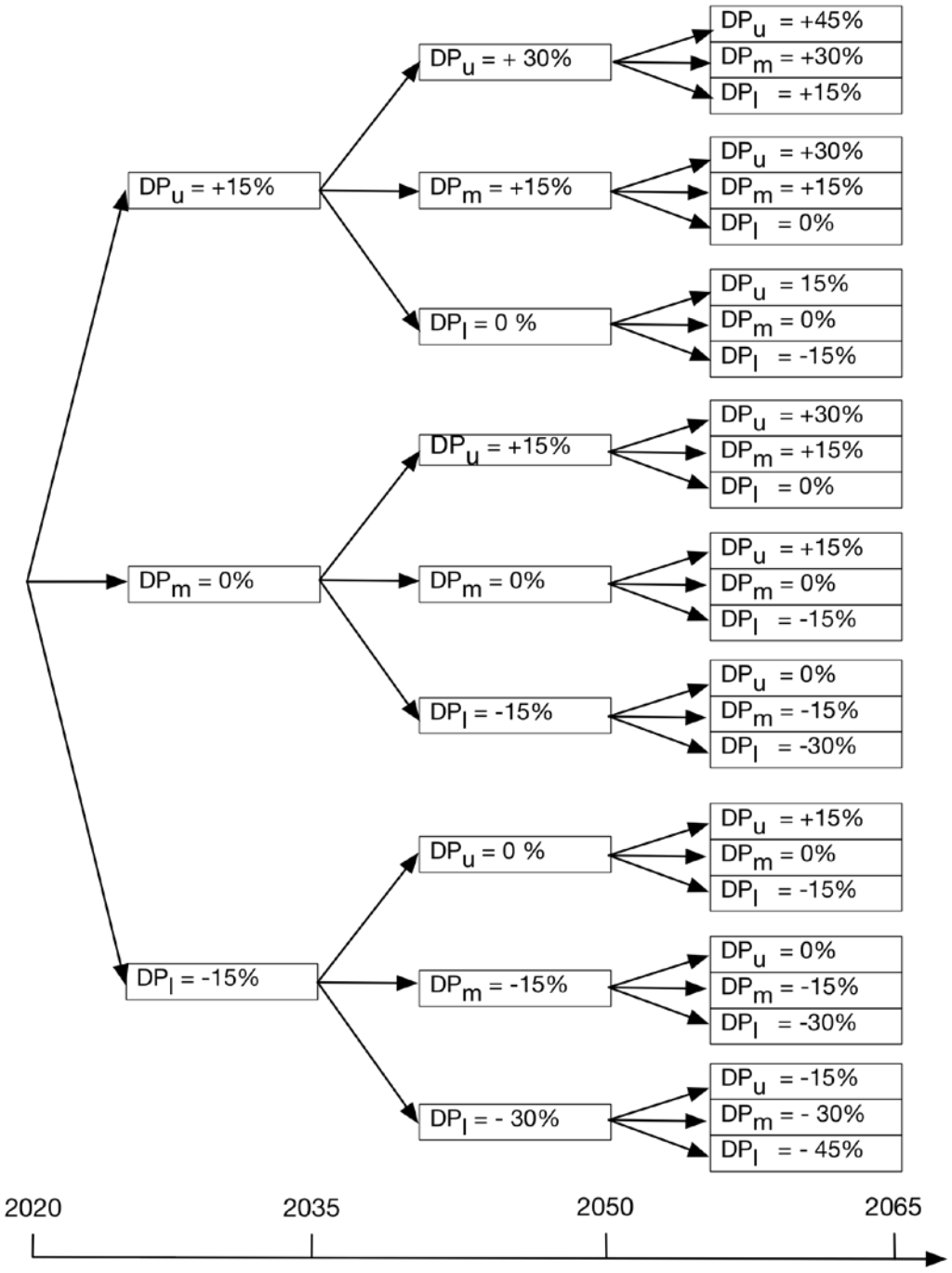

Figure 4.10 The trinomial scenario tree representing future precipitation changes. Each path shows the evolution of one possible scenario over the subsequent periods of 2020-2035, 2035-2049, and 2050-2065 respectively. Indices DP_l, DP_m, and DP_u represent scenario transitionings into lower, mid, and upper levels at each stage.

Table 4.3 Uncertainty range at each stage of the climate change scenario tree

Discrete time stages represented	Number of unique scenarios	Range of temperature change uncertainty	Range of precipitation change uncertainty
Stage 1 (year 2020)	1	-	-
Stage 2 (year 2035)	6	0.5 – 1.5°C	±15%
Stage 3 (year 2050)	36	1 - 4°C	±30%
Stage 4 (year 2065)	216	1 - 7°C	±45%

Overall, the scenario tree generation method presented here aims to provide a fuller evaluation of plausible climate changes over the forty-five year planning period. The proposed method provides at least two major advantages over the GCM-based scenarios-tree generation techniques (Ray et al. 2012; Cai et al. 2015) that are illustrated in Figure 4.11. First, the prosed procedure takes into account a broader range of uncertainty without being restricted to the results derived from GCM projections, especially from the mid-21st Century and onwards where the uncertainty in climate projections are expected to be the most. Second, the climate change factors used to define the scenario paths provides a uniform exploration of the uncertainty space, i.e., with a 1ºC step in the second and third stages, and a 1.5 ºC step in the fourth stage for temperature changes and with a %15 step for precipitation over the entire period (Figure 4.11). In contrast, if the scenario tree is developed based on GCM projections, the resulting scenarios would be clustered in certain areas of the climate uncertainty space (Figure 4.11). Given the fact that such clustering effects are likely to be dependent on many uncertainty factors, such as emission scenarios, initial model conditions or structural model similarities, this would be an important source of bias.

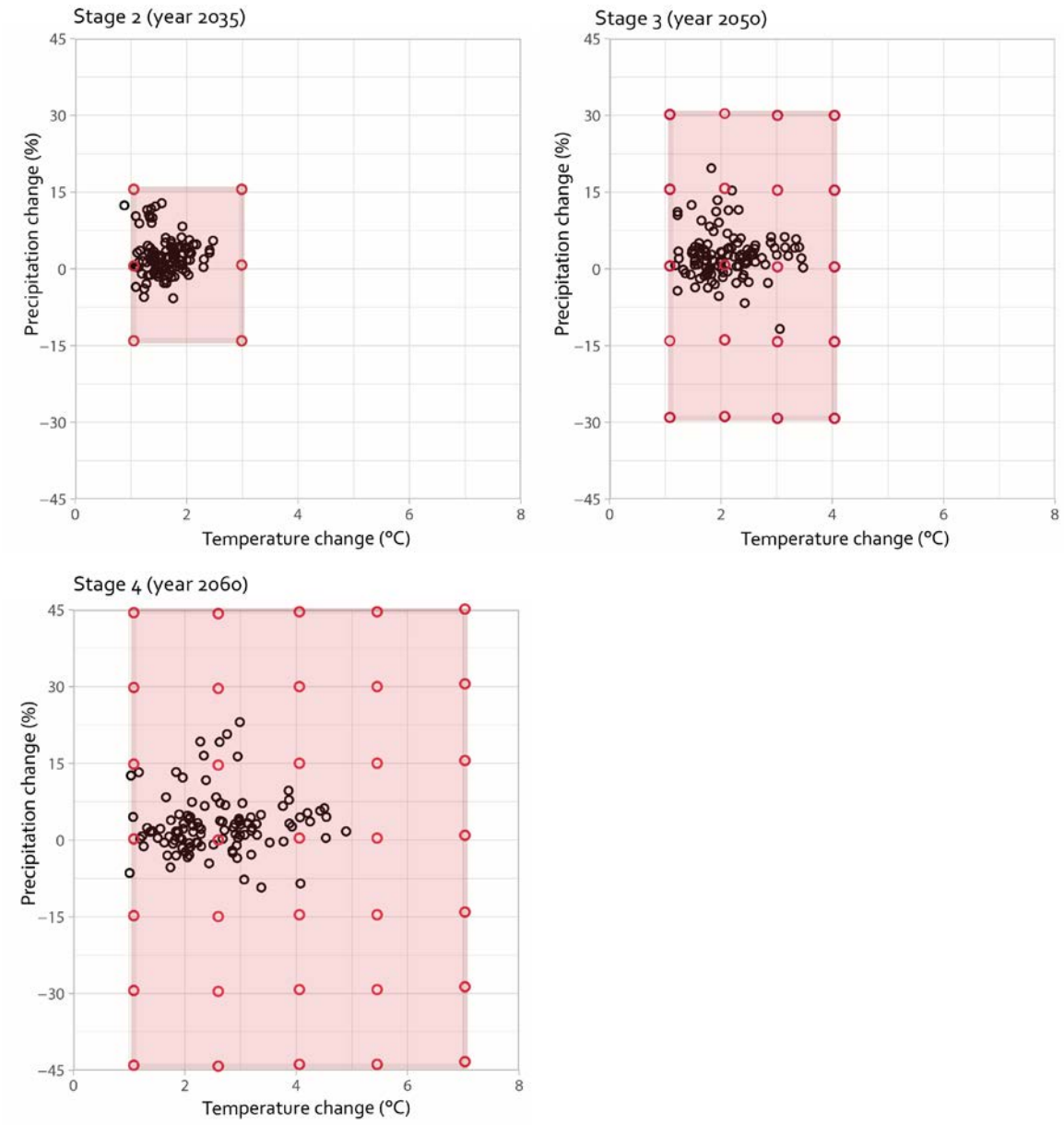

Figure 4.11 Representation of climate change uncertainty within the climate change scenarios at stage 2 (year 2035), stage 3 (year 2050), and stage 4 (year 2065) respectively. The circles in red color represent combined temperature and precipitation change factors applied at each stage. The circles in black color show associated mean temperature and precipitation changes from the GCM projections.

4.4.4.2.4. Obtaining transient climate scenarios

The last step of the scenario generation process is to obtain a set of forty-five-year transient climate scenarios reflecting both natural climate variability and long-term climate changes. This is done by dividing each of the five natural climate realizations into three equal

intervals (representing the periods of 2020-2035, 2035-2050, and 2050-2066 respectively). A total of 216 climate changes scenarios (Table 4.3) are then imposed over each of the natural variability realizations through additive or multiplicative change factors. For example, a 1.5ºC increase in the year 2035 is reflected in the first planning period (2020-2035) by a set of additive factors from 0 ºC (in the year 2020) to 1.5 ºC (in the year 2035). Similarly, a 15% increase in precipitation is reflected in the first planning period through a set of multiplicative factors from 0% (in the year 2020) to 15% (in the year 2035). The process results in a total of 1080 scenarios (216 climate change x 5 different climate scenarios organized through five climate scenario trees.

4.4.4.3 Generating belief dominated planning pathways

In the third step, a multi-stage SP model is repeatedly used to generate multiple flexible planning trajectories by taking into account the uncertainty associated with occurrence likelihoods of the plausible climate changes (Section 4.2.4.5) and the uncertainty arising from natural climate variability (Section 4.2.4.3).

The uncertainty resulting from the occurrence likelihoods of plausible climate changes is explored by varying the scenario tree transitioning probabilities (Figures 4.9 and 4.10). In doing this, four PMFs are specified for temperature changes to describe the probabilities of transitioning into a lower or an upper scenario $p(DT_{low})$ and $p(DT_{up})$. These four PMFs represent a range of beliefs about the future temperature changes referred as "mildly warm", "moderately warm", "very warm", and "extremely warm" futures (Figure 4.12 -a). For example, the probability of transitioning to a lower temperature change p(DT_{low}) is set to 0.8 under the "mildly warm" belief, and 0.2 under the "extremely warm" belief. Similarly, five PMFs are specified for precipitation changes to set the probabilities of

transitioning to a lower, medium, and an upper scenario, i.e., $p(DP_{low})$, $p(DP_{mid})$, and $p(DP_{up})$. These five PMFs describing alternative beliefs about future precipitation change are called as "very dry", "dry", "normal", "wet", "very wet" futures (Figure 4.12 –b). Under a "very dry" belief, a high value of 0.6 is assigned to p(DP_{low}). On the other extreme of a "very wet" belief, p(DP_{low}) is set to 0.1. These two sets of PMFs are then combined to obtain twenty bivariate PMFs of temperature and precipitation changes. In addition, one other bivariate PMF is specified as a "non-informative" belief to assign equal weights to all transition probabilities for temperature and precipitation changes.

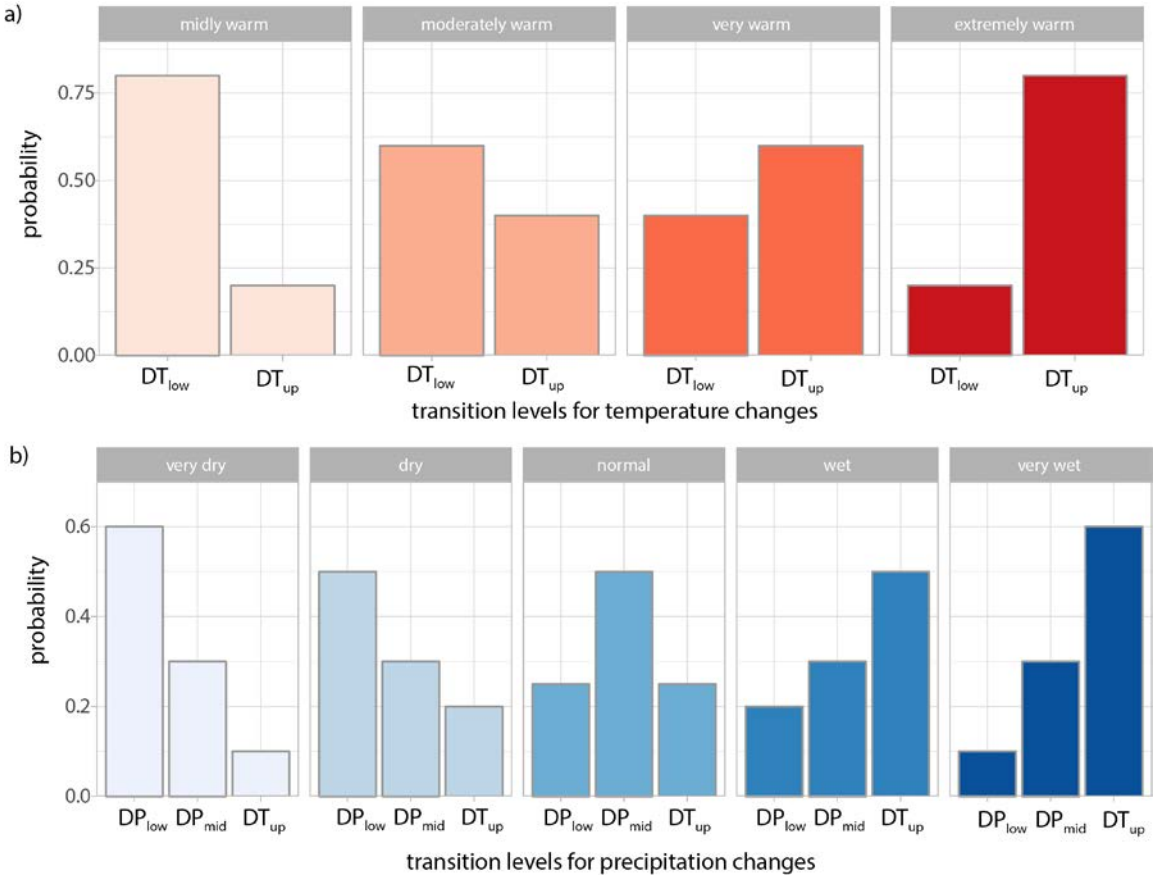

Figure 4.12 Belief functions defining the probability weights assigned for scenario transition levels a) temperature changes, b) precipitation changes.

Finally, the inventory of belief dominated planning trajectories is obtained by executing the SP model 130 times (from the combinations of 26 climate change beliefs and five natural variability realizations), resulting in a total of 28,080 belief dominated planning pathways.

4.4.4.4 Identifying robust development pathways using climate information

In the final phase of the analysis, the inventory of 28,080 belief dominated planning pathways obtained from the SP model are post-processed to identify one or few frequently found solutions. GCM projections are also incorporated at this phase, to inform the decision-making process on the solution pathways that are associated with 'more likely' futures. This was done by first calculating the mean basin discharge under each GCM projection, and then fitting the results to a Gaussian PDF. The specified PDF of mean discharges from the GCM projections is then used to weight the set of 28,080 solutions based on the mean discharge value associated with each solution.

4.5. Results

4.5.1. Variation in economic outputs under climate variability and change

Table 4.4 summarizes key findings from the set of 22,680 optimal planning trajectories obtained by solving the stochastic optimization repeatedly over 21 bivariate PMFs of temperature and precipitation changes and five climate variability realizations. Across this large inventory of solutions, the mean basin discharge varied from 80 to 396 km^3 per year, with an average of 196 km^3 per year. In contrast, mean basin discharge is 205 km^3 per year under the historic climate, and ranges from 187 to 220 km^3 per year across different natural climate variability realizations (i.e., without climate change effects).

The total NPV from the water resources system is found to be highly sensitive to climate conditions, ranging from about $27 Billion to $73 Billion. Natural climate variability itself also results in a considerable variation in NPV up to 20%. Irrigation and hydropower are the two largest sectors contributing to the NPV, ranging from 21 to $40 Billion, and from 20 to $27 Billion respectively (Table 4.4). The results of the stochastic analysis with under uniform probability weights yield very close results to the average values obtained from the 130 stochastic solutions, with almost equal NPV values of about $50 Billion. It is also important to note that that the costs of new infrastructure developments, especially the costs associated with the four new dams is about an order of magnitude less than the benefits from irrigation and hydropower (i.e., about 1 to $7 Billion) (Table 4.4).

Table 4.4 Summary of results across the optimization runs. Under the climate change analysis, "stoc. uniform" indicates the results under the uniform temperature and precipitation change PMFs. "Stoc. mean" and "Stoc. range" show the results across all evaluated PMFs. Under the historical climate analysis, "Hist. climate" represents results under historical climate time-series. "Var mean" and "Var range" represents the results across the five natural climate variability realizations.

Results	Mean Q (km3/yr)	NPV ($1B)	Irrig benefits ($1B)	HP benefits ($1B)	Dam costs ($1B)	Irrig infra costs ($1B)	Ecoflow penalty ($1B)
Climate change analysis							
Stoc. uniform	195	50.5	32	26	3.1	2	0.3
Stoc. mean	196	50.3	33	27	3	2.1	0.4
Stoc. range	173 – 218	27 - 73	7.6 – 13	6.8 - 9.1	1.1 - 6.7	0.7 - 3.2	0.2-0.6
Historical climate analysis							
Hist. climate	205	53	35	25	9.8	3.2	> 0.1
Nat. var mean	202	52	31	25	9.1	3	> 0.1
Nat. var range	187 - 220	50-61	42 - 48	27 - 36	8.3 - 10	1.8 - 3.5	0 - 0.1

4.5.2. Alternative water infrastructure planning trajectories

Figure 4.13 depicts the optimal dam development pathways obtained from the stochastic analysis. An interesting outcome of the analysis is that there are only eleven unique solutions across the database of 22,680 solutions. Among these optimal pathways, all of them suggests that the Taoussa Dam shall be postponed until 2035 or until 2050 (Figure 4.13). Another important conclusion is that all optimal pathways except for one indicate that The Fomi shall be implemented, with the largest capacity option of 6760 Mm^3. Besides these two solid findings, results strongly reflect underlying assumptions on climate scenarios, and the probabilistic beliefs about climate change.

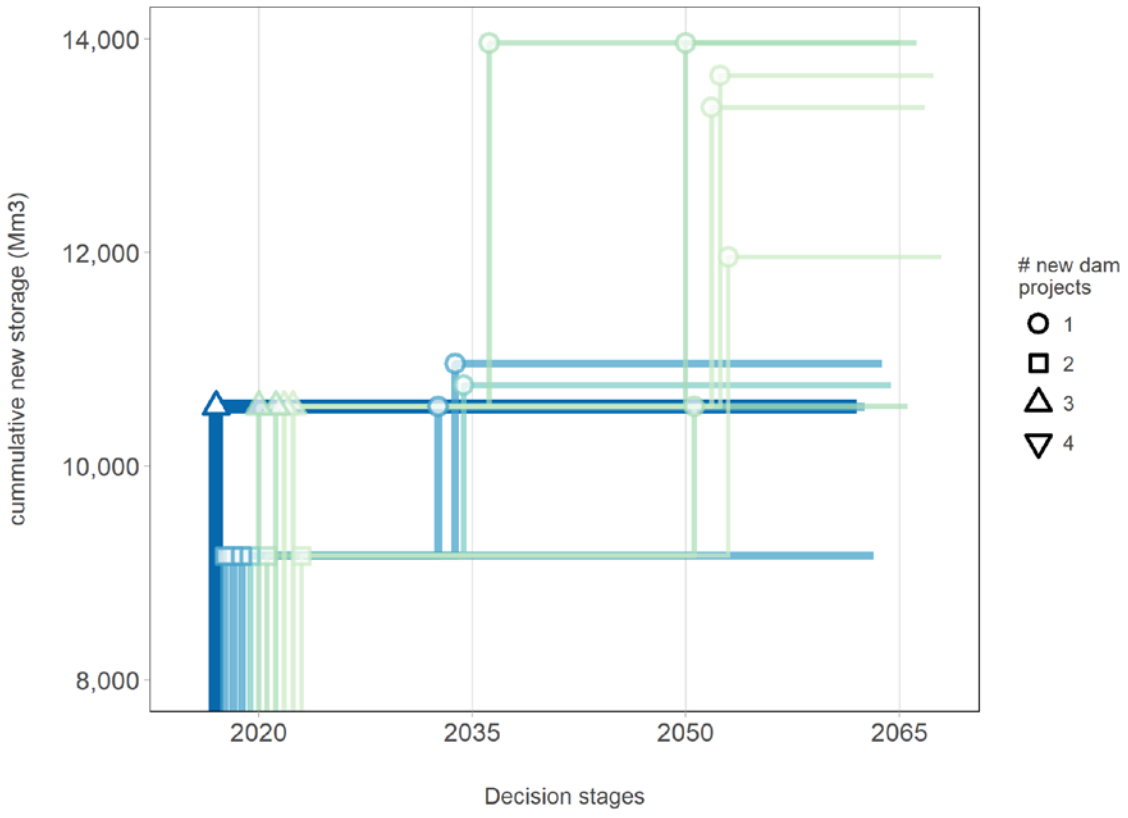

Figure 4.13 The optimal planning trajectories derived from the repeated stochastic optimization analysis. In the figure, x-axis shows the decision stages at the years 2020, 2035 and 2050 respectively. Y-axis marks the cumulative new storage capacity at each decision stage. The shapes indicate the number of new dam projects at each decision point. The color scheme indicates how often a solution trajectory is obtained (darker colors indicate a higher frequency).

Given that the solutions are derived from a broad range of climate uncertainties, one useful analysis on the results is to rank the pathways based on the appearance frequency within the entire solution database. Table 4.5 shows that first planning pathway, with one large dam (Fomi) and two small dams (Diaraguala and Kandadji), represents about 70% of all solutions. The second solution, which suggests a smaller capacity Fomi Dam is the second most frequent pathway, with a coverage of 10%. At this point, one can also make use of climate information to place a larger value on solutions associated with more plausible futures. In this work, we incorporated GCM information by first calculating mean basin discharge from each of the 110 GCM projections and then fitted the results to a Gaussian PDF. Next, we weighted each climate scenario based on their distance to the GCM-derived Gaussian distribution, and then computed a "climate-informed dominance" based on the weighted results. Column 7 on Table 4.5 shows that GCM-informed dominance is similar to the scenario neutral case, especially for the first the pathways.

Table 4.5 The features of the optimal water planning trajectories derived from repeated stochastic optimization analysis. Columns 2-5 shows the suggest capacity and the implementation year Column 6 shows the coverage of the solution within the entire database. Column 7 shows the weighted coverage based on GCM projections.

	Fomi Dam	Diaraguala	Taoussa	Kandadji	Dominance (%)	Climate-informed Dominance (%)
1	Large (2020)	Large (2020)	-	Small (2020)	68.9	67.2
2	Medium (2020)	Small (2020)	-	Small (2020)	10.2	12.8
3	Large (2020)	Small (2020)	-	Small (2020)	9.6	2.0
4	Large (2020)	Small (2020)	-	Small (2035)	6.8	10.1
5	Large (2020)	Large (2020)	-	Small (2035)	2.1	2.8
6	Large (2020)	Medium (2020)	Small (2035)	Small (2020)	0.9	1.6
7	Large (2020)	Small (2020)	-	Small (2035)	0.9	2.8
8	Large (2020)	Medium (2020)	Medium (2035)	Small (2020)	0.5	0.3
9	Large (2020)	Medium (2020)	Small (2035)	Small (2020)	0.1	0.0
10	Large (2020)	Medium (2020)	Small (2035)	Small (2020)	0.1	0.3
11	Large (2020)	Small (2020)		Small (2035)	0.0	0.0

The results depicted in Figure 4.13 and Table 4.5 can be further analyzed by revealing the climate conditions associated with most prominent planning pathways. We first parsed the range of mean basin discharges from the analysis (ranging from about 100 to 380 km3 per yr) to bins with interval sizes of 20 km3 per year and then identified most frequently found trajectory within each bin. Next, we visualized the results along with the probabilistic information derived from the GCM projections (Figure 4.14).

Figure 4.14 shows that that the two solutions previously depicted in Table 4.5 are superior to all others. Results show that the first planning trajectory is the most frequently found solution when the mean basin runoff is less than 140 km^3 per year, which is very plausible based on the current generation of climate model projections. As a result, the

planning trajectory suggesting to implement the Fomi and Kandadji Dams in Large size, and Diaraguala in small size is identified as the most robust solution.

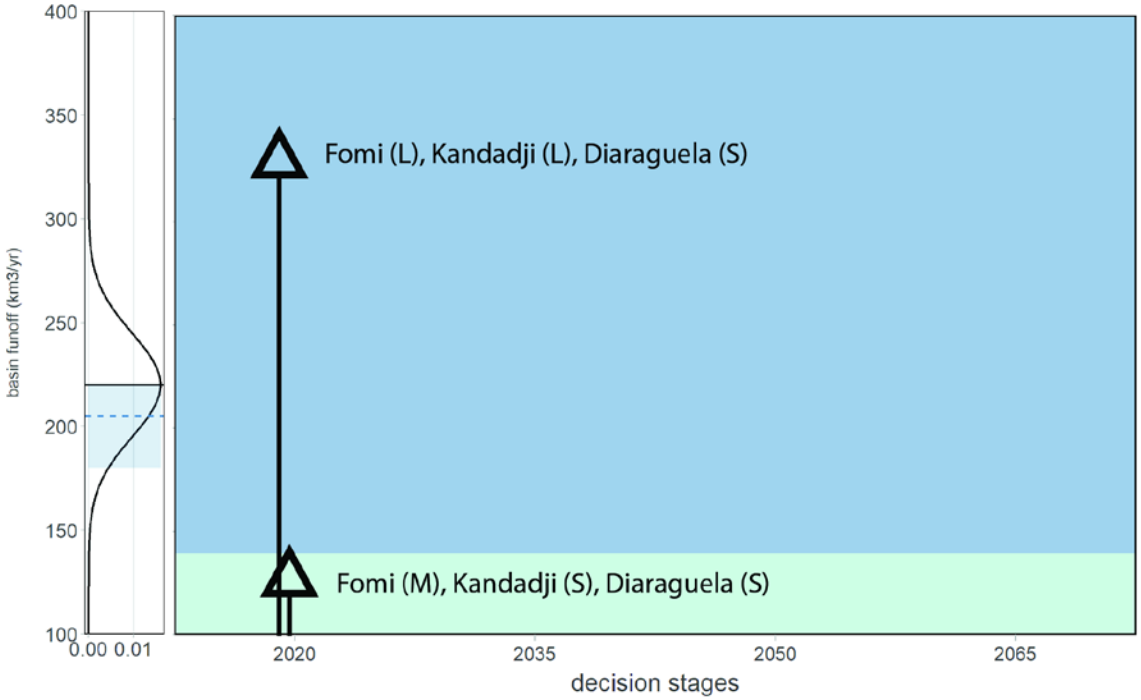

Figure 4.14 The final set of candidate planning trajectories identified through the analysis. In the figure, each color region indicates the mean run-off interval, where the indicated planning trajectory is the frequently found solution. The PDF on the left of the figure indicates the simulated runoff range from the GCM projections. The solid line is the mean of the GCM data. The gray ribbon indicates the natural variability range.

4.5.3. Value of stochastic analysis

In the final part of the study, we evaluated the added value gained by using a stochastic model based on the value of stochastic solution VSS (Birge and Francois 2011). In the analyses involving stochastic optimization, VSS shows the expected value of including uncertainty by quantifying the expected difference in cost for a decision based on stochastic analysis and one that ignores uncertainty. The VSS measure is calculated from the difference between the stochastic analysis, referred as the recourse problem solution (RP) and the expected value problem EEV:

$$VSS = RP - EEV$$

Equation 4.4

The parameter EEV measures how the mean value solution performs, allowing the second stage decisions and onwards to be chosen optimally as a function of using the EV solution and stochasticity (Birge and Louveaux 1997). EEV is calculated in three steps: i) solve the related average scenario problem, ii) fixing the first stage decisions for each scenario in the SP based on the average scenario solution, and iii) resolving the SP. We applied the three step procedure under the uniform scenario probabilities case for each climate variability trace obtained a range of VSS values ranging from $11 Million to $236 Million, and giving a value of $ 95 Million on average.

Figure 4.15 shows how VSS values change across the twenty probability distributions explored in the analysis (i.e., from each combination of the four temperature changes PMFs and the five precipitation change PMFs). The results, which are averaged over the five natural variability realizations show that the stochastic the stochastic solution provides the least added value under wet and mild futures, and the greatest benefits under moderately dry and warm conditions (Figure 4.15).

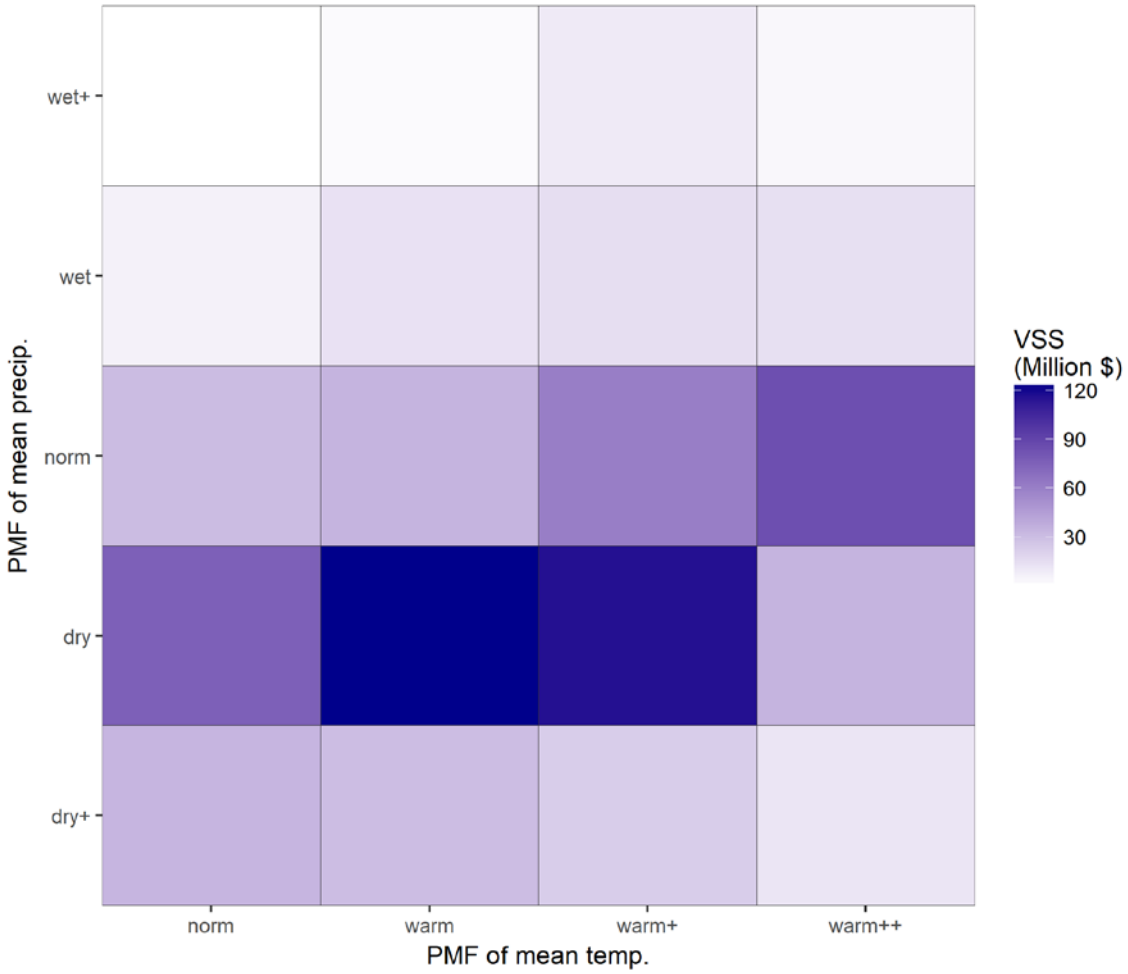

Figure 4.15 Variation in the value of the stochastic solution (VSS) measured under different probabilistic assumptions. Each value on the x-axis shows a PMF associated with the mean temperature changes described as normal, mildly warm, moderately warm, and very warm. Similarly, each value on the y-axis represents a PMF ranging from very dry, dry, normal, wet, and very wet climate futures.

The relatively low VSS value obtained in the analysis (i.e., less than 1% of the objective function value) can be attributed to a number of factors. First, the VSS calculation technique mainly focuses on the improvements in the first stage solution and therefore indicates a lower bound of the real VSS. Since the problem evaluated in this work make use of transient scenarios (i.e., scenarios that gradually evolve), the divergence among the climate conditions in the first period of the analysis is relatively small. A second factor contributing to low VSS values is the physical bounds defined for the irrigation development problem.

Results show that most scenarios, except for the very dry futures can provide make use of full irrigation area available.

4.6. Discussion and Conclusions

This work presented an analytical framework to support basin-level sequential water systems planning under climate uncertainty. The primary motivation for this framework is to apply the principles of bottom-up, robustness-based climate risk management to large-scale river basin planning problems that involve multiple sources of temporal and spatial complexities. To achieve this, the framework employs a multi-stage stochastic optimization approach with a number of key innovations over their existing use in water planning. First, the framework develops a scenario-tree generation technique that combines stochastically sampled climate realizations with transient temperature and precipitation change factors to provide a wide range of climate conditions without relying on climate models. Second, we address the challenge of assigning probability weights to scenarios in multi-stage optimization, which potentially limits their use in problems involving long-term climate changes. To circumvent the issue of assigning *ex-ante* probability weights, we systematically explore a wide range probabilistic distributions without making any prior preference. We then apply multi-stage stochastic optimization repeatedly over the domain of generated scenario trees and probability distributions in an attempt to obtain a diverse ensemble of optimal planning trajectories conditioned on the underlying assumptions. Within this large ensemble of solutions, we then identify a small subset of optimal sequences that are robust (insensitive) to underlying climate scenarios and probability weights and therefore are preferable under a deeply uncertain climate. At the final step, we make use of GCM projections for the final preference set of robust planning trajectories.

The framework is applied to the Niger River Basin to assess the sizing, timing, and sequencing of a number of water infrastructure projects considering long-term economic benefits over a period of forty-five years, on a seasonal basis, considering three decision stages corresponding to the years 2020, 2035, and 2050 respectively. As part of the application, a diverse portfolio of optimal planning trajectories was developed considering the sizing, timing, and sequencing of four large dams. The results are compared to those obtained from a more conventional deterministic optimization and found to be substantially different.

While our approach provides certain advantages over existing optimization or Monte-Carlo based frameworks, there are a number of caveats that can limit its application to real-world planning problems. First, the current scenario-generation procedure is designed to address climate change and does not consider the uncertainties associated with population, demand changes, or societal preferences which can also be significant over longer time scales. In the context of long-term sequential water infrastructure planning, several recent studies have explored multiple sources of uncertainties simultaneously (Jeuland and Whittington 2014; Beh et al. 2015b).

A second limitation is a computational burden related to repeated application of basin-scale multi-stage optimization (Mortazavi et al. 2012). For large-scale problems, as the Niger River Basin application introduced in this work, the use of detailed process-based models can be very prohibitive. In this work, we employed linear optimization model that runs at a seasonal step, to reduce the overall computational demand, however, at the expense of realism. One alternative is to replace process-based detailed modeling processes with statistical meta-models based on machine learning (Cai et al. 2015) or artificial neural networks (Beh et al. 2017).

4.7. Acknowledgments

This work was partially funded by the World Bank as part of the project "Climate Risk Assessment for the Niger River Basin." The authors would like to express their gratitude to Scot Steinscheineider for providing the weather generator code, and the Niger Basin Authority for providing hydroclimatic and socioeconomic data.

CHAPTER 5

CONCLUSIONS

The primary goal of this dissertation was to develop new, improved analytical methods to aid the planning of water infrastructure systems under a deeply uncertain future. In this context, the dissertation aimed to address three open research challenges faced in the contemporary practice of water systems planning. The first challenge is about how to design long-lived, costly water infrastructure systems under a deeply uncertain climate, and how to make the best use of GCM projections in the decision-making processes of such infrastructure (Chapter 2). The second challenge is how to quantify multiple, compounding sources of climate, socioeconomic, and demographic uncertainties in robustness-based water infrastructure planning by concurrently considering stakeholder beliefs and model outputs (Chapter 3). Finally, the third challenge is related to adaptive water planning at the basin-level. It deals with the question of how to plan and schedule multiple water infrastructure investments in the best way considering climate change uncertainty (Chapter 4).

The first study presented in Chapter 2 applied decision scaling concepts to the design of the turbine capacity for a run of the river hydropower facility. This study differs from the previous applications of decision scaling, which have been used to assess the impact of possible climate changes on a water resources system. Also, the work provided the first in depth comparison of the decision scaling method to a more conventional GCM-driven, top-down analysis of water infrastructure systems. The comparative analysis demonstrated the potential benefits of the proposed approach in three key areas: i) a fuller and more systematic exploration of the plausible climate changes, ii) better accounting for the potential effects of natural (inherent) uncertainty, and iii) a more reasonable and flexible use of external climate information in the decision analysis processes.

The work on Chapter 3 demonstrated an improved decision-analytical framework for making informed decisions in water systems planning under long-term climate and demographic uncertainty by explicitly considering subjective information or beliefs about the future states of the world. The framework integrates a bottom-up, robustness-based risk assessment approach called decision scaling with Bayesian network modeling, a popular tool for visualizing and propagating probabilistic information in complex systems. The coupled framework allows an explicit representation of conditional dependencies among various types of uncertainties and provides an estimation of the joint probability distribution of problematic conditions that were identified through an exhaustive vulnerability analysis. The proposed approach is expanding the existing method in several key directions. First, the probabilistic network approach allowed stakeholder beliefs and local information to be quantified and incorporated into the risk assessment process. The presented framework also allowed blending of multiple sources of information in a transparent, coherent probabilistic framework that can be easily communicated to the stakeholders and public. The results from the BNDS framework is also coupled with a data-mining algorithm, PRIM to obtain high-risk scenarios.

Chapter 4 presented an analytical framework to support basin-level sequential water systems planning under climate uncertainty. The primary motivation for this framework was to apply the principles of bottom-up, robustness-based climate risk management to large-scale river basin planning problems that involve multiple sources of temporal and spatial complexities. To achieve this, a multi-stage stochastic optimization method is developed with a number of key innovations over their existing use in water planning. First, the framework incorporated a new scenario-tree generation technique that combined stochastically sampled climate realizations with transient temperature and precipitation

change factors without relying on climate models. Second, since no prior assumption was made on the probability weights of climate change scenarios, a broad range of probability distributions were systematically explored within a multistage stochastic optimization framework. The analysis yielded a diverse ensemble of optimal planning trajectories conditioned on the underlying probabilistic assumptions. Finally, a small subset of infrastructure development pathways was identified that were found to be insensitive to the underlying climate scenarios and probability weights. Overall, the sequential water infrastructure planning framework presented in Chapter 4 shows an innovative way to use stochastic optimization under imprecise probabilistic information.

This dissertation demonstrated how subjective, inherently uncertain belief information could be integrated to robustness-based water resources planning for different types of problems. However, the value of the methods presented in this work is still unclear, and more work is needed to assess them. One shall also keep in mind that the methods presented in this work provide engineering-based, analytical solutions that are intended to aid decision-making processes. When designing complex water infrastructure systems, planners shall also consider the societal, political, and environmental concerns side with engineering solutions.

APPENDIX A

DESCRIPTION OF THE COUPLED HYDROLOGY AND WATER RESOURCES SYSTEM MODEL OF THE MWACHE SYSTEM

This section describes the details of the coupled water resources simulation model used for the analysis in Chapter 3. Monthly run-off from the Mwache River and reservoir operations are simulated using a coupled model application implemented in R. Basin hydrology are simulated via a two-compartment, parsimonious, lumped parameter watershed model (Thomas 1981; Martinez and Gupta 2010). The hydrology component of the coupled model application accepts monthly precipitation and potential evapotranspiration as inputs and generates monthly streamflow as output. Simulated streamflow is then fed to the reservoir simulation component, which calculates monthly storage volumes and the releases to the downstream users based on the principles of mass conservation and specified model parameters.

The entire drainage area at the upstream of the Mwache Dam (about 2275 km^2) is modeled as a single catchment due to the availability of only one streamflow gauge in the region (station 3MA03). The runoff response of the Mwache river is calibrated over a 10-year period from 1980 to 1990 against the observed streamflow record, using the Princeton University Terrestrial Hydrology Research Group's gridded meteorological data set (Sheffield et al. 2006). The predictive performance of the hydrologic model is evaluated using the Nash–Sutcliffe model efficiency (NSE) coefficient:

$$NSE = 1 - \frac{\sum_{t=1}^{T}(Q_0^t - Q_m^t)^2}{\sum_{t=1}^{T}(Q_0^t - \overline{Q_o})^2}$$

Equation A.1

where, Q_0^t is the observed discharge at period t; Q_m^t is modeled discharge at period t; $\overline{Q_o}$ Is the mean observed discharge over the simulation period T. NSE values range from -∞ to 1, in which a value of 1 corresponds to a perfect match of the modeled discharge to the observed data. The computed NSE value over the calibration period was found to be 0.43, which is decided to be as acceptable given the spatial and temporal limitations in the hydroclimate data (Figure A.1).

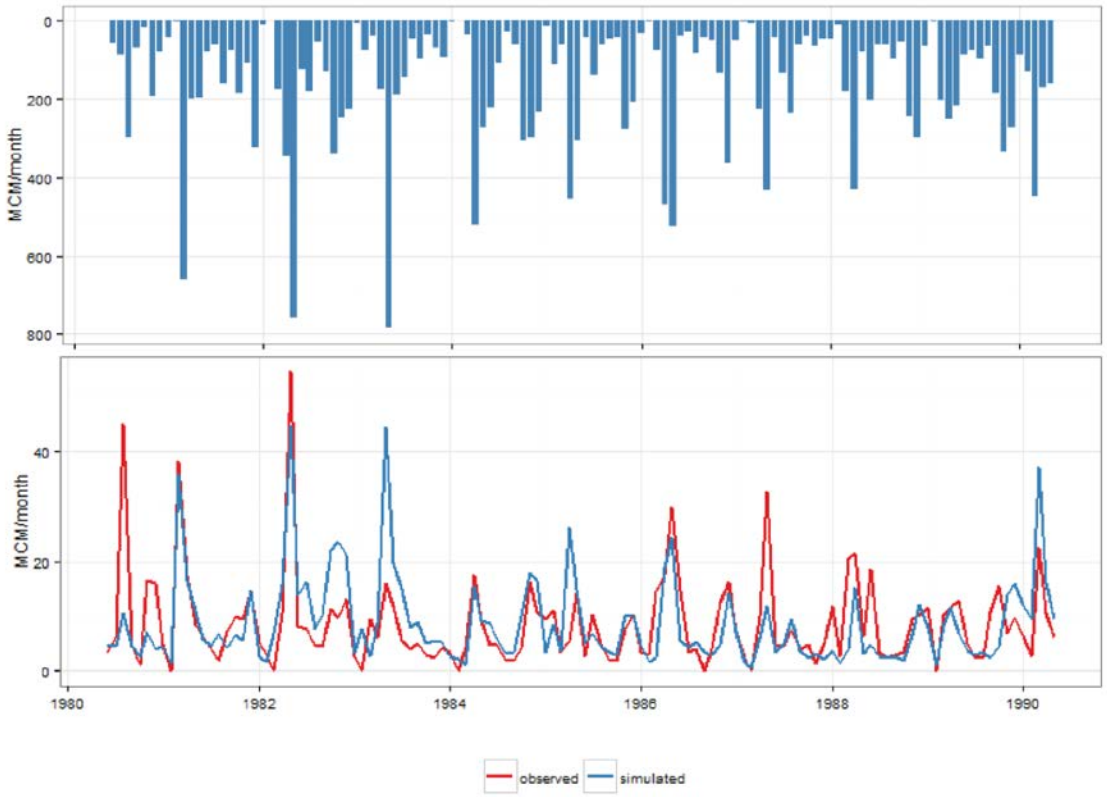

Figure A.1 Hydrologic calibration results for the Mwache River from June-1980 to May-1990. The top figure shows monthly rainfall (in Mm^3 per month). The bottom figure shows the observed vs. simulated streamflow (in Mm^3 per month).

The reservoir component of the simulation model is set considering all available information in the detailed design report of the Mwache Dam (CES 2014). For the scope of the analysis, two downstream water uses are considered that are the total municipal demand

from the target districts of Mombasa, and environmental flow requirements at the downstream of the Mwache Dam respectively. Monthly releases from the reservoir are calculated with the assumption that the priority is to meet the proposed environmental release targets by WRMA, and then meet the domestic demand target for the given month as much as possible. Adopted environmental release targets are defined based on the historical flow exceeded 95% percent of the times (i.e., Q95 value), which is in the order of 8 Mm^3 per year (Table A.1). Planned irrigation demand from Mwache Dam is low priority and was not included in this analysis.

Table A.1 Monthly Q95 values and the adopted environmental release targets for the Mwache Dam

Month	Q95 value (Mm^3)	Adopted flow target (Mm^3)
Jun	1.06	0.82
Jul	0.94	0.76
Aug	0.69	0.55
Sep	0.00	0.00
Oct	0.00	0.00
Nov	0.50	0.40
Dec	1.56	1.26
Jan	1.05	0.83
Feb	0.00	0.00
Mar	0.00	0.00
Apr	2.18	1.69
May	1.85	1.49

Mass balance in the reservoir ensures that at any given period t, the total inflow Q_t is equal to the sum of total outflow R_t, the net change in storage ΔS_t, and the losses L_t:

$$Q_t = R_t + \Delta S_t + L_t$$

Equation A.2

Reservoir storage volume in period t, S_t is constrained by the reservoir storage capacity K and the dead storage volume S_d. For simplicity, S_d is set to be 20 Mm^3 and assumed to be independent of K. The gradual reduction in the maximum active storage capacity is also considered due to the sediment accumulation in the reservoir. The sediment accumulation is estimated based on the trapping efficiency formula (Vörösmarty et al., 2003):

$$TE = 1 - (0.05 / \tau_r^{0.5})$$

Equation A.3

where TE is the annual sediment trapping efficiency (%) and τ_r is the mean water residence time in the reservoir given by the ratio of storage capacity to mean annual flow ($years^{-1}$). Based on the observed historical streamflow over the 1976-1990 period, the sediment trapping efficiency of the Mwache Dam is about 95% across the four design alternatives. Over the same period, annual sediment flux to the Mwache Dam is estimated to be 0.615 Mm^3 by the project consultant (CES 2014). Based on these estimates, annual sediment load trapped in the Mwache Dam is about 0.62 Mm^3 (Table A.2).

Table A.2 Annual sediment accumulation estimates under the storage design capacity estimates of 80, 100, 120, and 140 Mm^3 respectively.

Design storage capacity (Mm^3)	Residence time (yr^{-1})	Sediment trap efficiency (%)	Sediment accumulation (Mm^3 /year)
80	0.75	94.2	0.612
100	0.93	94.8	0.616
120	1.12	95.2	0.619
140	1.30	95.6	0.621

System performance was assessed by the metrics of water supply reliability and the NPV. The former metric, reliability indicates the proportion of months that the reservoir can meet the target demand (Hashimoto et al. 1982):

$$R_t = N_s/N$$

Equation A.4

where R_t is the reliability of the system, N_s is the number of months with no delivery deficit, and N is the total number of months over the planning period. NPV is defined as the total present value of benefits minus the present value cost of the project:

$$NPV = \sum_{t=1}^{T} \frac{(D(d,s) * p_w}{(1+r)^t} - C_d$$

Equation A.5

where d is the design alternative considered, s is the state of the world, C_d is the capital cost of the reservoir (million USD), $D(d,s)$ is the annual water delivery to the Mombasa city (Mm^3); $p_w$is the unit price charged for municipal water use (USD per m^3), T is the length of the project planning horizon (50 years), t is the serial year index from 1 to T=50, and r is the economic discount rate (%).

APPENDIX B

ADDITIONAL INFORMATION ON THE BAYESIAN NETWORK MODEL OF THE MWACHE SYSTEM

Conditional probability distributions for the specific sediment yield

The probability distribution of specific sediment yield (SSY) is assumed to be conditional on local land-use patterns and practices. Major land-use types at the upstream of the Mwache Dam location includes closed evergreen lowland forest, closed deciduous forest, deciduous woodland, closed grassland, open grassland with sparse shrubs, cropland, and habitation and roads respectively (CES 2014). The erosion class and specific sediment yield (SSY) associated with each land-use type are estimated previously by CES (2014), based on the guidelines provided by the Practice Manual for Water Supply Services in Kenya (Table B.1). According to Table B.1, urban areas (Habitat and roads) and agricultural croplands are associated with the highest sediment yields (1500 m^3 per km^2-year), whereas forest areas are associated with the lowest (500 m^3 per km^2-year).

Table B.1 Specific sediment yields for different land use types in the Mwache catchment

Land-use type	Area (km^2)	Erosion class	Specific Sediment Yield, SSY (m^3/ km^2-year)
Closed evergreen forest	45	Low	500
Closed deciduous forest	435	Low	500
Deciduous woodland	403	Low	500
Closed grassland	1055	Medium	1000
Open grassland	2.25	Medium	1000
Habitats and roads	113	High	1500
Crop lands	225.00	High	1500

Based on Table B.1, average SSY within the Mwache dam's catchment area is about 820 m^3 per km^2 – year, which results in an annual sediment loading of 2 Mm^3. Since this

loading rate is relatively high and would substantially reduce the effective lifetime of the reservoir, two upstream check-dams are planned to be constructed. These check-dams are expected to provide an overall sediment trapping efficiency %68 percent (CES 2014), which would reduce the SSY to Mwache Dam to about 265 m^3 per km^2 – year and the corresponding annual sediment loading to 0.65 Mm^3.

For the BN model, it is assumed that the reduced annual sedimentation loading (after considering the reductions due to check dams) will follow a truncated normal distribution, in which the parameters of mean and standard deviation will be conditional on economic development. Higher economic development is likely to result in greater urban and agricultural development within the region, which will also increase soil erosion and sediment loading according to Table B.1. The probability density distributions of SSY under low, medium and high development levels are illustrated in Figure B.1.

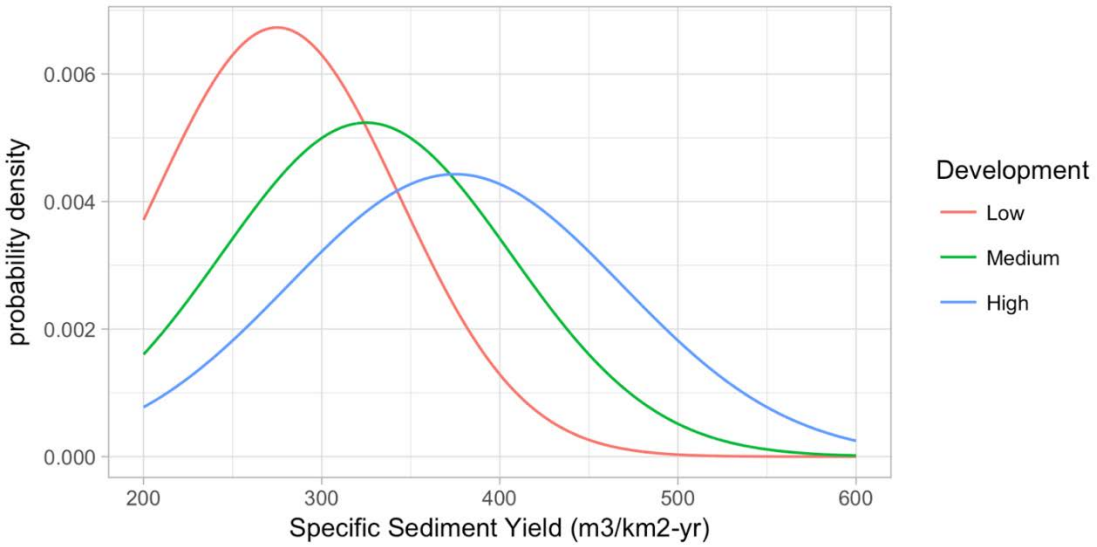

Figure B.1- Adopted probability density distributions of SSY under low, medium, and high economic development.

Conditional probability distribution for Per capita water demand

Per capita municipal water demand (PCD) in the Mombasa and the surrounding areas is assumed to be dependent on three factors: regional economic development, the price of unit water set by the Mombasa municipality, and the mean annual temperature increase due to long-term climate change. Historical water demand levels in the Mombasa city and the other towns within Coastal Kenya region is obtained from the Coastal Kenya's Water Supply Master Plan (Tahal, 2013). Based on Tahal (2013), region-wide per capita water demand ranges from 50 to 250 l per capita per day depending on the income level (Table B.2).

Table B.2 Per capita water demand concerning low, medium, and high-income levels and the income distribution for the three target districts of Mwache water supply

Income level	Municipal Demand (l/p-d)	Distribution of income classes over the target population			
		Mvita	Kisauni	Changamwe	combined
Low	50	35%	46%	46%	44%
Medium	150	60%	48%	48%	50%
High	250	5%	6%	6%	6%

Table B.2 shows the positive relationship between the household income level and the municipal water demand. Assuming that the current socioeconomic trends in the Coastal Kenya will continue over the next several decades, the municipal water is also expected to increase further. We also considered two other potential factors that may affect future water demand levels: increasing air temperature and the unit price of water defined by the municipality. Considering these three the conditional probability distribution of per capita demand, i.e., $P(PCD|Dev, \Delta Temp, Price)$ is given by:

$$TNORM(\mu = h(Dev, \Delta Temp, Price), \sigma^2 = \mu/3, a = 85, b = 150) \qquad \forall i, k$$

Equation B.1

where, h is the transfer function defining the mean of the Gaussian PDF. The transfer function h is defined as:

$$h(Dev, \Delta Temp, Price) = PCD_{dev} * 10\,\Delta Temp_{NORM} - 10\,Price_{NORM}$$

Equation B.2

where PCD_{dev} is equal to 85, 100, and 15 at the low, medium and high development levels and $\Delta Temp_{NORM}$ and $Price_{NORM}$ define values of mean temperature changes and the unit price of water normalized over the 0-1 interval. Figure B.2 shows examples of conditional PDFs of per capita demand based on the relationships shown on Equations B.1 and B.2.

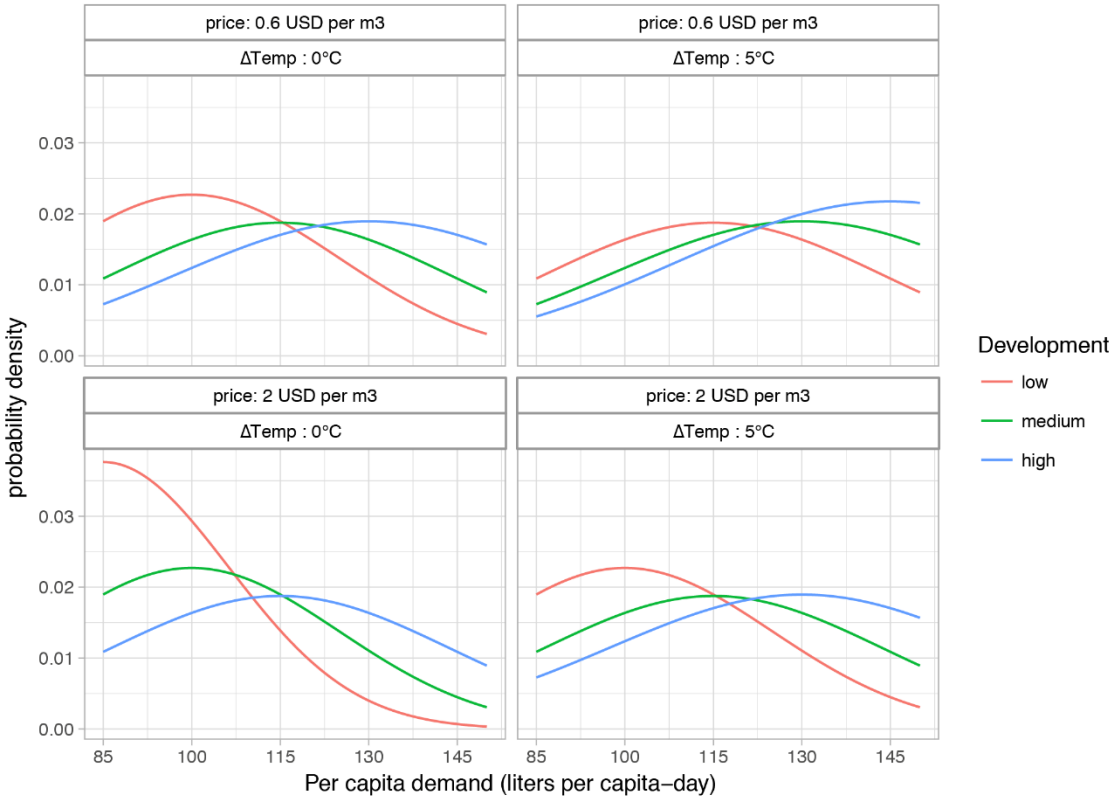

Figure B.2 The conditional likelihood of PCD based on unit price of water, temperature increases due to climate change, and socio-economic development.

APPENDIX C

DESCRIPTION OF STOCHASTIC MIXED-INTEGER PROGRAMMING MODEL OF THE NIGER RIVER BASIN

Multistage stochastic programming method

Stochastic programming (SP) (Dantzig 1955) is an extension to deterministic optimization to capture the dynamic uncertainties in a given problem. The purpose of an SP model is to find a sequence of decisions that is feasible across all possible instances of the random variables, and that maximizes the expectation of some objective function dependent on the decisions and random variables (Defourny et al. 2012). SP models can be formulated in two or more stages, where each stage represents the time-periods that the decisions are made. The simplest formulation is a two-stage recourse model, in which the decision maker takes some initial action x_1 under uncertainty. A recourse action, x_2 is then made in the second stage after the uncertainty is resolved. Hence, the actions taken in the second-stage actions aim to compensate for any bad effects of the first-stage decisions. The 2-stage SP formulation can be extended to a T-stage problem, in which the decisions taken at discrete time-periods $x = \{x_1,\ldots, x_{T_f}\}$ alternative with the observations of stochastic events

$\omega = \{\omega_1,\ldots, \omega_{T_f}\}$, i.e., $x_1, \omega_1,\ldots, x_{T_f-1}, \omega_{T_f-1}x_{T_f}, \omega_{T_f}$.

An essential requirement of multistage SP models is the "nonanticipativity" (or implementability) constraints to impose that the decisions made at any stage *t* only depend on previous events up to that stage, i.e., $x_T(\omega_1, \ldots\ \omega_{T_f-1})$. Based on this principle, a SP model can be formulated as:

$$\min_{x(\cdot)} Z = f_1(x_1) + E\left[f_2(x_2,\omega_2) + E\left[f_3(x_3,\omega_3) + E\left[\ldots + E[f_{T_f}\left(x_{T_f},\omega_{T_f}\right)\right]\right]\right]$$

$$
\begin{array}{llllll}
 & A_1x_1 & & & & = b_1 \\
 & B_2x_1 & +A_2x_2 & & & = b_2 \\
s.t. & & B_3x_2 & +A_3x_3 & & = b_3 \\
 & & & \ddots & & \vdots \\
 & & & & B_{T_f}x_{T_f-1} \quad +A_{T_f}x_{T_f} & = b_{T_f}
\end{array}
$$

$$0 \le x_t \; for \; t = 1, \ldots T_f$$

Equation C.1

where $f(x_t(\omega_t))$ is the expected value of the objective function at stage t; A and B are the technology and transition matrices, and b_1,… b_T are the right hand side coefficients (Birge and Francois 2011). Note that the problem formulation (2) relies on a specific representation of uncertain events, $\omega_1, \ldots, \omega_{T-1}$ in association with the decision stages.

A common way to express uncertainty in SP is to use a scenario-tree formulation, in which a scenario is defined as one possible realization of the random events from to the first stage to the final T_f (Dupacová et al. 2000). On Figure 15, the branching process in a scenario tree begins with the *root vertex*, in which the decisions are made in the absence of information, and terminates at the *leaf vertices*. Each vertex represents possible states of the future at given decision stages and have a conditional probability weight $p(v_i)$. A scenario is expressed by the set of vertices on its path s_j = {${v_{s_j}}^1$,..., ${v_{s_j}}^{T_f}$}. Thus, the probability of a scenario $p(s_j)$ is equal to the product of the conditional probabilities of all vertices that are in its path $p(s_i) = \prod_{t=1}^{T_f} p\left({v_{s_j}}^t\right)$.

Using a vertex-based notation, the objective function of the stochastic model is reformulated as a deterministic equivalent problem:

$$\min_{x(\cdot)} Z = \sum_{i=1}^{V_f} p(v_i).\ F(x^{v_i}, \omega)$$

Equation C.2

where, $F(x^{v_i}, \omega)$ is the objective function value for the vertex $v_i = 1, \ldots, V_f$. Note that the nonanticipativity constraints are implicit in given notation, since we directly solve the optimization model over the set of vertices.

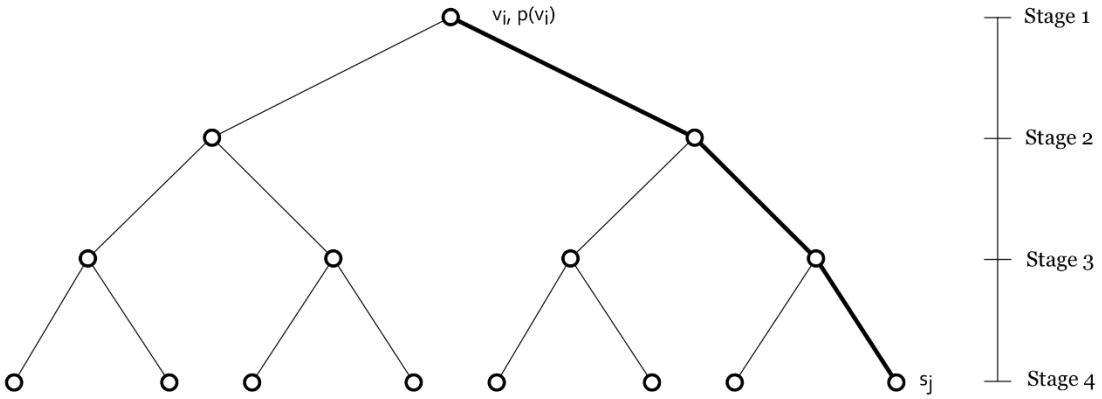

Figure C.1 Illustration of a generalized scenario tree. Each point in the scenario tree v_i is a vertex, with a probability weight of $p(v_i)$. The highlighted path represents one possible scenario s_j.

Formulation of the Niger River Basin model

The NRB optimization model is formulated as a multi-stage stochastic mixed-integer program (SMIP). The purpose of the model is to find an optimal sequence of infrastructure planning decisions for maximizing NPV of the system considering long-term climate uncertainty. There are three infrastructure decision stages at years 2020, 2035, and 2050, and three subsequent observation periods from 2020 to 2034, from 2035 to 2049, and from 2050 to 2064 respectively. The model runs at a seasonal time-step, with a wet season from May to November and a dry season from December to April respectively.

There are five major socioeconomic sectors in the optimization model: energy (hydropower), irrigation, fishing, municipal and industrial water use, and environmental flows. Figure 16 shows a conceptual diagram of the model indicating the linkages between the natural and the water resources systems.

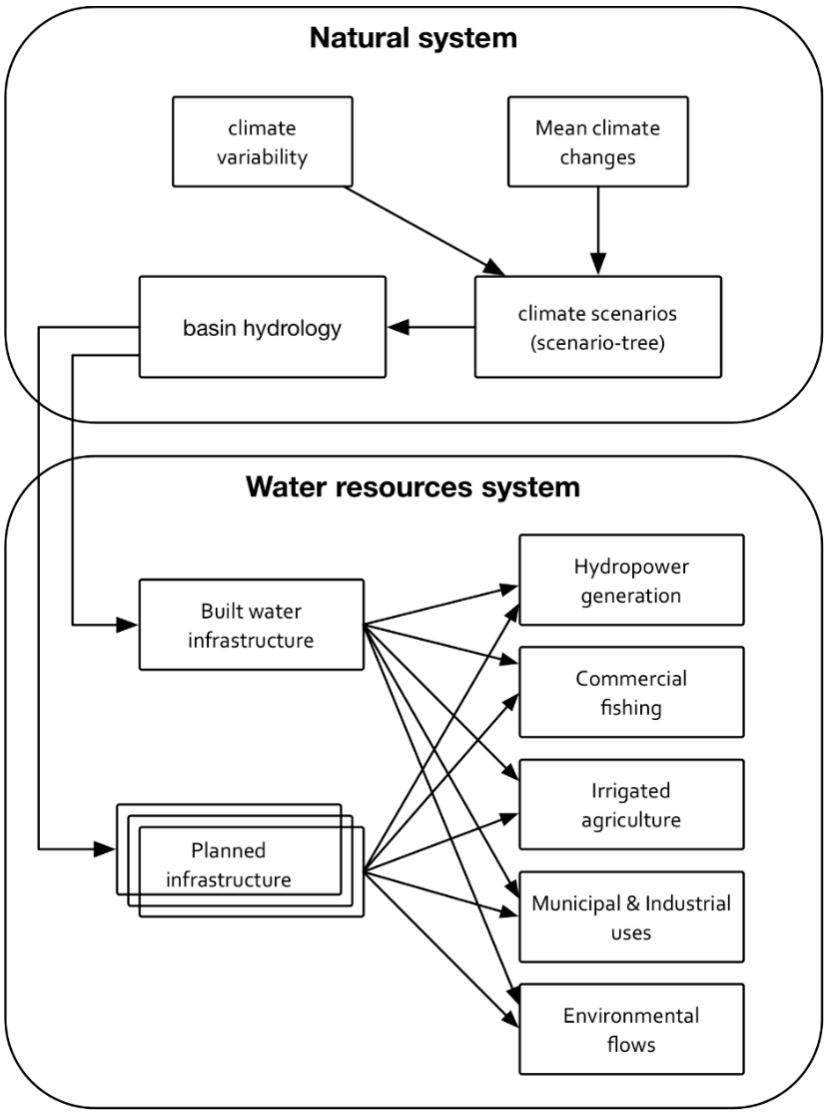

Figure C.2 Conceptual representation of the Niger River Basin long-term planning model. Arrows show major linkages between model components

The schematic of the Niger River Basin system

The Niger Basin water resources system is represented by a node-link network, in which nodes n represent various entities in the system (e.g., reservoirs, diversions) and the links set the connections among those entities (Mckinney et al. 1999; Rosegrant et al. 2000). The system consists of a total of 160 nodes including:

- 49 s*ource nodes* ($ns \in n$) representing the approximate locations of the sub-basins that provide monthly basin-runoff to the water resources system,
- *67 river nodes* ($nn \in n$) representing the water diversions and the river conjunctions,
- *12 reservoir nodes* ($nr \in n$) representing the locations of the existing and potential reservoirs,
- *2 wetland nodes* ($nw \in n$) representing prominent wetlands,
- *11 irrigation nodes* ($nr \in n$) representing the irrigation diversions aggregated at the level of development zones, and
- *19 domestic nodes* ($nr \in n$) represent the municipal and industrial water diversions aggregated based on spatial proximity.
- *28 environmental flow nodes* ($nr \in n$) representing the locations of minimum environmental flow targets.

Generation of basin runoff

For the scope of this work, basin runoff from the forty-nine catchments in the NRB is generated using a simple, physically-based, lumped-parameter 'abcd' hydrology model (Thomas 1981). Simulated runoff from each of the 49 sub-catchments is calibrated using the run-off data from the Niger Mike Basin model (BRLi and DHI 2007a) over a 60-year historical period (1948-20008). The goodness-of-fit of the developed abcd models are

summarized using the NSE measure (A.1). The results from the hydrological model calibration results are shown in Table C.1.

Table C.1 Results obtained from the hydrological calibration process

Catchment ID	Catchment latitude	Catchment area (km^2)	Nash-Sutcliffe Efficiency (NSE)
C05_11	11.25	15048.26	0.757
C06	10	15713.61	0.604
C07	9.5	12518.4	0.776
C08_09	10	5504.82	0.814
C10_59	9.5	19440.17	0.785
C12	11	21601.69	0.807
C13	11	5725.14	0.66
C14_17	6.13	10333.55	0.638
C15_57	10.5	34584.76	0.676
C16	12.25	19823.25	0.812
C19	12	34747.23	0.75
C53	14.5	26496.17	0.72
C21	15.5	136109	0.698
C23	16	81756	0.83
C24	15	42444	0.816
C25	15	12980	0.791
C26_28_29	13	38868	0.753
C27	14	5582	0.749
C30	12.5	9649	0.712
C31	13	34340	0.163
C32	11.5	9648	0.751
C33	12	34117	0.719

Table C.1 (Continued)

Catchment ID	Catchment latitude	Catchment area (km^2)	Nash-Sutcliffe Efficiency (NSE)
C34	11	13410	0.738
C40	13	33790	0.284
C62	12.5	3200	0.756
C63	13	15870	0.616
C64	12	4800	0.775
C65	12.5	43910	0.719
C66	10.5	791	0.669
C82	10.5	21080	0.797
C84	10	2.50E+04	0.719
C86_87	10.5	17950	0.687
C88	10.25	6380	0.558
C89	10.5	15800	0.782
C90	12.25	2380	0.38
C75	8	1640	0.721
C78_79	7.5	46626	0.731
C80	8	147640	0.719
C83	8.75	30650	0.795

Objective function of the optimization model

The objective of the model is to maximize long-term net economic benefits from water use and allocation given by the summation of discounted annual benefits from irrigated agriculture, hydropower production and fishing minus the cost of new water infrastructure investments and the penalties from environmental flow deficits:

$$max\ Z = \sum_{v} p_v \left(- \sum_{nr} CK_{nr}^{v} - \sum_{ni} CIRR_{ni}^{v} - \sum_{neco} \sum_{y} \sum_{m} PECO_{y,m,neco}^{v} \right.$$

$$\left. + \sum_{ni} \sum_{y} BIRR_{y,ni}^{v} + \sum_{nr} \sum_{y} \sum_{m} BHP_{y,m,nr}^{v} + \sum_{nr} \sum_{y} \sum_{m} BFSH_{y,m,nr}^{v} \right)$$

Equation C.3

where, v is a vertex in the scenario-tree representation of the problem, p_v is the probability weight of vertex v; *y* and m are sets indicating the year and the season; nr, ni, and $neco$ are river nodes corresponding to reservoirs, irrigation zones, and minimum flow sites; CK and $CIRR$ are the present value costs of new dams and hydro-agricultural infrastructure (in $1M); $BIRR$, BHP and $BFSH$ are discounted economic benefits from irrigated agriculture, hydropower generation, and fishing (in $1M); and $PECO$ is a penalizing term for not meeting the minimum flow requirements (in units of $1M).

The following sections introduce the equations used to formulate the constraints of the models. A list of all sets, decision variables, and parameters in the formulations is given on the Tables C.11, C.12 and C.13 respectively.

Formulations used for the new infrastructure decisions

This work assesses two types of new water infrastructure decisions: i) construction of new dams along the Niger River and its tributaries for providing water supply and hydropower, ii) expanding the capacity of the irrigation infrastructure schemes at the eleven irrigation development zones of the NRB.

The decisions related to new dam projects are modeled using two sets of binary variables: $X1$ and $X2$. The former variable, $X1$ indicates the timing and the capacity of the new dam project (4), whereas $X2$ reports whether a dam is already in place (5):

$$X1^{v}{}_{nr,a} = \begin{cases} 1, & if\ a\ dam\ project\ decision\ is\ made \\ 0, & otherwise \end{cases}$$

Equation C.4

$$X2^{v}{}_{nr} = \begin{cases} 1, & if\ a\ dam\ is\ in\ place \\ 0, & otherwise \end{cases}$$

Equation C.5

where, a specifies the capacity alternatives for each dam project. Table C.2 shows the three options (small, medium, and large sizes) defined for the Fomi, Diaraguala, Taussa, and Kandadji Dams along with their estimated capital costs.

Table C.2 Specified design capacity alternatives for the Fomi, Diaraguala, Taussa, and Kandadji Dams (in Million m^3). The associated present value capital costs are given in parentheses.

Name	Small size	Medium size	Large size
Fomi	5560 ($300M)	6160 ($384 M USD)	6760 ($520M)
Diaraguala	2400 ($150M)	2700 ($189 M USD)	3000 ($265M)
Taussa	2800 ($165M)	3100 ($209 M USD)	3400 ($300M)
Kandadji	1400 ($115M)	1600 ($146 M USD)	1800 ($210M)

A new dam can only be built in one vertex within a single scenario in order to ensure the nonanticipativity over the planning horizon:

$$\sum_{v \in map\_sv(s_i,v)} \sum_{a} X1^{v}{}_{nr,a} \leq 1$$

Equation C.6

where, $map\_sv(s_i, v)$ is a mapping set to define the collection of vertices in any given scenario s_i. For all existing dams, $X1$ is set to zero since no further modification, e.g., capacity expansion is allowed. The binary variable $X2$ is 1 for all existing variables, or when a new dam investment decision was made in the parent vertex:

$$X2^{v}{}_{nr} = X2^{pa}{}_{nr} + \sum_{a} X1^{v}{}_{nr,a}$$

Equation C.7

where, the set pa indicates the parent vertex of v. The parent-child relationships among the scenario-tree vertices are defined through the mapping set $map\_anc(v, pa)$. Equation C.8 states that $\mathrm{X1}$ and $\mathrm{X2}$ cannot take a value of 1 at the same time, since there is a lag between the time a new dam decision is made and the time that dam is in place and operational:

$$X2^{v}{}_{nr} + \sum_{a} X1^{v}{}_{nr,a} \leq 1$$

Equation C.8

The storage capacity of a new dam $KNEW$ (in Mm^3) is given by:

$$KNEW_{nr}^{v} = \sum_{a} k\_alter_{nr,a} * X1^{v}{}_{nr,a}$$

Equation C.9

where, $k\_alter_{nr,a}$ is the prespecified alternatives defined over the set $a \in A$.

Equation (10) sets the present value cost of a new dam investment CK (in $1M):

$$CK^{v}{}_{nr} = \sum_{a} (k\_cost_{nr,a} * X1^{v}{}_{nr,a}) \ * \ discf^{v}$$

Equation C.10

where, $k\_cost_{nr,a}$ is the cost associated with the selected design capacity and $discf^{v}$ is the discount factor associated with the vertex v. The reservoir storage capacity in place and operational at any vertex v_i is obtained from the summation of existing capacity K_{nr}^{pa} and new capacity $KNEW_{nr}^{pa}$ in the parent vertex pa:

$$K_{d,nr} = \sum_{anc\_map(v_i,pa)} K_{nr}^{pa} \ + \ KNEW_{nr}^{pa}$$

Equation C.11

Irrigation infrastructure decisions are modeled using continuous decisions variables. In each development zone, new irrigation infrastructure provides an additional irrigable land area for crop production. Based on the data provided by BRLi and DHI (2007), we consider two cases: i) expansion of the existing irrigated perimeter, represented by $AREAEXP$ (Mm^2), and ii) creation of new irrigation perimeter, represented by $AREANEW$ (Mm^2). The variables $AREAEXP$ and $AREANEW$ are constrained by the specified physical limits at each vertex v (Table C.3):

$$AREAEXP_{ni}^{v} \ \leq \ areaexp\_max^{\ v}_{ni}$$

Equation C.12

$$AREANEW_{ni}^{v} \leq areanew\_max_{ni}^{v}$$

Equation C.13

A third decision variable defines the total land area available for irrigated agriculture $AREADEV$ (Mm^2). The developed land area at any given vertex v_i, $AREADEV_{ni}^{v}$ is the summation of the existing land area and the new development at its parent vertex:

$$AREADEV_{ni}^{v} = AREADEV_{ni}^{pa} + AREAEXP_{ni}^{pa} + AREANEW_{ni}^{pa}$$

Equation C.14

Table C.3 Currently irrigable perimeter and potential expansions across eleven irrigation development zones in the NRB

Irrigation zone	Currently irrigable perimeter (Mm^2)	Maximum perimeter expansion (Mm^2)	Maximum new perimeter 2020 (Mm^2)	Maximum new perimeter 2035 (Mm^2)	Maximum new perimeter 2050 (Mm^2)
DZ 1	147	71	283	1,415	1,415
DZ 2	1,162	2,280	253	1,267	1,267
DZ 3	44	236	944	4,721	4,721
DZ 4	208	35	139	693	693
DZ 5	541	334	1,334	6,671	6,671
DZ 6	35	18	71	357	357
DZ 7	462	304	1,217	6,084	6,084
DZ 8	214	323	2,905	14,525	14,525
DZ 9	129	360	1,442	7,210	7,210
DZ 10	50	156	1,403	7,016	7,016
DZ 11	56	74	670	3,348	3,348
TOTAL	3,047	4,191	10,661	53,306	53,306

The total cost of new irrigation developments $CIRR$ (in \$1M) in is calculated from the summation of present value costs of the investments. Based on BRLi and DHI (2007), it

is assumed that the unit costs of expanding the existing irrigated perimeter and creation of new perimeter are 0.5 $1M per Mm^2 and 1.2 $1M per Mm^2 respectively:

$$CIRR_{ni}^{v} = 0.5 * AREAEXP_{ni}^{v} + 1.2 * AREANEW_{ni}^{v}$$

Equation C.15

Conservation of mass balance

Conservation of water balance across the river basin system is maintained by an accounting of all inflows, releases, and storages. At any given river node *n,* year y, and season m, the releases $QOUT$ is equal to the summation of all inflows from the upstream nodes QIN minus the summation of the irrigation diversions $DIVIRR$ and the municipal and industrial diversions $DIVMI$:

$$QOUT_{y,m,n}^{v} = \sum_{n1 \in in} QIN_{y,m,n1}^{v} - \sum_{ni \in out} DIVIRR_{y,m,ni}^{v} - \sum_{nd \in out} DIVMI_{y,m,nd}^{v}$$

Equation C.16

where, for a given node n, $n1$ specifies the upstream node $(n1 \in in)$; ni, nd specify diversions for irrigation uses $(ni \in out)$ and the municipal uses $(nd \in out)$ respectively.

For reservoirs and natural lakes, the mass conservation equation (C.16) is modified to impose additional constraints:

$$QOUT_{y,m,nr}^{v} = QIN_{y,m,nr}^{v} + STRINI_{y,m,nr}^{v} - STR_{y,m,nr}^{v} - NEVAP_{y,m,nr}^{v}$$

Equation C.17

where, $STRINI$ and STR are storage volumes at the beginning and at the end of the given period (in Mm^2), NEVAP is the net evaporative loss from the reservoir surface during a given period (in Mm^2). The equation defining the initial storage volume $STRINI$ take three cases:

$$STRINI^{v}_{y,m,nr} = \begin{cases} STR^{pa}_{y_f,m_f,nr} + 0.8 * KNEW^{pa}_{nr} , & if\ y = 1, m = 1 \\ STR^{v}_{y_{f-1},1,nr} , & if\ \ y > 1, m = 1 \\ STR^{v}_{y,m-1,nr} & if\ m > 1 \end{cases}$$

Equation C.18

where, y_f and m_f are the final year and season. On equation (18), a special case is the first condition (y = 1 and m =1). In this case, $STRINI$ takes its value from the final period of its parent vertex pa. If a new investment decision is made at the parent node, $STRINI$ is set to 80 percent of the storage volume $KNEW$. Reservoir storage volume STR is constrained by the physical capacity K and the inactive storage volume k_dead:

$$K\_dead_{nr} * X2^{v}_{nr} \ \leq \ STR^{pa}_{y,m,nr} \ \leq K_{d,nr}$$

Equation C.19

Net evaporative losses $NEVAP$ is calculated from the average lake surface area, $RAREA$ (Mm^2) and a pre-calculated adjusted seasonal average evaporation rate $nevapr\_adj^{v}_{y,m,nr}$ (m):

$$NEVAP^{v}_{y,m,nr} = SAREA^{v}_{y,m,nr}, * nevapr\_adj^{v}_{y,m,nr}$$

Equation C.20

On Equation C.20, adjust net evaporation rate $nevapr\_\mathrm{adj}$ modifies the baseline net evaporation rates based on Hargreaves equation Lu et al. (2005). This provides a rough estimate of the effects of long-term temperature changes on lake evaporation.

Average lake surface area $SAREA$ is a linear function of the average storage volume in the given period, with intercepts $av\_c0_{m,nr}$ and slopes $av\_c1_{m,nr}$ defined for each reservoir and each season:

$$SAREA_{d,y,m,nr} = av\_c0_{m,nr} * X2_{d,nr} + av\_c0_{m,nr} * \frac{STRINI^{d}_{y,m,nr} + STR^{d}_{y,m,nr}}{2}$$

Equation C.21

The seasonal water balance in the Inland Delta, Mali is represented through a separate set of equations due to its prominence on the overall water budget of the NRB. The Inland Delta is one of the largest wetland systems in the entire African continent that extends downstream from KeMacina on the Niger River and Douna on the Bani River, to the station Dire in the north. The total surface area of the Inland Delta is about 73 000 km^2, of which about 40,000 km^2 was designated as a Ramsar site in 2004 by Mali (Mahé et al. 2009). On average, the Niger River loses about 40% percent of its flow in the Inland Delta due to evaporation, varying from 24 to 48% based on the year (Mahé et al. 2009).

In this work, our goal is to provide a reasonable estimate of the seasonal evaporative water losses from the wetland area as well as the inflows and outflows from the wetlands using simple, linear equations. More detailed analyses of the Inland Delta's physical hydrology and the wetland dynamics is presented by (Kuper et al. 2003; Passchier et al. 2005; Zwarts et al. 2005; Dadson et al. 2010). The wetland system in the Inland Delta Region is represented by two lakes, i.e., a south lake (DELTAS) and a north lake (DELTAN)

respectively. In this representation, the Niger flow enters to the wetland system from the south lake after it converges with Bani River, then routed to the north lake and exits.

In any period, intermediate lake volumes are calculated based on the previous season's storage $STRINI$, current inflow from the upstream node QIN, and the current net evaporative losses $NEVAP$:

$$STR\_INT^{v}_{y,m,nw} = STRINI^{v}_{y,m,nw} + QIN^{v}_{y,m,nw} - NEVAP^{v}_{y,m,nw}$$

Equation C.22

where, the set nw represents t DELTAS and DELTAN respectively. $SAREA$ is expressed as a linear function of the inflow and previous months' storage volume:

$$SAREA^{v}_{y,m,nw} = av\_c0_{m,nw} * QIN^{v}_{y,m,nw} + av\_c0_{m,nw} * STRINI^{v}_{y,m,nw}$$

Equation C.23

The outflows from the wetlands are calculated in two steps. First, an initial outflow $QOUTINI$ is calculated as a linear function of inflow QIN and previous season's storage $STRINI$:

$$QOUTINI^{v}_{y,m,nw} = deltaq\_c0_{m,nw} * QIN^{v}_{y,m,nw} + deltaq\_c1_{m,nw} * STRINI^{v}_{y,m,nw}$$

Equation C.24

The relationship between $QOUTINI$ and $STRINI$ is defined as follows using an additional set of binary variables X_3:

$$STRINI^{v}_{y,m,nw} \leq QOUTINI^{v}_{y,m,nw} + \left(1 - X3^{v}_{y,m,nw}\right) * M$$

Equation C.25

$$STRINI^{v}_{y,m,nw} \geq QOUTINI^{v}_{y,m,nw} - X3^{v}_{y,m,nw} * M$$

Equation C.26

where, M is a very large number (in this case 500,000) used for the integer formulation. Finally, the actual outflow from the lakes $QOUT$ is computed through a series of constraints to ensure that mass balance laws are not violated.

Equations C.27 through C.30 represents linearized approximations of the mass-balance in the wetlandsnd, which are specified based on the MikeBasin model the NRB system (BRLi and DHI, 2007):

$$QOUT^{v}_{y,m,nw} \geq STRINI^{v}_{y,m,nw} - (1 - X3^{v}_{y,m,nw}) * M$$

Equation C.27

$$QOUT^{v}_{y,m,nw} \leq STRINI^{v}_{y,m,nw}$$

Equation C.28

$$QOUT^{v}_{y,m,nw} \geq STRINI^{v}_{y,m,nw} - X3^{v}_{y,m,nw} * M$$

Equation C.29

$$QOUT^{v}_{y,m,nw} \leq QOUTINI^{v}_{y,m,nw}$$

Equation C.30

Benefits from hydropower

Economic benefits from hydropower production is approximated using a set of linear equations defined for each site nr and season m:

$$HP^{v}_{y,m,nr} = hp_{c0_{nr,m}} * RHP^{v}_{y,m,nr} + hp_{c1_{nr,m}} * STR^{v}_{y,m,nr}$$

Equation C.31

where, HP is the hydropower output (in MW), RHP is release through the turbines (Mm^2); and hp_c0 and hp_c1 are coefficients defined for each reservoir and season obtained by linear regression. HP variable is constrained by maximum plant capacity hp_max, and RHP cannot exceed total releases to downstream $QOUT$:

$$RHP^{v}_{y,m,nr} \leq QOUT^{v}_{y,m,nw}$$

Equation C.32

$$HP^{v}_{y,m,nr} \leq HP\_max_{nr} * \quad X2^{v}{}_{nr}$$

Equation C.33

Based on the approximated hydropower production, discounted annual benefits from hydropower production BHP ($1M) is:

$$BHP^{v}_{y,m,nr} = HP^{v}_{y,m,nr} * 3.6 * hp\_price \ *discf^{v}{}_{y}$$

Equation C.34

where, hp_price is the unit price of electricity generated, which is assumed as 0.123 $1M per GWh (BRLi and DHI 2007).

Benefits from irrigation

Irrigation benefits are calculated based on the crop yield obtained at each season. Each season, the model decides on how much area to allocate for each crop type c based on water availability and economic profitability. The model considers a number of crop types including sugar cane (all year), market gardening products (all year), grains (wet and dry

season) and rice (wet and dry season). The distribution of these crop types over the eleven irrigation development zones is shown in Table C.4.

Table C.4 Crop types considered in each irrigation district

Irrig_Zone	Sugar cane	GrainsWS	GrainsDS	Market G.	RiceWS	RiceDS
DZ_1	x	x	x	x	x	x
DZ_2	x	x	x	x	x	x
DZ_3	x	x	x	x	x	x
DZ_4	x	x	x	x	x	x
DZ_5		x	x	x	x	x
DZ_6	x	x	x	x	x	x
DZ_7	x	x	x	x	x	x
DZ_8	x		x	x	x	x
DZ_9	x	x	x	x	x	x
DZ_10		x	x	x	x	x
DZ_11		x	x		x	

The summation of the area allocated to each crop type $AREACROP$ is constrained by the irrigable land area $AREADEV_{ni}^{v}$:

$$\sum_{c} AREACROP_{c,y,m,ni}^{v} \cdot crop\_cal_{ni,c,m} \leq AREADEV_{ni}^{v}$$

Equation C.35

where, the parameter $crop\_cal$ specifies the cropping season for each crop type c in each irrigation district ni. The total amount of irrigation water required at each season $DIVIRR$ is obtained by multiplying the crop water requirements cwr (in mm per month), and the area allocated to each crop type $AREACROP$:

$$DIVIRR^{v}_{y,m,ni} = \sum_{c} AREACROP^{v}_{c,y,m,ni} * cwr_{ni,c,m} * (1e-3)$$

Equation C.36

The area devoted for each crop type c in each irrigation development zone is constrained by the specified lower and upper limits as specified in Tables C.5 and C.6 respectively.

$$AREACROP^{v}_{c,y,m,ni} \leq AREADEV^{v}_{ni} * crop\_max_{c,n}$$

Equation C.37

$$AREACROP^{v}_{c,y,m,ni} \geq AREADEV^{v}_{ni} * crop\_min_{c,n}$$

Equation C.38

Table C.5 – Minimum amount of land area devoted to each crop type in each irrigation development zone (in %)

Crop type	DZ 1	DZ 2	DZ 3	DZ 4	DZ 5	DZ 6	DZ 7	DZ 8	DZ 9	DZ 10	DZ 11
RiceWS	50%	50%	50%	50%	60%	0%	0%	30%	30%	30%	60%
RiceDS	0%	30%	50%	50%	20%	0%	0%	0%	0%	0%	30%
GrainsWS	0%	0%	0%	0%	0%	50%	50%	30%	30%	30%	0%
GrainsDS	0%	0%	0%	0%	0%	30%	50%	30%	30%	30%	0%
Market Gard.	0%	0%	0%	0%	0%	0%	0%	0%	0%	0%	0%
Sugar cane	0%	0%	0%	0%	0%	0%	0%	0%	0%	0%	0%

Table C.6 Maximum amount of land area devoted to each crop type in each irrigation development zone (in %)

Crop type	DZ 1	DZ 2	DZ 3	DZ 4	DZ 5	DZ 6	DZ 7	DZ 8	DZ 9	DZ 10	DZ 11
RiceWS	50%	50%	50%	50%	60%	0%	0%	30%	30%	30%	60%
RiceDS	0%	30%	50%	50%	20%	0%	0%	0%	0%	0%	30%
GrainsWS	0%	0%	0%	0%	0%	50%	50%	30%	30%	30%	0%
GrainsDS	0%	0%	0%	0%	0%	30%	50%	30%	30%	30%	0%
Market Gard.	0%	0%	0%	0%	0%	0%	0%	0%	0%	0%	0%
Sugar cane	0%	0%	0%	0%	0%	0%	0%	0%	0%	0%	0%

Finally, the economic benefits from irrigated agriculture $BIRR$ is calculated based on the yield from each crop type:

$$BIRR_{d,y,ni} = \sum_{c} AREACROP_{d,c,y,ni} \left(crop\_yield_{c,ni} \, . crop\_price_{c,ni} - crop\_cost_{c,ni}\right)$$

Equation C.39

where $crop\_yield$ is the average crop yield specified for each crop type c (in 1,000 tons per Mm^2), $crop\_price$ is the selling price of the crop (in 1$M per Mm^2), and crop cost is the total costs associated with the specified crop type in (in 1$M per Mm^2).

The data associated with average crop yields in each development zone (kg/m^2), selling price of the each crop in each development zone ($/kg), and average crop costs for each development zone ($/m^2$) are obtained from BRLi and DHI (2007a, b) and shown on Tables C.7, C.8, and C.9 respectively.

Table C.7 Average crop yield in each irrigation district (kg/m^2)

Crop type	DZ1	DZ2	DZ3	DZ4	DZ5	DZ6	DZ7	DZ8	DZ9	DZ10	DZ11
RiceWS	0.40	0.55	0.13	0.12	0.45	0.45	0.00	0.45	0.45	0.00	0.00
RiceDS	0.45	0.45	0.45	0.45	0.45	0.45	0.00	0.00	0.40	0.00	0.00
GrainsWS	0.00	0.00	0.00	0.00	0.00	0.00	0.30	0.00	0.00	0.00	0.00
GrainsDS	0.00	0.00	0.00	0.00	0.30	0.00	0.30	0.30	0.30	0.30	0.30
Market Gard.	3.00	3.00	3.00	0.00	3.00	3.00	0.00	0.00	0.00	0.00	0.00
Sugar cane	9.00	9.00	0.00	0.00	0.00	0.00	0.00	9.00	9.00	9.00	0.00

Table C.8 - Selling price of each crop in each irrigation district (in \$1M per Mm^2)

Crop type	DZ1	DZ2	DZ3	DZ4	DZ5	DZ6	DZ7	DZ8	DZ9	DZ10	DZ11
RiceWS	0.25	0.25	0.25	0.25	0.25	0.25	0.00	0.25	0.25	0.00	0.00
RiceDS	0.25	0.25	0.25	0.25	0.25	0.25	0.00	0.00	0.25	0.00	0.00
GrainsWS	0.00	0.00	0.00	0.00	0.00	0.00	0.22	0.00	0.00	0.00	0.00
GrainsDS	0.00	0.00	0.00	0.00	0.22	0.00	0.22	0.22	0.22	0.22	0.22
Market Gard.	0.12	0.12	0.12	0.00	0.12	0.12	0.00	0.00	0.00	0.00	0.00
Sugar cane	0.05	0.05	0.00	0.00	0.00	0.00	0.00	0.05	0.05	0.05	0.00

Table C.9 - The cost of each crop type in each irrigation district (in \$1M per Mm^2)

Crop type	DZ1	DZ2	DZ3	DZ4	DZ5	DZ6	DZ7	DZ8	DZ9	DZ10	DZ11
RiceWS	0.06	0.08	0.02	0.02	0.08	0.08	0.00	0.08	0.08	0.00	0.00
RiceDS	0.07	0.07	0.07	0.07	0.08	0.08	0.00	0.00	0.08	0.00	0.00
GrainsWS	0.00	0.00	0.00	0.00	0.00	0.00	0.04	0.00	0.00	0.00	0.00
GrainsDS	0.00	0.00	0.00	0.00	0.04	0.00	0.04	0.04	0.04	0.04	0.04
Market Gard.	3.00	3.00	3.00	0.00	3.00	3.00	0.00	0.00	0.00	0.00	0.00
Sugar cane	9.00	9.00	0.00	0.00	0.00	0.00	0.00	9.00	9.00	9.00	0.00

Benefits from fisheries

The benefits from fishery activities are assumed to be as a function of reservoir surface area $SAREA$:

$$BFISH^{v}_{y,m,nr} = SAREA^{v}_{y,m,nr} * fish\_prod * fish\_price$$

Equation C.40

where $fish\_prod$ is the fish productivity constant assumed as 10 tons per Mm^2 – year and $fish\_price$ is the selling price of the fish assumed to be equal to $300 per tons based on BRLi and DHI (2007b). Municipal and industrial (M&I) demands are introduced as hard constraints to the model, i.e., required to be satisfied to obtain a feasible solution:

$$DIVMI^{v}_{y,m,nd} = target\_mi^{v}_{m,nd} \; {}^{*}cf\_mi^{v}$$

Equation C.41

where, $target\_mi$ is the seasonal M&I demand specified at site nd and vertex v, cf_mi is a multiplier for increasing the demand in the second period (2035-2049) to two-folds, and in the third period (2050-2064) to four-folds respectively. For this work, the baseline M&I demand estimates are obtained from BRLi and DHI (2007a).

Environmental flows

Environmental flow requirements are imposed at 28 nodes points along the Niger River and its tributaries, based on the previously adopted standards (BRLi and DHI 2007b; NBA 2008) and based on the general recommendations of Zwarts et al. (2005) (Table C.10). The flow deficits from the targets are penalized through a set of linear functions:

$$QECODEF^{v}_{y,m,neco} = eco\_target_{n,m} - QECO^{v}_{y,m,neco}$$

Equation C.42

$$PENECO^{v}_{y,m,neco} = eco\_wcoef_{neco} * QECODEF^{v}_{y,m,neco} \; / \; eco\_target_{n,m}$$

Equation C.43

$$QECO^{v}_{y,m,neco} \leq QOUT^{v}_{y,m,neco}$$

*Equation C.*44

$$QECO^{v}_{y,m,neco} \leq eco\_target_{n,m}$$

Equation C.45

where, $eco\_target_{n,m}$ is the minimum flow target (Mm^3/season), eco_wcoef_{neco} is a subjective weighting factor (dimensionless), $QECO^{v}_{y,m,neco}$ is the variable representing environmental flows (Mm^3/season), $QECODEF^{v}_{y,m,neco}$ is the deficit between the minimum flow target and environmental flows, and finally $PENECO$ is the penalizing variable used in the objective function.

Table C.10 Environmental flow requirements employed in the optimization model

Node ID	Wet season Flow target (Mm^3)	Dry season Flow target (Mm^3)	Weighting factor (dimensionless)
SELIN	780	780	10
FOMI	156	156	10
DIARA	156	156	10
TAOUS	1,260	1,260	10
KANDA	1,260	1,260	10
KAINJ	318	318	10
JEBBA	2,340	2,340	10
SHIRO	2,340	2,340	10
LAGDO	2,700	2,700	10
DADIN	1,260	1,260	10
Node 24	10,000	1,000	8
Node 16	2,820	2,820	5
Node 17	780	780	5
Node 18	780	780	5
Node 23	780	780	5
Nodes 30, 31, 32, 52, 53, 55, 56, 57, 58, 59, 60, 61, and 62	1,200	1,200	5

Table C.11 Sets specified in the optimization model

Index	Description
t	decision stages, T = {t1, t2, t3, t4}
v	scenario tree vertices, V = {v1, …, v67}
s	scenarios, S = {v1, ..., v45}
pa(v)	parents of the vertices
map_anc(d, pa)	parent-child vertex mapping function
map_vt(v, t)	vertex-decision stage mapping function
map_sv(s, v)	scenario-vertex mapping function
n	all nodes
nn	simple nodes
ns	supply nodes
ni	irrigation diversion nodes
nd	municipal and industrial diversion nodes
nr	reservoir nodes (existing and planned)
nw	wetland nodes
neco	flow requirement nodes
y	serial year, Y = {1, …,15}
m	seasons {dry season, wet season)
yf(y)	terminal year, 15
mf(m)	terminal season, dry season
c	crop types {ricews, riceds, grainsws, grainsds, market gardening, sugarcane}
a	reservoir capacity alternatives {small, medium, large}

Table C.12 Decision variables specified in the optimization model

Variable	Unit/type	Description
AREACROP	Mm^2	area allocated to each crop type
AREADEV	Mm^2	total irrigable land area
AREAEXP	Mm^2	expansion of irrigated perimeter
AREANEW	Mm^2	creation of new irrigated perimeter
BIRR	$1M	Benefits from irrigated agriculture
DIRR	Mm3/season	diversions for irrigation
DMI	Mm3/season	diversion for municipal and industrial use
HPGEN	MWh/season	hydroelectric generated
K	Mm3	Reservoir storage capacity
KNEW	Mm3	New reservoir capacity
NEVAP	m/month	Net evaporation from reservoir surface
PENECO	$1M	Penalty term for not meeting environmental flows
QECO	Mm^3/season	Environmental flow target
QECODEF	Mm^3/season	Environmental flow deficit
QIN	Mm^3/season	Inflows to node
QOUT	Mm^3/season	Outflows from node
QOUT_INI	Mm^3/season	Outflows from node (initial calculation)
RHP	Mm^3/season	flow through turbines
SAREA	Mm^2	Reservoir surface area
STR	Mm^3	Reservoir storage
STR_INI	Mm^3	Initial storage volume in reservoir
X1	binary	new dam decisions
X2	binary	dam indicator
X3	binary	flow calculation variable
Z	$1M	Objective function
Z_BFISH	$1M	Benefits from fisheries
Z_BHP	$1M	Benefits from hydroelectric production
Z_BIRR	$1M	Benefits from irrigated agriculture
Z_CIRR	$1M	Present value cost of new irrigation infrastructure
Z_CK	$1M	Present value cost of new dams
Z_PENECO	$1M	Penalizing term for environmental flow deficits

Table C.13 Parameters specified in the optimization model

Parameter	Unit/Type	Description
areaexp_max	Mm^2	maximum limit for irrigation perimeter expansion
areanew_max	Mm^2	maximum limit for irrigation perimeter creation
area_base	Mm^2	irrigable land area at the initial period
av_c0	Mm^2	reg. coefficient for reservoir area-volume curve (1)
av_c1	-	reg. coefficient for reservoir area-volume curve (2)
cf_mi		coefficient for gradual increases in M&I demand
crop_cal	binary	cropping calendar
crop_cost	\$1M/ Mm^2	unit cost of crop production
crop_price	\$/kg	unit selling price of each crop
crop_wr	mm/season	crop water requirement
crop_yield	kg/ Mm^2	average yield of each crop
delta_area_max	Mm^2	maximum inundated area in the wetlands
delta_qout_c0	-	reg. coefficient for wetland outflow (1)
delta_qout_c1	-	reg. coefficient for wetland outflow (2)
delta_sarea_c0	-	reg. coefficient for wetland surface area (1)
delta_sarea_c1	-	reg. coefficient for wetland surface area (2)
discf	-	Discount coeff. assigned to annual benefits
discf_cap	-	Discount coeff. assigned to capital investments
discr	%	discount rate used in the analysis
eco_target	Mm^3/season	minimum environmental flow targets
eco_wcoef	-	weighting factor for environmental flow nodes
evapr	m/season	net evaporation rate from reservoir surfaces
evap_adj	m/season	Adjusted net evaporation rate (based on temp.)
fish_price	\$/ Mm^2	unit price of fish catch
hp_c0	-	reg. coefficient for hydropower calculation (1)
hp_c1	-	reg. coefficient for hydropower calculation (2)
hp_max	MWh	maximum capacity for hydroelectric generation
hp_price	1\$M/GWh	economic value of hydroelectricity
k_alter	Mm^3	design capacity alternatives for new dams
K_cost	1\$M	cost of new dam alternatives
k_dead	Mm^3	inactive storage of reservoir
lv_c0	m	reg. coefficient for reservoir level-volume curve (1)
lv_c1	-	reg. coefficient for reservoir level-volume curve (2)
pr_arc	-	conditional probability weight of each vertex
pr_path	-	joint probability weight of each vertex
target_mi	Mm^3/season	target M&I demand

BIBLIOGRAPHY

Aguilera PA, Fernández A, Fernández R, et al (2011) Bayesian networks in environmental modelling. Environ Model Softw 26:1376–1388. doi: 10.1016/j.envsoft.2011.06.004

Aller SPWEW, Waller SW (2011) Bayesian Belief Networks in Environmental Modeling: A Review o Recent Progress.

Andersen I, Ousmane D, Jarosewich-Holder M, Olivery J-C (2005) The Niger River Basin: A Vision for Sustainable Management. The Internatonal Bank for Reconstruction and Development / The World Bank, Washington, DC

AOCHYCOS (2015) Streamflow data for the Niger River.

Arnell NW, Gosling SN (2013) The impacts of climate change on river flow regimes at the global scale. J Hydrol 486:351–364. doi: 10.1016/j.jhydrol.2013.02.010

Arnell NW, Lloyd-Hughes B (2014) The global-scale impacts of climate change on water resources and flooding under new climate and socio-economic scenarios. Clim Change 122:127–140. doi: 10.1007/s10584-013-0948-4

Åström H, Friis Hansen P, Garré L, Arnbjerg-Nielsen K (2014) An influence diagram for urban flood risk assessment through pluvial flood hazards under non-stationary conditions. J Water Clim Chang 5:276–286. doi: 10.2166/wcc.2014.103

Barnett J, Graham S, Mortreux C, et al (2014) A local coastal adaptation pathway. Nat Clim Chang 4:1103–1108. doi: 10.1038/nclimate2383

Barsugli J, Vogel J, Kaatz L, et al (2012) Two Faces of Uncertainty: Climate Science and Water Utility Planning Methods. J Water Resour Plan Manag 138:389–395. doi: 10.1061/(ASCE)WR.1943-5452.0000188

Batchelor C, Cain J (1999) Application of belief networks to water management studies. Agric Water Manag 40:51–57. doi: 10.1016/S0378-3774(98)00103-6

Becker L, Yeh WW (1974) Optimal Timing, Sequencing, and Sizing of Multiple Reservoir Surface Water Supply Facilities. Water Resour Res 10:57–62. doi: 10.1029/WR010i001p00057

Bednarek AT (2001) Undamming Rivers: A Review of the Ecological Impacts of Dam Removal. Environ Manage 27:803–814. doi: 10.1007/s002670010189

Beh EHY, Dandy GC, Maier HR, Paton FL (2014) Optimal sequencing of water supply options at the regional scale incorporating alternative water supply sources and multiple objectives. In: International Environmental Modelling and Software Society (iEMSs) 2012 International Congress on Environmental Modelling and Software. Elsevier Ltd, pp 137–153

Beh EHY, Maier HR, Dandy GC (2015a) Scenario driven optimal sequencing under deep uncertainty. Environ Model Softw 68:181–195. doi: 10.1016/j.envsoft.2015.02.006

Beh EHY, Zheng F, Dandy GC, et al. (2017) Robust optimization of water infrastructure planning under deep uncertainty using metamodels. Environ Model Softw 93:92–105. doi: 10.1016/j.envsoft.2017.03.013

Beh H, Maier H, Dandy G (2015b) Adaptive, multiobjective optimal sequencing approach for urban water supply augmentation under deep uncertainty. Water Resour Res 51:1529–1551. doi: 10.1002/2015WR016967.Received

Ben-Haim Y (2006) Info-gap decision theory: Decisions under severe uncertainty. Academic Press, San Diego

Bertone E, Sahin O, Richards R, Roiko A (2015) Bayesian Network and System Thinking modelling to manage water quality related health risks from extreme events. In: The 21st International Congress on Modelling and Simulation (MODSIM), Gold Coast, Australia. 29th November – 4th December 2015.

Bhave AG, Conway D, Dessai S, Stainforth DA (2016) Barriers and opportunities for robust decision making approaches to support climate change adaptation in the developing world. Clim Risk Manag 14:1–10. doi: 10.1016/j.crm.2016.09.004

Biasutti M, Giannini A (2006) Robust Sahel drying in response to late 20th century forcings. Geophys Res Lett 33:10–13. doi: 10.1029/2006GL026067

Birge JR, Francois L (2011) Introduction to stochastic programming. Springer, New York

Bishop CH, Abramowitz G (2013) Climate model dependence and the replicate Earth paradigm. Clim Dyn 41:885–900. doi: 10.1007/s00382-012-1610-y

Black DC, Wallbrink PJ, Jordan PW (2014) Towards best practice implementation and application of models for analysis of water resources management scenarios. Environ Model Softw 52:136–148. doi: 10.1016/j.envsoft.2013.10.023

Borgomeo E, Hall JW, Fung F, et al (2014) Risk-based water resources planning: Incorporating probabilistic nonstationary climate uncertainties. Water Resour Res 4840–4847. doi: 10.1002/2015WR017273

Borsuk M, Clemen R, Maguire L, Reckhow K (2001) Stakeholder Values and Scientific Modeling in the Neuse River Watershed. Gr Decis Negot 10:355–373. doi: 10.1023/A:1011231801266

Braga B, Conejo JGL, Becker L, Yeh WG (1985) Capacity Expansion of Sao Paulo Water Supply. J Water Resour Plan Manag I:238–252.

Brekke LD, Maurer EP, Anderson JD, et al (2009) Assessing reservoir operations risk under climate change. Water Resour Res 45:1–16. doi: 10.1029/2008WR006941

BRLi, DHI (2007a) Establishment of a water management model for the Niger River Basin, Final Report. Niamey, Niger

BRLi, DHI (2007b) Establishment of a Water Resources Model for the Niger Basin. Addendum for the elaboration of the economic module. Niamey, Niger

Brooke A, Kendrick D, Meeraus A, Rosenthal RE (1988) GAMS: A user's guide.

Brooks N (2004) Long term perspectives and future prospects Drought in the African Sahel : Long term perspectives and future prospects. Norwich, UK

Brown C (2011) Decision-Scaling for Robust Planning and Policy under Climate Uncertainty.

Brown C, Ghile Y, Laverty M, Li K (2012) Decision scaling: Linking bottom-up vulnerability analysis with climate projections in the water sector. Water Resour Res 48:1–12. doi: 10.1029/2011WR011212

Brown C, Lall U (2006) Water and economic development: The role of variability and a framework for resilience. Nat Resour Forum 30:306–317.

Brown C, Meeks R, Hunu K, Yu W (2011a) Hydroclimate risk to economic growth in sub-Saharan Africa. Clim Change 106:621–647. doi: 10.1007/s10584-010-9956-9

Brown C, Werick W, Leger W, Fay D (2011b) A decision-analytic approach to managing climate risks: Application to the upper great lakes. J Am Water Resour Assoc 47:524–534. doi: 10.1111/j.1752-1688.2011.00552.x

Brown C, Wilby RL (2012) An Alternate Approach to Assessing Climate Risks. Eos, Trans Am Geophys Union 93:401–402. doi: 10.1029/2012EO410001

Bryant BP, Lempert RJ (2010) Thinking inside the box: A participatory, computer-assisted approach to scenario discovery. Technol Forecast Soc Change 77:34–49. doi: 10.1016/j.techfore.2009.08.002

Budescu D V., Broomell SB, Lempert RJ, Keller K (2014) Aided and unaided decisions with imprecise probabilities in the domain of losses.

Bussi G, Dadson SJ, Prudhomme C, Whitehead PG (2016) Modelling the future impacts of climate and land-use change on suspended sediment transport in the River Thames (UK). J Hydrol 542:357–372. doi: 10.1016/j.jhydrol.2016.09.010

Butcher WS, Haimes YY, Hall WA (1969) Dynamic Programming for the Optimal Sequencing of Water Supply Projects. Water Resour Res 5:1196–1204.

Buurman J, Babovic V (2016) Adaptation Pathways and Real Options Analysis: An approach to deep uncertainty in climate change adaptation policies. Policy Soc 35:137–150. doi: 10.1016/j.polsoc.2016.05.002

Cai X, Zeng R, Valocchi A, Song J (2015) Strategic planning for drought mitigation under climate change. J Water Resour Plan Manag 141:1–10. doi: 10.1061/(ASCE)WR.1943-5452.0000510.

Cannon AJ (2015) Selecting GCM scenarios that span the range of changes in a multimodel ensemble: Application to CMIP5 climate extremes indices. J Clim 28:1260–1267. doi: 10.1175/JCLI-D-14-00636.1

Castelletti A, Soncini-Sessa R (2007) Bayesian Networks and participatory modeling in water resource management. Environ Model Softw 22:1075–1088. doi: 10.1016/j.envsoft.2006.06.003

Castelletti A, Soncini-Sessa R (2006) A procedural approach to strengthening integration and participation in water resource planning. Environ Model Softw 21:1455–1470. doi: 10.1016/j.envsoft.2005.07.013

Catenacci M, Giupponi C, Borsuk ME, et al. (2013) Integrated assessment of sea-level rise adaptation strategies using a Bayesian decision network approach. Environ Model Softw 44:87–100. doi: 10.1016/j.envsoft.2012.10.010

Cervigni R, Liden R, Neumann JE, Strzepek M (2015) Enhancing the Climate Resilience of Africa's Infrastructure: The Power and Water Sectors. Africa Development Forum series. International Bank for Reconstruction and Development / The World Bank, Washington, DC

CES (2014) The Mwache Multi-Purpose Dam Project: Detailed Design Report.

Chan T, Ross H, Hoverman S, Powell B (2010) Participatory development of a Bayesian network model for catchment-based water resource management. Water Resour Res 46:1–12. doi: 10.1029/2009WR008848

Chan TUT., Hart B. BT, Kennard MJ, et al. (2012) Bayesian network models for environmental flow decision making in the daly river, northern territory, Australia. River Res Appl 28:283–301. doi: 10.1002/rra.1456

Charney JG (1975) Dynamics of deserts and drought in the Sahel. Q J R Meteorol Soc 101:193–202. doi: 10.1002/qj.49710142802

Chung G, Lansey K, Bayraksan G (2009) Reliable water supply system design under uncertainty. Environ Model Softw 24:449–462. doi: 10.1016/j.envsoft.2008.08.007

Conway D, Persechino A, Ardoin-Bardin S, et al. (2009) Rainfall and Water Resources Variability in Sub-Saharan Africa during the Twentieth Century. J Hydrometeorol 10:41–59. doi: 10.1175/2008JHM1004.1

Creaco E, Franchini M, Walski TM (2015) Taking Account of Uncertainty in Demand Growth When Phasing the Construction of a Water Distribution Network. J Water Resour Plan Manag 141:4014049. doi: 10.1061/(ASCE)WR.1943-5452.0000441

Crétat J, Vizy EK, Cook KH (2014) How well are daily intense rainfall events captured by current climate models over Africa? Clim Dyn 42:2691–2711. doi: 10.1007/s00382-013-1796-7

Culley S, Noble S, Yates A, et al (2016) A bottom-up approach to identifying themaximum operational adaptive capacity of water resource systems to a changing climate. Water Resour Res 52:6751– 6768. doi: 10.1002/2015WR018253

Dadson SJ, Ashpole I, Harris P, et al (2010) Wetland inundation dynamics in a model of land surface climate: Evaluation in the Niger inland delta region. J Geophys Res Atmos 115:1–7. doi: 10.1029/2010JD014474

Dantzig GB (1955) Linear programming under uncertainty. Manage Sci 197–206. doi: 10.1007/978-1-4419-1642-6_1

David B, Jr WW, Member S, et al. (1997) FINDING ROBUST SOLUTIONS TO WATER RESOURCES PROBLEMS. J Water Resour Plan Manag 123:49–58. doi: 10.1061/(ASCE)0733-9496(1997)123:1(49)

Davidson O, Halsnæs K, Huq S, et al. (2003) The development and climate nexus: The case of sub-Saharan Africa. Clim Policy. doi: 10.1016/j.clipol.2003.10.007

Dawsey WJJ, Minsker BSS, VanBlaricum VLL (2006) Bayesian belief networks to integrate monitoring evidence of water distribution system contamination. J Water Resour Plan Manag 132:234–241. doi: 10.1061/(ASCE)0733-9496(2006)132:4(234)

Defourny B, Ernst D, Wehenkel L (2012) Multistage stochastic programming: A scenario tree based approach to planning under uncertainty. Decis Theory Model … 97–143. doi: 10.4018/978-1-60960-165-2.ch006

Deser C, Phillips A, Bourdette V, Teng H (2012) Uncertainty in climate change projections: The role of internal variability. Clim Dyn 38:527–546. doi: 10.1007/s00382-010-0977-x

Dessai S, Hulme M (2009) Climate prediction: a limit to adaptation. Adapt to Clim … 64–78. doi: http://dx.doi.org/10.1017/CBO9780511596667.006

Dessai S, Hulme M (2007) Assessing the robustness of adaptation decisions to climate change uncertainties: A case study on water resources management in the East of England. Glob Environ Chang 17:59–72. doi: 10.1016/j.gloenvcha.2006.11.005

Dessai S, Hulme M (2004) Does climate adaptation policy need probabilities? Clim Policy 4:107–128. doi: 10.1080/14693062.2004.9685515

Dessai S, Sluijs J (2007) Uncertainty and climate change adaptation: A scoping study. Utrecht

Dittrich R, Wreford A, Moran D (2016) A survey of decision-making approaches for climate change adaptation: Are robust methods the way forward? Ecol Econ 122:79–89. doi: 10.1016/j.ecolecon.2015.12.006

Dixit AK, Pindyck RS (1994) Investment under uncertainty. Princeton University Press

Döll P, Jiménez-Cisneros B, Oki T, et al (2014) Integrating risks of climate change into water management. Hydrol Sci J 60:4–13. doi: 10.1080/02626667.2014.967250

Dosio A, Panitz HJ (2016) Climate change projections for CORDEX-Africa with COSMO-CLM regional climate model and differences with the driving global climate models. Clim Dyn 46:1599–1625. doi: 10.1007/s00382-015-2664-4

Draper AJ, Jenkins MW, Kirby KW, et al. (2003) Economic-Engineering Optimization for California Water Management. J water Resour Plan Manag 129:155–164. doi: 10.1061/(ASCE)0733-9496(2003)129:3(155)

Dupacová J, Consigli G, Wallace SW (2000) Scenarios for Multistage Stochastic Programs. Ann Oper Res 100:25–53. doi: 10.1023/A:1019206915174

Dyer F, ElSawah S, Croke B, et al. (2014) The effects of climate change on ecologically-relevant flow regime and water quality attributes. Stoch Environ Res Risk Assess 28:67–82. doi: 10.1007/s00477-013-0744-8

Enserink B, Kwakkel JH, Veenman S (2013) Coping with uncertainty in climate policy making: (Mis)understanding scenario studies. Futures 53:1–12. doi: 10.1016/j.futures.2013.09.006

Evans J., Ji F, Gab A, Ekström M (2013) Optimally choosing small ensemble members to produce robust climate simulations. Environ Res Lett 8:44050. doi: 10.1088/1748-9326/8/4/044050

Fankhauser S, Smith JB, Tol RSJJ (1999a) Weathering Climate Change: Some Simple Rules to Guide Climate Change Adaptation. Ecol Econ 30:67–78. doi: 10.1016/S0921-8009(98)00117-7

Fankhauser S, Smith JB, Tol RSJJ (1999b) Weathering climate change: some simple rules to guide adaptation decisions. Ecol Econ 30:67–78. doi: 10.1016/S0921-8009(98)00117-7

Fatichi S, Rimkus S, Burlando P, Bordoy R (2014) Does internal climate variability overwhelm climate change signals in streamflow? The upper Po and Rhone basin case studies. Sci Total Environ 493:1171–1182. doi: 10.1016/j.scitotenv.2013.12.014

Fenton NE, Neil M, Caballero JG (2006) Using Ranked Nodes to Model Qualitative Judgments in Bayesian Networks. IEEE Trans. Knowl. Data Eng.

Fontaine B, Roucou P, Gaetani M, Marteau R (2011) Recent changes in precipitation, ITCZ convection and northern tropical circulation over North Africa (1979-2007). Int J Climatol 31:633–648. doi: 10.1002/joc.2108

Forster PM, Andrews T, Good P, et al (2013) Evaluating adjusted forcing and model spread for historical and future scenarios in the CMIP5 generation of climate models. J Geophys Res Atmos 118:1139–1150. doi: 10.1002/jgrd.50174

Franczyk J, Chang H (2009) Spatial analysis of water use in Oregon, USA, 1985-2005. Water Resour Manag 23:755–774. doi: 10.1007/s11269-008-9298-9

Friedman JH, Fisher NI (1999) Bump Hunting in High-Dimensional Data. Statics Comput 9:123–143. doi: 10.1023/A:1008894516817

Fung F, Watts G, Lopez A, et al (2013) Using Large Climate Ensembles to Plan for the Hydrological Impact of Climate Change in the Freshwater Environment. Water Resour Manag 27:1063–1084. doi: 10.1007/s11269-012-0080-7

Furlong C, De Silva S, Guthrie L, Considine R (2016) Developing a water infrastructure planning framework for the complex modern planning environment. Util Policy 38:1–10. doi: 10.1016/j.jup.2015.11.002

Gersonius B, Ashley R, Pathirana A, Zevenbergen C (2013) Climate change uncertainty: Building flexibility into water and flood risk infrastructure. Clim Change 116:411–423. doi: 10.1007/s10584-012-0494-5

Getoor L, Rhee JT, Koller D, Small P (2004) Understanding tuberculosis epidemiology using structured statistical models. Artif Intell Med 30:233–256. doi: 10.1016/j.artmed.2003.11.003

Giannini A, Biasutti M, Held IM, Sobel AH (2008) A global perspective on African climate. Clim Change 90:359–383. doi: 10.1007/s10584-008-9396-y

Giordano T (2012) Adaptive planning for climate resilient long-lived infrastructures. Util Policy 23:80–89. doi: 10.1016/j.jup.2012.07.001

Giorgi F (2005) Climate change prediction. Clim Change 73:239–265. doi: 10.1007/s10584-005-6857-4

Giuliani M, Castelletti A (2016) Is robustness really robust? How different definitions of robustness impact decision-making under climate change. Clim Change 135:409–424. doi: 10.1007/s10584-015-1586-9

Grijsen JG, Brown C, Tarhule A, et al. (2013) Climate Risk Assessment for Water Resources Development in the Niger River Basin Part II: Context and Climate Projections. Clim Var - Reg Themat patterns 37–56. doi: 10.5772/56707

Groves D, Mao Z, Liden R, et al. (2015) Enhancing the climate resilience of Africa's infrastructure: The power and water sectors. In: Cervigni R, Liden R, Neumann JE, Strzepek KM (eds) Enhancing the Climate Resilience of Africa's Infrastructure: The Power and Water Sectors. Africa Development Forum series. International Bank for Reconstruction and Development / The World Bank, Washington, DC, pp 131–154

Groves DG, Lempert RJ (2007) A new analytic method for finding policy-relevant scenarios. Glob Environ Chang 17:73–85. doi: 10.1016/j.gloenvcha.2006.11.006

Groves DG, Yates D, Tebaldi C (2008) Developing and applying uncertain global climate change projections for regional water management planning. Water Resour Res 44:1–16. doi: 10.1029/2008WR006964

Groves DG, Zhimin M, Evan B, et al (2014) Enhancing the Climate Resilience of African Hydropower and Irrigation Infrastructure.

Haasnoot M, Kwakkel JH, Walker WE, ter Maat J (2013) Dynamic adaptive policy pathways: A method for crafting robust decisions for a deeply uncertain world. Glob Environ Chang 23:485–498. doi: 10.1016/j.gloenvcha.2012.12.006

Haasnoot M, Middelkoop H, Beek E Van, Deursen WPA Van (2011) A method to develop management strategies for an uncertain future. Sustain Dev 381:369–381. doi: 10.1002/sd

Haasnoot M, Middelkoop H, Offermans A, et al. (2012) Exploring pathways for sustainable water management in river deltas in a changing environment. Clim Change 115:795–819. doi: 10.1007/s10584-012-0444-2

Haguma D, Leconte R, Krau S, et al. (2014) Water Resources Optimization Method in the Context of Climate Change. J Water Resour Plan Manag 141:1–9. doi: 10.1061/(ASCE)WR.1943-5452.0000445.

Hall A (2014) Projecting regional change. Science (80-) 346:1460–1462. doi: 10.1126/science.aaa0629

Hall J, Murphy C (2012) Adapting water supply systems in a changing climate. Water Supply Syst Distrib Environ Eff 353:30.

Hall JW, Borgomeo E (2013) Risk-based principles for defining and managing water security. Philos Trans A Math Phys Eng Sci 371:20120407. doi: 10.1098/rsta.2012.0407

Hall JWW, Henriques JJJ, Hickford AJJ, et al. (2015) Assessing the long-term performance of cross-sectoral strategies for national infrastructure. J Infrastruct Syst 20:1–12. doi: 10.1061/(ASCE)IS.1943-555X.0000196

Hallegatte S (2009) Strategies to adapt to an uncertain climate change. Glob Environ Chang 19:240–247. doi: 10.1016/j.gloenvcha.2008.12.003

Hamarat C, Kwakkel JH, Pruyt E (2013) Adaptive Robust Design under deep uncertainty. Technol Forecast Soc Change 80:408–418. doi: 10.1016/j.techfore.2012.10.004

Hansman RJ, Magee C, Neufville R De, et al. (2006) Research agenda for an integrated approach to infrastructure planning, design, and management. Int J Crit Infrastructures 2:146. doi: 10.1504/IJCIS.2006.009434

Hashimoto T, Stedinger JR, Loucks DP (1982) Reliability, resiliency, and vulnerability criteria for water resource system performance evaluation. Water Resour Res 18:14–20. doi: 10.1029/WR018i001p00014

Haughton N, Abramowitz G, Pitman A, Phipps SJ (2015) Weighting climate model ensembles for mean and variance estimates. Clim Dyn 45:3169–3181. doi: 10.1007/s00382-015-2531-3

Hawkins E, Sutton R (2011) The potential to narrow uncertainty in projections of regional precipitation change. Clim Dyn 37:407–418. doi: 10.1007/s00382-010-0810-6

Heal G, Millner A (2014) Uncertainty and decision making in climate change economics. Rev Environ Econ Policy 8:120–137. doi: 10.1093/reep/ret023

Held IM, Delworth TL, Lu J, et al (2005) Simulation of Sahel drought in the 20th and 21st centuries. Proc Natl Acad Sci U S A 102:17891–17896. doi: 10.1073/pnas.0509057102

Henriksen HJ, Barlebo HC (2008) Reflections on the use of Bayesian belief networks for adaptive management. J Environ Manage 88:1025–1036. doi: 10.1016/j.jenvman.2007.05.009

Herman JD, Reed PM, Zeff HB, et al. (2015) How Should Robustness Be Defined for Water Systems Planning under Change? J Water Resour Plan Manag 141:4015012. doi: 10.1061/(ASCE)WR.1943-5452.0000509

Hirsch RM (2011) A Perspective on nonstationarity and water management. J Am Water Resour Assoc 47:436–446. doi: 10.1111/j.1752-1688.2011.00539.x

Huntington DE, Lyrintzist CS (1998) Improvements to and limitations of Latin hypercube sampling. Prob Engng Mech 13:245–253. doi: 10.1016/S0266-8920(97)00013-1

Hurd BH, Callaway M, Smith J, Kirshen P (2004) Climatic change and U.S. water resources: From modeled watershed impacts to national estimates. J Am Water Resour Assoc 40:129–148. doi: 10.1111/j.1752-1688.2004.tb01015.x

Hurwicz L (1951) A class of criteria for decision-making under ignorance.

IPCC (2013a) The Physical Science Basis. The contribution of Working Group I to the Fifth Assessment Report of the Intergovernmental Panel on Climate Change. In: Stocker TF, Qin D, Plattner GK, et al. (eds) Climate Change 2013. Cambridge University Press, Cambridge, United Kingdom and New York, NY, USA, p 29

IPCC (2013b) Climate Change 2013: The Physical Science Basis. The contribution of Working Group I to AR5. Cambridge University Press, Cambridge

Janicot S, Caniaux G, Chauvin F, et al. (2011) Intraseasonal variability of the West African monsoon. Atmos Sci Lett 12:58–66. doi: 10.1002/asl.280

Jensen F V., Nielsen TD (2007) Bayesian networks and decision graphs. J Phys A Math Theor 44:85201. doi: 10.1007/978-0-387-68282-2

Jeuland M (2010) Social discounting of large dams with climate change uncertainty. Water Altern 3:185–206.

Jeuland M, Whittington D (2014) Water resources planning under climate change: Assessing the robustness of real options for the Blue Nile. Water Resour Res 2086–2107. doi: 10.1002/2013WR013705.Received

Jury MR, Mwafulirwa ND (2002) Climate variability in Malawi, Part 1: Dry summers, statistical associations and predictability. Int J Climatol 22:1289–1302. doi: 10.1002/joc.771

Kang D, Lansey K (2014) Multiperiod Planning of Water Supply Infrastructure Based on Scenario Analysis. J Water Resour Plan Manag 140:40–54. doi: 10.1061/(ASCE)WR.1943-5452.0000310

Kasprzyk JJR, Nataraj S, Reed PM, Lempert RJ (2013) Many objective robust decision making for complex environmental systems undergoing change. Environ Model Softw 42:55–71. doi: 10.1016/j.envsoft.2012.12.007

Keeney RL, Consultants W, Francisco S (1982) Decision Analysis : An Overview. Oper Res 30:803–838.

Kirshen P, Caputo L, Vogel R, et al. (2014) Adapting Urban Infrastructure to Climate Change: A Drainage Case Study. J Water Resour Plan Manag 141:1 to 11. doi: 10.1061/(ASCE)WR.1943-5452.0000443

Kjaerulff UB, Anders LM (2013) Bayesian networks and influence diagrams. Springer

Knutti R (2008) Should we believe model predictions of future climate change? Philos Trans A Math Phys Eng Sci 366:4647–4664. doi: 10.1098/rsta.2008.0169

Knutti R, Masson D, Gettelman A (2013) Climate model genealogy: Generation CMIP5 and how we got there. Geophys Res Lett 40:1194–1199. doi: 10.1002/grl.50256

Kocabas V, Dragicevic S (2013) Bayesian networks and agent-based modeling approach for urban land-use and population density change: A BNAS model. J Geogr Syst 15:403–426. doi: 10.1007/s10109-012-0171-2

Korteling B, Dessai S, Kapelan Z (2013) Using Information-Gap Decision Theory for Water Resources Planning Under Severe Uncertainty. Water Resour Manag 27:1149–1172. doi: 10.1007/s11269-012-0164-4

Koutsoyiannis D (2014) Reconciling hydrology with engineering. Hydrol Res 45:2–22. doi: 10.2166/nh.2013.092

Kuikka S, Varis O (1997) Uncertainties of climatic change impacts in Finnish watersheds: A Bayesian network analysis of expert knowledge. Boreal Environ Res 2:109–128.

Kumar V, Holzkaemper A, Surridge B, et al. (2008) Bayesian challenges in integrated catchment modeling. iEMSs 2008 Int Congr Environ Model Softw Integr Sci Inf Technol Environ Assess Decis Mak 1–11.

Kunkel KE, Karl TR, Brooks H, et al. (2013) Monitoring and understanding trends in extreme storms: State of knowledge. Bull Am Meteorol Soc 94:499–514. doi: 10.1175/BAMS-D-11-00262.1

Kuper M, Mullon C, Poncet Y, Benga E (2003) Integrated modeling of the ecosystem of the Niger river inland delta in Mali. Ecol Modell 164:83–102. doi: 10.1016/S0304-3800(03)00006-1

Kwakkel J, Walker W, Haasnoot M (2016) Coping with the Wickedness of Public Policy Problems: Approaches for Decision Making under Deep Uncertainty. J Water Resour Plan Manag 142:1816001. doi: 10.1061/(ASCE)WR.1943-5452.0000626

Kwakkel JH, Haasnoot M, Walker WE (2015) Developing dynamic adaptive policy pathways: a computer-assisted approach for developing adaptive strategies for a deeply uncertain world. Clim Change 132:373–386. doi: 10.1007/s10584-014-1210-4

Kwakkel JH, Walker WE (2010) Grappling with uncertainty in the long-term development of infrastructure systems. 3rd Int Conf Next Gener Infrastruct Syst Eco-Cities, INFRA 2010 - Conf Proc. doi: 10.1109/INFRA.2010.5679228

Kwon H-HH, Lall U, Khalil AFF (2007) Stochastic simulation model for nonstationary time series using an autoregressive wavelet decomposition: Applications to rainfall and temperature. Water Resour Res 43:1–15. doi: 10.1029/2006WR005258

L'Hote Y, Mahe G, Bonaventure S (2003) The 1990s rainfall in the Sahel: the third driest decade since the beginning of the century. Hydrol Sci J 48:493–496. doi: 10.1623/hysj.48.3.493.45283

Lall U, Sharma A (1996) A nearest neighbor bootstrap for resampling hydrologic time series. Water Resour Res 32:679–693.

Laprise R, Hernández-Díaz L, Tete K, et al. (2013) Climate projections over CORDEX Africa domain using the fifth-generation Canadian Regional Climate Model (CRCM5). Clim Dyn 41:3219–3246. doi: 10.1007/s00382-012-1651-2

Le Barbe L, Lebel T, Tapsoba D (2002) Rainfall variability in West Africa during the years (1950-1990). J Clim 15:187–202. doi: 10.1175/1520-0442(2002)015<0187:RVIWAD>2.0.CO;2

Lebel T, Ali A (2009) Recent trends in the Central Sahel rainfall regime (1990 - 2007).

Ledbetter R, Prudhomme C, Arnell N (2012) A method for incorporating climate variability in climate change impact assessments: Sensitivity of river flows in the Eden catchment to precipitation scenarios. Clim Change 113:803–823. doi: 10.1007/s10584-011-0386-0

Lee E, Park Y, Shin JG (2009) Large engineering project risk management using a Bayesian belief network. Expert Syst Appl 36:5880–5887. doi: 10.1016/j.eswa.2008.07.057

Lempert R, McKay S (2011) Some thoughts on the role of robust control theory in climate-related decision support. Clim Change 107:241–246. doi: 10.1007/s10584-011-0135-4

Lempert R, Nakicenovic N, Sarewitz D, Schlesinger M (2004) Characterizing climate change uncertainty for decision makers. Clim Change 65:1–9. doi: 10.1023/B:CLIM.0000037561.75281.b3

Lempert RJ (2002) A new decision sciences for complex systems. Proc Natl Acad Sci U S A 99 Suppl 3:7309–7313. doi: 10.1073/pnas.082081699

Lempert RJ (2003) Shaping the Next One Hundred Years: New Methods for Quantitative, Long-Term Policy Analysis.

Lempert RJ, Bryant BP, Bankes SC (2008) Comparing Algorithms for Scenario Discovery. Work Pap 1–35.

Lempert RJ, Collins MT (2007) Managing the risk of uncertain threshold responses: Comparison of robust, optimum, and precautionary approaches. Risk Anal 27:1009–1026. doi: 10.1111/j.1539-6924.2007.00940.x

Lempert RJ, Groves DG (2010) Identifying and evaluating robust adaptive policy responses to climate change for water management agencies in the American west. Technol Forecast Soc Change 77:960–974. doi: 10.1016/j.techfore.2010.04.007

Lempert RJ, Groves DG, Popper SW (2006) A general, analytic method for generating robust strategies and narrative scenarios. Manage Sci 52:514–528. doi: 10.1287/mnsc.l

Lienou G (2013) Integrated Future Needs and Climate Change on the River Niger Water Availability. 2013:887–893. doi: 10.4236/jwarp.2013.59090

Lopez A, Fung F, New M, et al. (2009) From climate model ensembles to climate change impacts and adaptation: A case study of water resource management in the southwest of England. Water Resour Res. doi: 10.1029/2008WR007499

Loucks DP, Stedinger J, Douglas AH (1981) Water resource systems planning and analysis. Prentice-Hall

Loucks DP, Van Beek E, Stedinger JR, et al. (2005) Water resources systems planning and management: an introduction to methods, models, and applications. UNESCO, Paris

Lu J, Sun G, McNulty SG, Amatya DM (2005) A COMPARISON OF SIX POTENTIAL EVAPOTRANSPIRATION METHODS FOR REGIONAL USE IN THE SOUTHEASTERN UNITED STATES. J Am Water Resour Assoc 41:621–633. doi: 10.1111/j.1752-1688.2005.tb03759.x

Lund JR, Israel M (1995) Optimization of Transfers in Urban Water Supply Planning. J Water Resour Plan Manag 121:41–48. doi: 10.1061/(ASCE)0733-9496(1995)121:1(41)

Maas A, Hufschmidt MM, Dorfman R, et al. (1962) Design of water-resource systems. Harvard University Press., Cambridge, MA

Mahé G, Bamba F, Soumaguel A, et al (2009) Water losses in the inner delta of the River Niger : water balance and flooded area. Hydrol Process 23:3157–3160. doi: 10.1002/hyp

Mahmoud M, Liu Y, Hartmann H, et al. (2009) A formal framework for scenario development in support of environmental decision-making. Environ Model Softw 24:798–808. doi: 10.1016/j.envsoft.2008.11.010

Maier HR, Guillaume JHA, van Delden H, et al. (2016) An uncertain future, deep uncertainty, scenarios, robustness, and adaptation: How do they fit together? Environ Model Softw 81:154–164. doi: 10.1016/j.envsoft.2016.03.014

Marino S, Hogue IB, Ray CJ, Kirschner DE (2008) A methodology for performing global uncertainty and sensitivity analysis in systems biology. J Theor Biol 254:178–196. doi: 10.1016/j.jtbi.2008.04.011

Mariotti L, Coppola E, Sylla MB, et al. (2011) Regional climate model simulation of projected 21st-century climate change over an all-Africa domain: Comparison analysis of nested and driving model results. J Geophys Res Atmos. doi: 10.1029/2010JD015068

Markowitz HM (1952) Portfolio Selection. J Finance 7:77–91.

Martínez-Santos P, Henriksen HJ, Zorrilla P, Martínez-Alfaro PE (2010) Comparative reflections on the use of modeling tools in conflictive water management settings: The Mancha Occidental aquifer, Spain. Environ Model Softw 25:1439–1449. doi: 10.1016/j.envsoft.2008.11.011

Martinez GGF, Gupta HVH (2010) Toward improved identification of hydrological models: A diagnostic evaluation of the " abcd " monthly water balance model for the conterminous United States. Water Resour Res 46:W08507. doi: 10.1029/2009WR008294

Matrosov ES, Padula S, Harou JJ (2013) Selecting Portfolios of Water Supply and Demand Management Strategies Under Uncertainty-Contrasting Economic Optimisation and "Robust Decision Making" Approaches. Water Resour Manag 27:1123–1148. doi: 10.1007/s11269-012-0118-x

McInerney D, Lempert R, Keller K (2012) What are robust strategies in the face of uncertain climate threshold responses?: Robust climate strategies. Clim Change 112:547–568. doi: 10.1007/s10584-011-0377-1

McKay MD, Beckman RJ, Conover WJ (1979) Comparison of Three Methods for Selecting Values of Input Variables in the Analysis of Output from a Computer Code. Technometrics 21:239–245. doi: 10.1080/00401706.1979.10489755

Mckinney DC, Cai X, Rosegrant MW, et al. (1999) Modeling Water Resources Management at the Basin Level: Review and Future Directions.

Mendelsohn R, Williams L (2006) The distributional impact of climate change on rich and poor countries. Environ Dev Econ 159–178. doi: 10.1017/S1355770X05002755

Mesbah SM, Kerachian R, Nikoo MR (2009) Developing real time operating rules for trading discharge permits in rivers: Application of Bayesian Networks. Environ Model Softw 24:238–246. doi: 10.1016/j.envsoft.2008.06.007

Millner A, Dietz S (2011) Adaptation to climate change and economic growth in developing countries. Polit Sci 1:1–33. doi: 10.2139/ssrn.1935349

Milly P, Betancourt J, Falkenmark M, et al. (2015) On Critiques of "'Stationarity is Dead: Whither Water Management?"' Water Resour Res 7785–7789. doi: 10.1002/2015WR017408.Received

Milly PCD, Betancourt J, Falkenmark M, et al. (2008a) Stationarity Is Dead: Whither Water Management? Science (80-) 319:573–574.

Milly PCD, Betancourt J, Falkenmark M, et al. (2008b) Climate change. Stationarity is dead: whither water management? Science 319:573–574. doi: 10.1126/science.1151915

Molina (2013) Stochastic hydro-economic model for groundwater management using Bayesian networks: El Salobral-Los Llanos aquifer system. J Chem Inf Model 53:1689–1699. doi: 10.1017/CBO9781107415324.004

Molle F, Wester P, Hirsch P (2010) River basin closure: Processes, implications, and responses. Agric Water Manag 97:569–577. doi: 10.1016/j.agwat.2009.01.004

Moody P, Brown C (2013) Robustness indicators for evaluation under climate change: Application to the upper Great Lakes. Water Resour Res 49:3576–3588. doi: 10.1002/wrcr.20228

Moody P, Brown C (2012) Modeling stakeholder-defined climate risk on the Upper Great Lakes. Water Resour Res 48:1–15. doi: 10.1029/2012WR012497

Mortazavi M, Kuczera G, Cui L (2012) Multiobjective optimization of urban water resources: Moving toward more practical solutions. Water Resour Res 48:1–15. doi: 10.1029/2011WR010866

Moss RHRH, Edmonds JAJA, Hibbard KAKA, et al. (2010) The next generation of scenarios for climate change research and assessment. Nature 463:747–756. doi: 10.1038/nature08823

Mulvey JM, Vanderbei RJ, Zenios SA, John M Mulvey, Robert J Vanderbei SAZ (2008) Robust Optimization of Large-Scale Systems. Oper Res 43:264–281. doi: 10.1287/opre.43.2.264

Murphy J., Booth BB., Collins M, et al. (2007) A methodology for probabilistic predictions of regional climate change from perturbed physics ensembles. Philos Trans R Soc A Math Phys Eng Sci 365:1993–2028. doi: 10.1098/rsta.2007.2077

Namara RE, Barry B, Owusu ES, Ogilvie A (2011) An Overview of the Development Challenges and Constraints of the Niger Basin and Possible Intervention Strategies. Colombo, Sri Lanka

Nazemi A, Wheater HS (2014) Assessing the Vulnerability of Water Supply to Changing Streamflow Conditions. Eos (Washington DC). doi: 10.1029/2011WR011212.Mote

Nazemi A, Wheater HS, Chun KP, Elshorbagy A (2013) A stochastic reconstruction framework for the analysis of water resource system vulnerability to climate-induced changes in river flow regime. 49:291–305. doi: 10.1029/2012WR012755

NBA (2008) A Shared Vision for the River Niger Basin. Niamey, Niger. Niamey, Niger, Niger

Neufville R (2003) Real Options: Dealing With Uncertainty in Systems Planning and Design. Integr Assess 4:26–34. doi: 10.1076/iaij.4.1.26.16461

New M, Hulme M (2000) Representing uncertainty in climate change scenarios: a Monte-Carlo approach. Integr Assess 1:203–213. doi: 10.1023/A:1019144202120

Newton AC (2010) Use of a Bayesian network for Red Listing under uncertainty. Environ Model Softw 25:15–23. doi: 10.1016/j.envsoft.2009.07.016

Nicholson S (2000) The nature of rainfall variability over Africa on time scales of decades to millennia. Glob Planet Change 26:137–158. doi: 10.1016/S0921-8181(00)00040-0

Nicholson SE (2009) A revised picture of the structure of the "' monsoon "' and land ITCZ over West Africa. 1155–1171. doi: 10.1007/s00382-008-0514-3

Nicholson SE (2013) The West African Sahel: A Review of Recent Studies on the Rainfall Regime and Its Interannual Variability. ISRN Meteorol 2013:32. doi: 10.1155/2013/453521

Noi LVT, Nitivattananon V (2015) Assessment of vulnerabilities to climate change for urban water and wastewater infrastructure management: Case study in Dong Nai river basin, Vietnam. Environ Dev 16:119–137. doi: 10.1016/j.envdev.2015.06.014

Norconsult (1996) Lower Fufu Hydropower Project Pre-feasibility study Final Report Volume II Initial Environmental Assessment.

O'Hagan A, Buck CE, Daneshkhan A, et al. (2006) Uncertain Judgments: Eliciting Experts' Probabilities. John Wiley & Sons, Ltd

O'Neill BC, Kriegler E, Riahi K, et al. (2014) A new scenario framework for climate change research: The concept of shared socioeconomic pathways. Clim Change 122:387–400. doi: 10.1007/s10584-013-0905-2

Obada E, Alamou E, Zandagba J, et al. (2017) Change in Future Rainfall Characteristics in the Mekrou Catchment (Benin), from an Ensemble of 3 RCMs (MPI-REMO, DMI-HIRHAM5 and SMHI-RCA4). Hydrology 4:14. doi: 10.3390/hydrology4010014

Ogilvie A, Mahé G, Ward J, et al. (2010) Water, agriculture and poverty in the Niger River basin. Water Int 35:594–622. doi: 10.1080/02508060.2010.515545

Olmstead SM (2014) Climate change adaptation and water resource management: A review of the literature. Energy Econ 46:500–509. doi: 10.1016/j.eneco.2013.09.005

Oyebande L, Odunuga S (2010) Climate change impact on water resources at the transboundary level in West Africa: the cases of the Senegal, Niger and Volta basins. Spec Issue Anal Clim Chang impacts water Resour Dev Econ successes challenges 4:163–172. doi: 10.2174/1874378101004010163]

Ozer P, Demarée G, Vandiepenbeeck M (2003) Discussion of "Analysis of a Sahelian annual rainfall index from 1896 to 2000; the drought continues." Hydrol Sci J 489–496:489–572.

Paeth H, Hall NMJ, Gaertner MA, et al (2011) Progress in regional downscaling of west African precipitation. Atmos Sci Lett 12:75–82. doi: 10.1002/asl.306

Pahl-Wostl C (2007a) The implications of complexity for integrated resources management. Environ Model Softw 22:561–569. doi: 10.1016/j.envsoft.2005.12.024

Pahl-Wostl C (2007b) Transitions towards adaptive management of water facing climate and global change. Water Resour Manag 21:49–62. doi: 10.1007/s11269-006-9040-4

Passchier R, Maaten R, Meijer K (2005) Integrated Water Resources Modelling of the Upper Niger River (Mali).

Patricola CM, Cook KH (2010) Northern African climate at the end of the twenty-first century: An integrated application of regional and global climate models. Clim Dyn 35:193–212. doi: 10.1007/s00382-009-0623-7

Pearl J (1988) Probabilistic Reasoning in Intelligent Systems: Networks of Plausible Inference. Morgan Kaufmann, San Mateo, CA. Pearl,

Pielke R et al. (2012) Regional Climate Downscaling: What's the Point? Eos (Washington DC) 93:52–53. doi: 10.1002/wea543.Wilby

Pollino CA, White AK, Hart BT (2007) Examination of conflicts and improved strategies for the management of an endangered Eucalypt species using Bayesian networks. Ecol Modell 201:37–59. doi: 10.1016/j.ecolmodel.2006.07.032

Polonik W, Wang Z (2010) PRIM analysis. J Multivar Anal 101:525–540. doi: 10.1016/j.jmva.2009.08.010

Priscoli JD (1998) Water and civilization: Using history to reframe water policy debates and to build a new ecological realism. Water Policy 1:623–636. doi: 10.1016/S1366-7017(99)00019-7

Prudhomme C, Wilby RL, Crooks S, et al. (2010) Scenario-neutral approach to climate change impact studies: Application to flood risk. J Hydrol 390:198–209. doi: 10.1016/j.jhydrol.2010.06.043

Randall D, Cleland L, Kuehne CS (1997) Water supply planning simulation model using mixed-integer linear programming "engine."

Ranger N, Reeder T, Lowe J (2013) Addressing "deep" uncertainty over long-term climate in major infrastructure projects: four innovations of the Thames Estuary 2100 Project. EURO J Decis Process 1:233–262. doi: 10.1007/s40070-013-0014-5

Ray PA, Kirshen PH, Watkins Jr DW (2012) Staged Climate Change Adaptation Planning for Water Supply in Amman, Jordan. J Water Resour Plan Manag 138:403–411. doi: 10.1061/(ASCE)WR.1943-5452.0000172.

Ray PA, Watkins DW, Vogel RM, Kirshen PH (2014) Performance-based evaluation of an improved robust optimization formulation. J Water Resour Plan Manag 140:1–9. doi: 10.1061/(ASCE)WR.1943-5452.0000389

Reed PM, Hadka D, Herman JD, et al. (2013) Evolutionary multiobjective optimization in water resources: The past, present, and future. Adv Water Resour 51:438–456. doi: 10.1016/j.advwatres.2012.01.005

Richards R, Sanó M, Roiko A, et al. (2013) Bayesian belief modeling of climate change impacts for informing regional adaptation options. Environ Model Softw 44:113–121. doi: 10.1016/j.envsoft.2012.07.008

Rittel HWJ, Webber MM (1973) Dilemmas in a General Theory of Planning. Policy Sci 4:155–169. doi: 10.1007/BF01405730

Rocheta E, Sugiyanto M, Johnson F, et al. (2014) How well do general circulation models represent low-frequency rainfall variability? Water Resour Res 50:2108–2123. doi: 10.1002/2012WR013085

Rosegrant MW, Ringler C, McKinney DC, et al. (2000) Integrated economic-hydrologic water modeling at the basin scale: The Maipo river basin. Agric Econ 24:33–46. doi: 10.1016/S0169-5150(00)00113-4

Roudier P, Ducharne A, Feyen L (2014) Climate change impacts on runoff in West Africa: A review. Hydrol Earth Syst Sci 18:2789–2801. doi: 10.5194/hess-18-2789-2014

Rougier J, Goldstein M (2014) Climate Simulators and Climate Projections. Annu Rev Stat Its Appl 1:103–123. doi: 10.1146/annurev-statistics-022513-115652

Sahinidis N V. (2004) Optimization under uncertainty: State-of-the-art and opportunities. Comput Chem Eng 28:971–983. doi: 10.1016/j.compchemeng.2003.09.017

Schiermeier Q (2007) Get practical, urge climatologists. Nature 448:234–235. doi: 10.1038/448234c

Schlef KE (2014) Documentation of the Niger River Basin WEAP Model. Amherst, MA

Schleich J, Hillenbrand T (2009) Determinants of residential water demand in Germany. Ecol Econ 68:1756–1769. doi: 10.1016/j.ecolecon.2008.11.012

Schwartz P (1996) The Art of the Long View. Crown Pub, New York, NY

Sheffield J, Goteti G, Wood EF (2006) Development of a 50-yr, high resolution global dataset of meteorological forcings for land surface modeling. J Clim 13:3088–3111. doi: 10.1175/JCLI3790.1

Shongwe ME, van Oldenborgh GJ, van den Hurk B, van Aalst M (2011) Projected Changes in Mean and Extreme Precipitation in Africa under Global Warming. J Clim Clim 24:3718–3733.

Sillmann J, Kharin V V., Zwiers FW, et al (2013) Climate extremes indices in the CMIP5 multimodel ensemble: Part 2. Future climate projections. J Geophys Res Atmos 118:2473–2493. doi: 10.1002/jgrd.50188

Simon HA (1955) A behavioral model of rational choice. Q J Econ 69:99–118. doi: 10.2307/1884852

Singh R, Wagener T, Crane R, et al. (2014) A vulnerability driven approach to identify adverse climate and land use change combinations for critical hydrologic indicator thresholds: Application to a watershed in Pennsylvania, USA. Water Resour Res 50:3409–3427. doi: 10.1002/2013WR014988

Sissoko K, van Keulen H, Verhagen J, et al. (2011) Agriculture, livelihoods and climate change in the West African Sahel. Reg Environ Chang 11:119–125. doi: 10.1007/s10113-010-0164-y

Stainforth D., Allen M., Tredger E., Smith L. (2007a) Confidence, uncertainty and decision-support relevance in climate predictions. Philos Trans R Soc A Math Phys Eng Sci 365:2145–2161. doi: 10.1098/rsta.2007.2074

Stainforth DA, Aina T, Christensen C, et al. (2005) Uncertainty in predictions of the climate response to rising levels of greenhouse gases. Nature 433:403–6. doi: 10.1038/nature03301

Stainforth DA, Downing TE, Washington R, et al. (2007b) Issues in the interpretation of climate model ensembles to inform decisions. Phil Trans R Soc A 365:2163–2177. doi: 10.1098/rsta.2007.2073

Steinschneider S, Brown C (2013) A semiparametric multivariate, multisite weather generator with low-frequency variability for use in climate risk assessments. Water Resour Res 49:7205–7220. doi: 10.1002/wrcr.20528

Steinschneider S, McCrary R, Mearns LO, Brown C (2015a) The effects of climate model similarity on probabilistic climate projections and the implications for local, risk-based adaptation planning. Geophys Res Lett 42:5014–5022. doi: 10.1002/2015GL064529

Steinschneider S, Mccrary R, Wi S, et al (2015b) Expanded Decision-Scaling Framework to Select Robust Long-Term Water-System Plans under Hydroclimatic Uncertainties. J Water Resour Plan Manag 141:4015023. doi: 10.1061/(ASCE)WR.1943-5452.0000536

Stewart-Koster B, Bunn SE, MacKay SJ, et al (2010) The use of Bayesian networks to guide investments in flow and catchment restoration for impaired river ecosystems. Freshw Biol 55:243–260. doi: 10.1111/j.1365-2427.2009.02219.x

Stouffer RJ, Eyring V, Meehl GA, et al (2017) CMIP5 scientific gaps and recommendations for CMIP6. Bull Am Meteorol Soc 98:95–105. doi: 10.1175/BAMS-D-15-00013.1

Strzepek K, Jacobsen M, Boehlert B, Neumann J (2013) Toward evaluating the effect of climate change on investments in the water resources sector: insights from the forecast and analysis of hydrological indicators in developing countries. Environ Res Lett 8:44014. doi: 10.1088/1748-9326/8/4/044014

Strzepek K, Yohe G, Neumann J, Boehlert B (2010) Characterizing changes in drought risk for the United States from climate change. Environ Res Lett 5:44012. doi: 10.1088/1748-9326/5/4/044012

Sultan B, Janicot S (2003) The West African monsoon dynamics. Part II: The "preonset" and "onset" of the summer monsoon. J Clim 16:3407–3427. doi: 10.1175/1520-0442(2003)016<3407:TWAMDP>2.0.CO;2

Sultan B, Janicot S, Diedhiou A (2003) The West African monsoon dynamics. Part I: Documentation of intraseasonal variability. J Clim 16:3389–3406. doi: 10.1175/1520-0442(2003)016<3389:TWAMDP>2.0.CO;2

Sylla MB, Elguindi N, Giorgi F, Wisser D (2016) Projected robust shift of climate zones over West Africa in response to anthropogenic climate change for the late 21st century. Clim Change 134:241–253. doi: 10.1007/s10584-015-1522-z

Syvitski JPM (2003) Supply and flux of sediment along hydrological pathways: Research for the 21st century. Glob Planet Change 39:1–11. doi: 10.1016/S0921-8181(03)00008-0

Tahal (2013) Consultancy Services for Water Supply Master Plan for Mombasa and Other Towns Within Coast Province: Draft Water Supply Master Plan Main Report.

Taleb NN (2007) The black swan: The impact of the highly improbable. doi: 10.2139/ssrn.1490769

Tarhule A, Zume JT, Grijsen JG (2012) Exploring temporal hydroclimatic variability in the Niger Basin (1901-2006) using observed and reanalysis data.

Taylor KE, Stouffer RJ, Meehl GA (2012) An overview of CMIP5 and the experiment design. Bull Am Meteorol Soc 93:485–498. doi: 10.1175/BAMS-D-11-00094.1

The Kenya Gazette (2012) October 26, 2012.

Thomas A (1981) Improved Methods for National Water Assessment. Water Resources Contract: WR15249270.

Turner SWD, Blackwell RJ, Smith MA, Jeffrey PJ (2016) Risk-based water resources planning in England and Wales: challenges in execution and implementation. Urban Water J 13:182–197. doi: 10.1080/1573062X.2014.955856

Turner SWD, Marlow D, Ekstr M, Jeffrey PJ (2014) Linking climate projections to performance: A yield-based decision scaling assessment of a large urban water resources system. Water Resour Res 50:3553–3567. doi: 10.1002/2013WR015156.Received

Uusitalo L (2007) Advantages and challenges of Bayesian networks in environmental modeling. Ecol Modell 203:312–318. doi: 10.1016/j.ecolmodel.2006.11.033

Vetter T, Huang S, Aich V, et al. (2015) Multi-model climate impact assessment and intercomparison for three large-scale river basins on three continents. Earth Syst Dyn 6:17–43. doi: 10.5194/esd-6-17-2015

Vicuna S, Dracup JA, Lund JR, et al. (2010) Basin-scale water system operations with uncertain future climate conditions: Methodology and case studies. Water Resour Res 46:1–19. doi: 10.1029/2009WR007838

Vorosmarty CCJ, Green P, Salisbury J, Lammers RB (2014) Global Water Resources: Vulnerability from Climate Change and Population Growth. Science (80-) 289:284–288. doi: 10.1126/science.289.5477.284

Vörösmarty CJ, Meybeck M, Fekete B, et al. (2003) Anthropogenic sediment retention: Major global impact from registered river impoundments. Glob Planet Change 39:169–190. doi: 10.1016/S0921-8181(03)00023-7

Wald A (1950) Statistical Decision Functions. New York

Walker W., Harremoes P, Rotmans J, et al. (2003) Defining uncertainty: A Conceptual Basis for Uncertainty Management. Integr Assess 4:5–17.

Walker WE, Haasnoot M, Kwakkel JH (2013) Adapt or perish: A review of planning approaches for adaptation under deep uncertainty. Sustain 5:955–979. doi: 10.3390/su5030955

Weaver CP, Lempert RJ, Brown C, et al. (2013) Improving the contribution of climate model information to decision making: The value and demands of robust decision frameworks. Wiley Interdiscip Rev Clim Chang 4:39–60. doi: 10.1002/wcc.202

Webby RB, Adamson PT, Boland J, et al. (2007) The Mekong-applications of value at risk (VaR) and conditional value at risk (CVaR) simulation to the benefits, costs, and consequences of water resources development in a large river basin. Ecol Modell 201:89–96. doi: 10.1016/j.ecolmodel.2006.07.033

Weigel AP, Knutti R, Liniger MA, Appenzeller C (2010) Risks of model weighting in multimodel climate projections. J Clim 23:4175–4191. doi: 10.1175/2010JCLI3594.1

Weitzman ML (2009) On Modeling and Interpreting the Economics of Catastrophic Climate Change. Rev Econ Stat 91:1–19. doi: 10.1162/rest.91.1.1

Whateley S, Steinschneider S, Brown C (2016) Selecting Stochastic Climate Realizations to Efficiently Explore a Wide Range of Climate Risk to Water Resource Systems. J Water Resour Plan Manag 142:1–7. doi: 10.1061/(ASCE)WR.1943-5452.0000631.

Whateley S, Steinschneider S, Brown C (2014) A climate change range-based method for estimating robustness for water resources supply. Water Resour Res 50:1–18. doi: 10.1002/2013WR014979.Reply

Wilby RL (2008) A review of recent trends and projected climate changes for Niger, West Africa. A technical brief for Tierfund.

Wilby RL, Dessai S (2010) Robust adaptation to climate change. Weather 65:176–180. doi: 10.1002/wea.504

Wise RM, Fazey I, Stafford Smith M, et al. (2014) Reconceptualising adaptation to climate change as part of pathways of change and response. Glob Environ Chang 28:325–336. doi: 10.1016/j.gloenvcha.2013.12.002

Woodward M, Kapelan Z, Gouldby B (2014) Adaptive flood risk management under climate change uncertainty using real options and optimization. Risk Anal 34:75–92. doi: 10.1111/risa.12088

Wurbs R (1993) Reservoir system simulation and optimization models. J water Resour Plan Manag 119:455–472.

Yang YCE, Wi S, Ray PA, et al. (2016) The future nexus of the Brahmaputra River Basin: Climate, water, energy and food trajectories. Glob Environ Chang 37:16–30. doi: 10.1016/j.gloenvcha.2016.01.002

Yet B, Constantinou A, Fenton N, et al. (2016) A Bayesian network framework for project cost, benefit and risk analysis with an agricultural development case study. Expert Syst Appl 60:141–155. doi: 10.1016/j.eswa.2016.05.005

Young K, Hall JW (2015) Introducing system interdependency into infrastructure appraisal: from projects to portfolios to pathways. Infrastruct Complex 2:2. doi: 10.1186/s40551-015-0005-8

Zwarts L, Beuering VB, Kone B, Wymenga E (2005) The Niger, a lifeline: effective water management in the Upper Niger Basin.